COMPUTATIONAL ANALYSES OF GROUNDWATER TRAVEL TIME - A PRELIMINARY STUDY

Prepared for

Nuclear Regulatory Commission
Contract NRC-02-88-005

Prepared by

R. T. Green
A. C. Bagtzoglou
G. W. Wittmeyer
B. Sagar
R. G. Baca

Center for Nuclear Waste Regulatory Analyses
San Antonio, Texas

October 1992

CONTENTS

CONTENTS (Cont'd)

FIGURES

FIGURES (Cont'd)

FIGURES (Cont'd)

TABLES

ACKNOWLEDGMENTS

This report was prepared to document work performed by the Center for Nuclear Waste Regulatory Analyses (CNWRA) for the U.S. Nulcear Regulatory Commission under Contract No. NRC-02-88-005. The activities reported here were performed on behalf of the NRC Office of Nuclear Material Safety and Safeguards, Division of High-Level Waste Management. The report is an independent product of the CNWRA and does not necessarily reflect the views or regulatory position of the NRC.

The authors wish to thank Drs. Wesley C. Patrick and Randall D. Manteufel, of the CNWRA, for their in-depth and thorough reviews of this report. Their editorial comments and suggestions made significant contributions to the clarity and readability of the final manuscript. The authors also thank Ms. Mary Ann Gruhlke and Mr. Arturo Ramos who prepared and assembled the report.

1 INTRODUCTION

1.1 PROGRAMMATIC BACKGROUND

In the code of federal regulations Title 10, Section 60.113 titled "Performance of particular barriers after permanent closure," performance objectives for the engineered barriers and the geologic setting are stated. The one related to the geologic setting, which is the subject of this report, is stated as follows.

> "Geologic setting. The geologic repository shall be located so that pre-waste-emplacement groundwater travel time along the fastest path of likely radionuclide travel from the disturbed zone to the accessible environment shall be at least 1,000 years or such other travel time as may be approved or specified by the commission."

As a step towards streamlining its licensing process, the U. S. Nuclear Regulatory Commission (NRC) and the Center for Nuclear Waste Regulatory Analyses (CNWRA) are analyzing the high-level waste (HLW) regulations so that institutional, regulatory, and technical uncertainties (see Weiner et al., 1990 for definitions) can be reduced prior to the submission of the license application. The pre-waste groundwater travel time (GWTT) objective stated above has also been subjected to such an analysis. The full details of this analysis are presently being documented by the NRC. To date, no institutional and regulatory uncertainties have been identified in the GWTT objective. This means that the institutional responsibilities for the implementation of the rule and what needs to be demonstrated by the Department of Energy (DOE) are clear. However, the specific computational approaches by which the DOE may demonstrate (and the NRC may determine) compliance with the GWTT objective are not well defined at this time. Consequently, the issue of how compliance is to be demonstrated (or determined) is an important technical uncertainty.

Three technical uncertainties have been identified in the GWTT rule. These are: (i) in a variably-saturated, fractured, layered, heterogeneous medium, it may not be possible to uniquely define the fastest path of radionuclide travel; (ii) the definition of disturbed zone is not precise; and (iii) it is not clear how much, if any, mass of water is to be associated with the flow tube used in computing the GWTT. In order to resolve these uncertainties, it has been assumed that ground water travel time refers to the time that a water particle of undefined mass will take in travelling between two specified locations or a specified distance. The need for clarification (and possible resolution) of technical uncertainties associated with the geologic setting performance measure is the motivation for the work reported here.

1.2 TECHNICAL BACKGROUND

In principle, experimental and/or calculational methods may be used for demonstrating or determining compliance with a performance objective like the GWTT. Because of the long time involved (e.g., 1,000 years) and large space scales (i.e., several kilometers) in the GWTT objective, it is doubtful that an *in situ* field experiment could be conducted under conditions of interest. While it is possible to think of spatially abbreviated and temporally accelerated tracer experiments for measuring travel times in the field, such experiments have too many difficulties associated with their execution and, to date, such experiments have predominately been performed in saturated media. Thus, mathematical models are the desired practical means for demonstrating compliance with the GWTT objective.

Stated simply, GWTT is the residence time of a parcel of water moving along a particular flow path between two points of interest. The flow path is determined by the fluid pressure field that exists prior to the emplacement of the waste. The phrase pre-waste-emplacement is interpreted to mean that: (i) future evolution of the site is not to be considered in calculating the GWTT, that is, the site (e.g., hydraulic property distribution) and its environment (e.g., recharge rate) are to be assumed to remain static; (ii) the effect of radiogenic heat (e.g., buoyancy forces and fracture dilations) is to be neglected outside the "disturbed zone"; and (iii) individual flow path represents the likely path for radionuclide travel with the effects of molecular diffusion, hydrodynamic dispersion, and other chemical effects (e.g., adsorption and desorption) neglected. On this conceptual basis, the GWTT can be thought of as the fundamental performance characteristic of a geologic medium.

With the assumptions stated above, the basic analysis approach for the calculating the GWTT for various flow paths consists of: (i) conceptualize the domain — locate the boundaries, determine the heterogeneities at an appropriate scale, provide geometric representation to fractures and stratigraphy, and determine the initial pressure distribution; (ii) develop a mathematical representation of water flow in the domain (the current concepts are based on mass conservation in a rigid, non-deforming, heterogeneous medium with water velocities sufficiently small that the inertia forces can be neglected); (iii) develop a computer based numerical model that implements the mathematical model; (iv) use site data and the numerical model to predict the pressure field which may either be transient (if episodic recharge is to be considered for example) or steady-state; (v) use an appropriate constitutive equation (generally the Darcy's equation although its applicability to extremely low permeability media is questionable), to determine the velocity field; and (vi) finally, use an appropriate procedure for tracking particle motion, to calculate travel times along various paths.

Several technical questions are inherent in the above approach. First, what is an appropriate scale for representing the heterogeneities? Both the pressure and the velocities derived from them depend upon this scale. Also, the effort for characterizing the site is directly dependent upon this scale. Second, how should smaller but important features, such as fractures, be accounted for in calculations? The usual equivalent porous media approximation is based on equivalence of Darcy fluxes and may be inappropriate for estimating particle travel times. That is, water flux is a quantity integrated over area, which is not true for travel time. This problem is also intimately connected to site characterization. For example, if fractures must be represented as discrete entities, then all fractures must be hydraulically characterized. That is, not only the fracture geometry must be determined, but also the *in situ* hydraulic properties of the fractures must be determined. Third, how should one convert the Eulerian velocities into Lagrangian particle velocities? Generally, the two are considered equivalent. A particle is assigned the Eulerian velocity at a location which is then held constant until another location is determined. Fourth, what mass, if any, should be associated with the water particle? Generally, the particle is assumed to have infinitesimal mass to avoid consideration of effects of particle size, but this assumption can lead to unrealistically small estimates of 'fastest' travel time. Finally, how does one verify and validate a model to assure that the travel time estimates are reasonable?

In a heterogeneous fractured-porous medium, there are numerous (in theory infinite) particle paths. The GWTT rule requires that the fastest path of likely radionuclide travel be identified and that the travel time associated with that path be calculated. In addition, the rule specifies the starting location of the particle to be the edge of a zone that encompasses the disturbances expected to be created by repository construction and waste emplacement. The end point for the particle is the boundary that defines the accessible environment.

The objective of work reported here was to investigate computational aspects of the GWTT that may help in resolving the technical issues discussed above. This work is ongoing and is expected to continue in FY93. Only the preliminary phase of the work is reported here which consists of three aspects of the computational problem: (i) calculation of disturbed zone, (ii) model complexities for unsaturated flow, and (iii) probabilistic methods for saturated flow.

1.3 REPORT ORGANIZATION

The material presented in Sections 2 to 4 form the main body of the report. In each of these sections, a different aspect of the computational problem is discussed.

In Section 2, an analysis of coupled heat and flow is presented that was aimed at defining the extent of the disturbed zone in the unsaturated zone. The disturbed zone is interpreted to mean that zone surrounding the repository in which the speed with which water moves may be enhanced because of repository construction and waste emplacement. This enhancement may be due to a modification in the hydraulic properties (e.g., hydraulic conductivity) or due to creation of forces (e.g., buoyancy) not present in the absence of the repository. This first analysis estimates the extent of the thermally disturbed zone for two cases: (i) "cool repository" (i.e., low areal power density); and (ii) "hot repository."

In Section 3, a deterministic analysis of water travel time through the unsaturated zone is presented that focuses on the effects of model complexity (i.e., spatial variation in unsaturated hydraulic conductivity and moisture retention functions). Transient, two-dimensional, unsaturated flow through a vertical cross section is modeled using data for the Las Cruces Trench experiment. Computations of water pathlines and travel times are presented and compared.

Section 4 describes a probabilistic analysis of travel times in a saturated porous medium. The Nearest Neighbor Model (NNM) is used to generate a three-dimensional representation of hydraulic conductivity as a spatially correlated stochastic field. Travel times are calculated for each random field which are then analyzed statistically, in a Monte Carlo fashion, to estimate probability distributions. In this way, the uncertainty in predicted GWTT is related to parameter variability, such as the standard deviation of the log-conductivity.

A summary of all the analyses including the conclusions and future questions is included in Section 5.

2 ANALYSIS OF THE DISTURBED ZONE OF A HIGH-LEVEL WASTE REPOSITORY IN RESPONSE TO DIFFERENT THERMAL LOADINGS

2.1 STATEMENT OF THE PROBLEM

In order to account for the potential disturbance due to the construction of the repository and subsequent emplacement of waste, the groundwater travel time (GWTT) rule in Code of Federal Regulations (CFR) 10 CFR 60.113 stipulates that the GWTT be calculated from the edge of a "disturbed zone" to the accessible environment boundary. Therefore, some volume of the host rock surrounding the repository is to be designated the disturbed zone for which credit is not to be taken during the estimation of GWTT. It may be noted that even though GWTT is required to be calculated for pre-waste-emplacement conditions only, because of the provision of a disturbed zone, the GWTT is considered a post-closure performance measure. In this sense, the disturbed zone should include all rock volume which is expected to experience disturbances impacting (presumably negatively) the GWTT. Such disturbance would include those that may change the hydraulic properties of the rock and those that would change the hydraulic gradient. Mechanical, chemical, and thermal effects of repository construction and waste emplacement can all modify hydrologic properties and/or hydraulic gradients in some volume of the rock surrounding the repository. The objective of this work is to study the relation of the disturbed zone to the presence of radiogenic heat.

There is an inherent difficulty in determining the extent of the disturbed zone, in that its extent is dependent upon the definition assigned to the disturbed zone. The definition of "disturbed zone" as stated in 10 CFR Part 60 is

> "Disturbed zone means that portion of the controlled area the physical or chemical properties of which have changed as a result of underground facility construction or as a result of heat generated by the emplaced radioactive wastes such that the resultant change of properties may have a significant effect on the performance of the geologic repository."

There is confusion in this definition in that the phrase "significant effect" does not have an unambiguous meaning. It is assumed that "significant effect" in this definition refers to effects that significantly alter repository performance in a negative way (e.g., increase cumulative release, reduce GWTT, and reduce containment period).

The temperature and moisture regimes of the geological setting of a high-level waste (HLW) repository will be affected by the thermal loading from waste decay heat. The degree to which these regimes will be affected is a function of the amount of heat emitted by the waste. The thermal loading of the repository, referred to as the areal power density (APD), which is most desirable to the performance of a repository is currently a subject of scrutiny.

A repository with a low APD is referred to as a "cool repository" in contrast to one with a high APD which is referred to as a "hot repository". In support of the case for a cool repository is the rationale that low temperature regimes are better understood and therefore the performance of a low APD

repository can be estimated with greater confidence (Eriksson, 1991). A low APD can be achieved by either aging the waste prior to emplacement or by configuring the waste packages at large distances.

Conversely, emplacement of younger waste or a closer configuration of canisters will lead to a higher APD. Such a condition is suggested to be advantageous for repository performance (Buscheck, 1991, Buscheck and Nitao, 1992) especially for unsaturated repositories as is the case at Yucca Mountain. According to this concept, an increased APD would create higher repository temperatures which would dry out the region proximal to the repository for long periods of time. This would isolate the waste container from liquid water for longer periods after emplacement, reducing potential for aqueous corrosion and also removing liquid transport pathways for contaminants. It may be worth noting that the current repository design for the Yucca Mountain site is based on a low APD (e.g., thermal loading of 57 kW/acre) (Site Characterization Plan, 1988).

The intent of this analysis is to investigate the effect of two different APDs upon the temperature and liquid saturation regimes at a hypothetical repository setting similar to Yucca Mountain. Particular emphasis is directed at assessing the effect of changes in the APD upon the extent of the "disturbed zone" as it is used in 10 CFR 60.113 as part of the GWTT rule.

2.2 TECHNICAL APPROACH

The numerical code, V-TOUGH (Pruess, 1987, and Nitao, 1989), was used to simulate the flow of water, air and heat through a partially-saturated porous medium as a means to assess the size and significance of the disturbed zone at a geologic HLW repository. A vertical grid, which was adapted to incorporate the geometrical nature of the repository, was used to represent a cross section with similarities to Yucca Mountain. Although data representative of Yucca Mountain were used where possible, the model did not accurately replicate processes present at that site. The intent of this analysis is to provide generic insight into the effect of different APDs upon the extent of the disturbed zone and not make predictions of processes at Yucca Mountain.

Additionally, sensitivities of temperature and liquid saturation regimes to rock matrix permeabilities were evaluated. These analyses were conducted using permeabilities greater than what are expected at the proposed repository horizon to enhance convection, because convection was small when published matrix permeability values were used in the model.

2.3 MODEL ASSUMPTIONS

The modeled domain was assumed to be homogeneous and isotropic. The hydrologic properties assigned to the medium were similar to those of the Topopah Springs welded tuff (Klavetter and Peters, 1986). Properties of both the fractures and the matrix were incorporated into the model through application of an equivalent composite medium (ECM)(Nitao, 1988). The ECM approach leads to a medium characteristic curve which is double valued (popularly known as double humped) at the point where the matrix and the fracture characteristic curves intersect. This can introduce large numerical instability in the solution of the flow equation.

As depicted in Figure 2-1, the model cross section was 2000 meters in the horizontal dimension and 580 meters in the vertical dimension. By assuming symmetry, the modeled cross section represented only one half of the repository. The numerical grid assumed cylindrical geometry and consisted of 1080

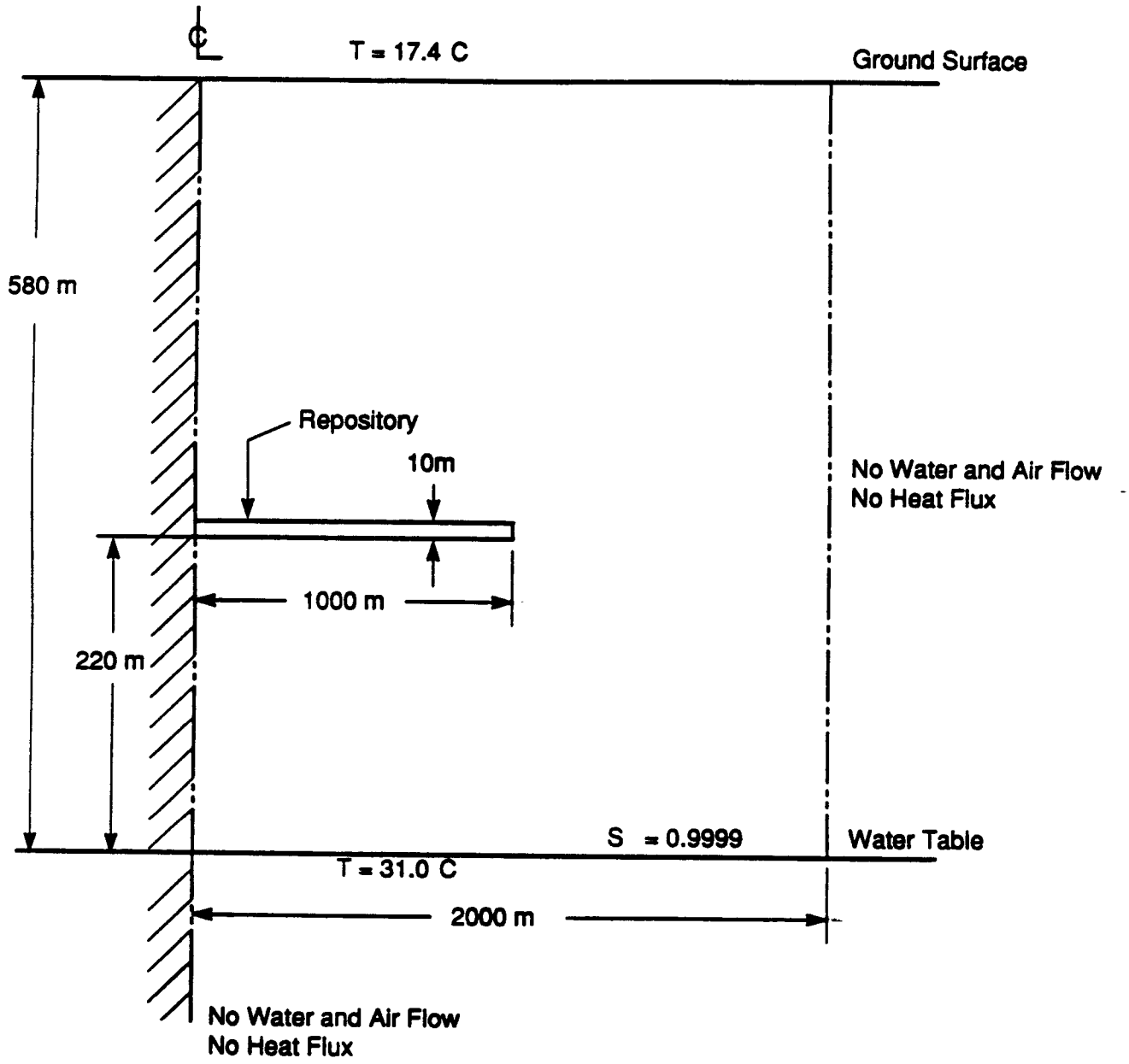

Figure 2-1. Model configuration

rectilinear elements with 24 in the vertical (z) dimension and 45 in the horizontal (x or radial) dimension. Although the cross section was only one element deep in the y-direction, the radial or cylindrical nature of the problem was incorporated into the model by increasing the y-dimension of the elements as the distance from the origin (center line of the repository) was increased. By incorporating this modification, a quasi-three-dimensional model was formulated to represent heat and water movement at the repository scale in cylindrical geometry.

The repository was modeled as a cylindrical disk with a radius of 1000 meters and a thickness of 10 meters. It was located 360 meters below the ground surface and 220 meters above the lower boundary which was the water table. The inner vertical boundary corresponded to the center line of the repository and was assigned zero fluxes of heat, air and water based on its symmetry. Constant temperatures were assigned to both the ground surface and water table boundaries. The bottom boundary was modeled as the water table by setting the liquid saturation at 0.9999. Water and air were permitted to cross both the upper and lower boundaries but no infiltrating water flux was introduced. The outer vertical boundary, located 2000 meters from the repository center line, was established to have no heat, air, or water flux.

A linear geothermal gradient of 23.5 K/km was imposed upon the model by maintaining the surface boundary at 17.4 C and the lower boundary at 31.0 C (Brandshaug, 1991). Initial liquid saturation gradient varied linearly from 50 percent at ground surface to 60 percent above the water table (Buscheck and Nitao, 1992). The heat load of the repository was established at two different values to examine the effect of these loads upon the temperature and liquid saturation regimes present at the repository. The two APDs evaluated in this analysis were 57 kW/acre (cool repository) and 114 kW/acre (hot repository).

For both APDs, the heat source was characterized with a thermal power decay source. This thermal power decay was representative of a 10-year old combination of 60 percent PWR spent fuel and 40 percent BWR spent fuel [Sandia National Laboratory (SNL), 1987] that was normalized and approximated by a piece-wise linear function (Brandshaug, 1991). Normalized thermal power coefficients used to define these linear segments are presented in Table 2.1 (Brandshaug, 1991).

This analysis incorporated media characteristics similar to those from Yucca Mountain, however, because this model was not fully representative of Yucca Mountain, the results are only meaningful in a qualitative sense at this time. Parameters used in these models were primarily selected from two documents, Klavetter and Peters (1986), and Nitao (1988). A summary of these values is presented in Table 2-2.

2.4 MODEL SIMULATIONS

Four sets of simulations were performed in this analysis. Water flow and heat transfer were simulated for two APDs at two matrix permeabilities. The APDs used in the simulations (57 and 114 kW/acre) were appropriate for a cool and a hot repository, respectively (Buscheck and Nitao, 1992). The two matrix permeabilities were 1.9 E-18 m^2 and 1.9 E-15 m^2. The latter permeability is greater than matrix permeabilities typically assigned to the Topopah Springs tuff, however, this set of simulations was performed to accentuate the effect of heat convection, since only heat conduction was observed in the simulations at matrix permeabilities of 1.9 E-18 m^2.

Table 2-1. Normalized thermal power decay (from Brandshaug, 1991)

Time (years)	Normalized Thermal Power
10	1.0000
20	0.7786
50	0.4763
100	0.2618
200	0.1488
500	0.0880
1,000	0.0515
2,000	0.0276
5,000	0.0178
10,000	0.0128

Each set of simulations has been graphically illustrated at three time intervals, 200, 500, and 1000 years. Figures 2-2 to 2-4 illustrate temperature at an APD of 57 kW/acre with a permeability of 1.9 E-18 m^2. Figures 2-5 to 2-7 illustrate liquid saturation for the same set of assumptions. Temperature and liquid saturation at an APD of 114 kW/acre at a permeability of 1.9 E-18 m^2 are similarly presented in Figures 2-8 to 2-13. Similar sets of simulations for APDs of 57 and 114 kw/acre and a matrix permeability of 1.9 E-15 m^2 are presented in Figures 2-14 to 2-25.

2.5 DISCUSSION OF RESULTS

A homogeneous medium, no surface recharge, and linear initial saturation gradient were integral assumptions in this analysis. As a result, initial liquid saturation at the repository depth was set at about 56 percent. The analysis by Buscheck and Nitao (1991) using a vertical one-dimensional steady-state ECM model for surface recharge fluxes of 0, 0.045, and 0.132 mm/yr resulted in predicted repository depth saturations of 68, 85, and 95 percent, respectively. Their model incorporated the properties of the various hydro-stratigraphic units. The Reference Information Base (RIB) indicates measured saturation at the 300 m level to be 60 percent $\pm$ 20 percent. Therefore, the initial saturation of 56 percent is within the range of observed data.

The assumption of a homogeneous medium and no infiltration detracts from a more representative saturation. However, since the intent of this analysis was to evaluate the extent of the

Table 2-2. List of property values

Definition	Value	Units
Matrix density	25800	kg/m^3
Matrix porosity	0.11	-
Fracture porosity	1.8E-3	-
Matrix permeability: Low estimate High estimate	 1.9E-18 1.9E-15	 m^2
Fracture permeability	1.0E-11	m^2
Specific heat of rock	840	J/kg-K
Thermal conductivity, dry	1.74	W/m-K
Thermal conductivity, wet	2.3	W/m-K
Gas pressure (ambient atmospheric pressure)	1.0E5	N/m^2
Gravitational acceleration	9.81	m/s^2
Matrix tortuosity (estimate)	0.5	-
Fracture tortuosity (estimate)	0.5	-
α, van Genuchten parameter, matrix	0.567E-02	1/m
β, van Genuchten parameter, matrix	1.798	-
α, van Genuchten parameter, fracture	1.2851	1/m
β, van Genuchten parameter, fracture	4.23	-

disturbed zone in the region proximal to the repository, the negative impact of these assumptions was minimum. The assumption of a constant temperature boundary at the surface is reasonable, since relatively short-term annual temperature fluctuations should only be detectable in the near surface. The assumption of constant temperature at the bottom boundary (water table), however, is more restrictive. Groundwater fluxes through the saturated zone are assumed to be sufficiently high to remove heat that could otherwise elevate the temperature of the water table.

Results of simulations with a permeability of 1.9 E-18 m^2 based upon use of the ECM were similar to simulations performed using a matrix-only characterization (not shown) of the medium. This similarity is explained by the fact that matrix water and air permeabilities were too small to permit significant water or water vapor movement during the time interval of interest.

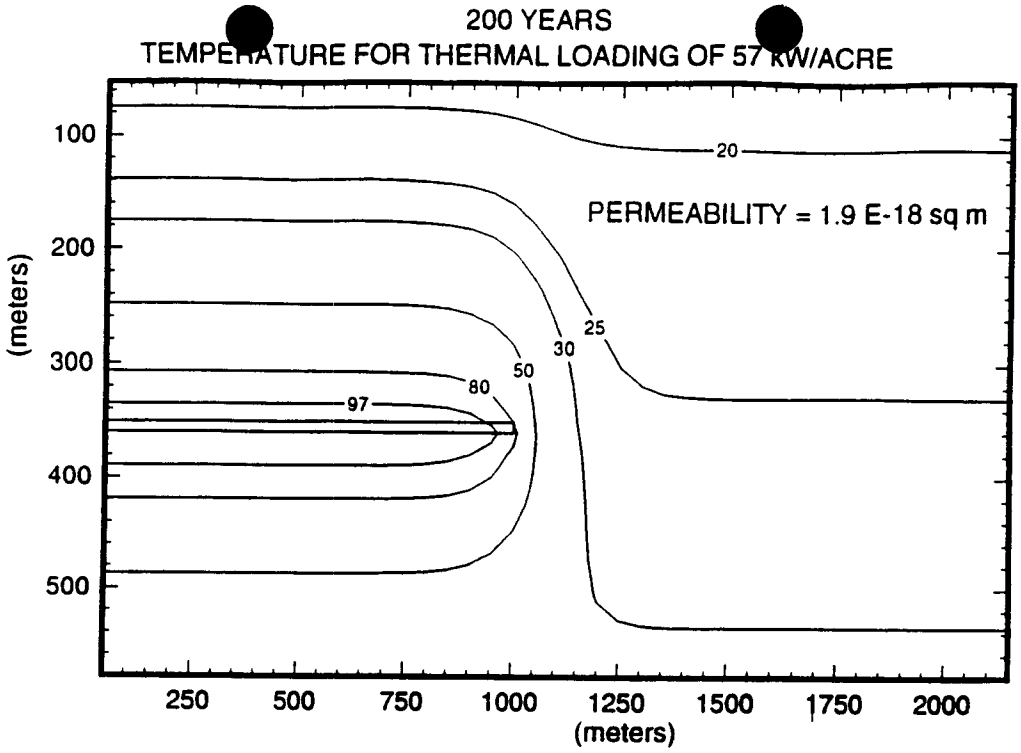

Figure 2-2. Temperature (°C) at 200 years with an APD of 57 kW/acre and a permeability of 1.9 E-18 m^2

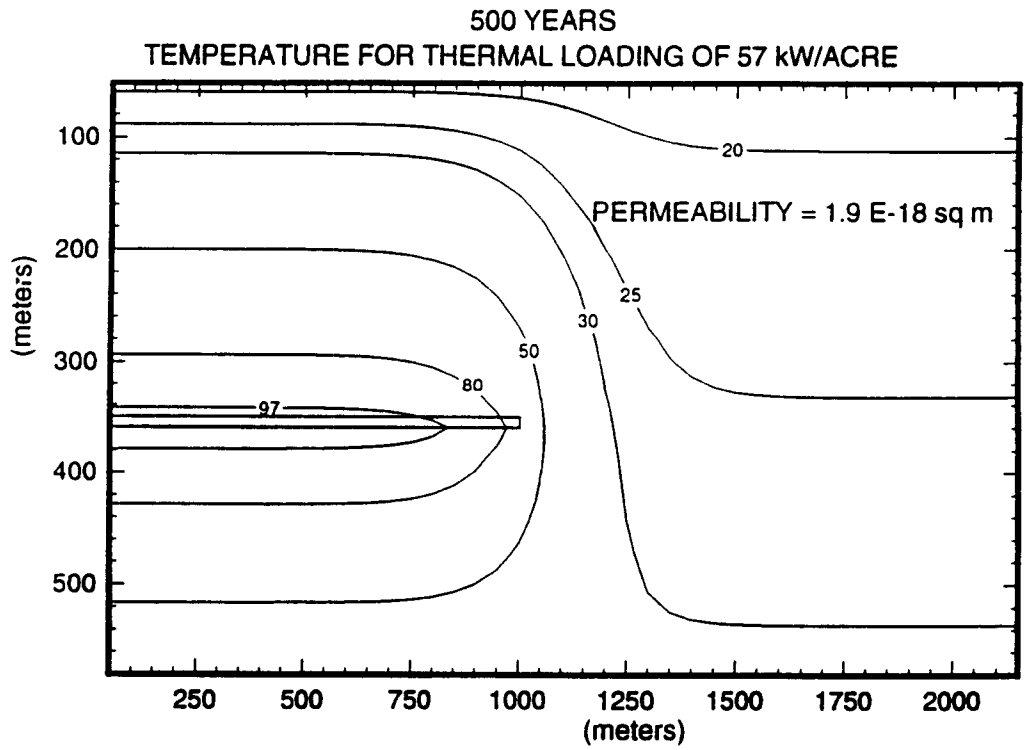

Figure 2-3. Temperature (°C) at 500 years with an APD of 57 kW/acre and a permeability of 1.9 E-18 m^2

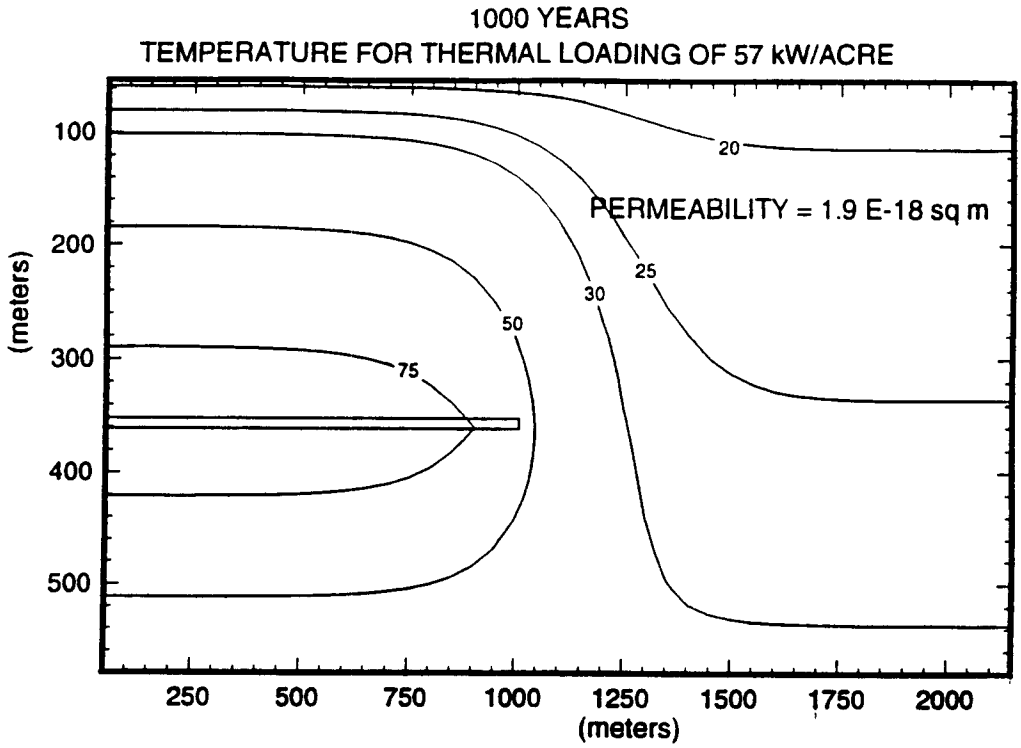

Figure 2-4. Temperature (°C) at 1000 years with an APD of 57 kW/acre and a permeability of 1.9 E-18 m²

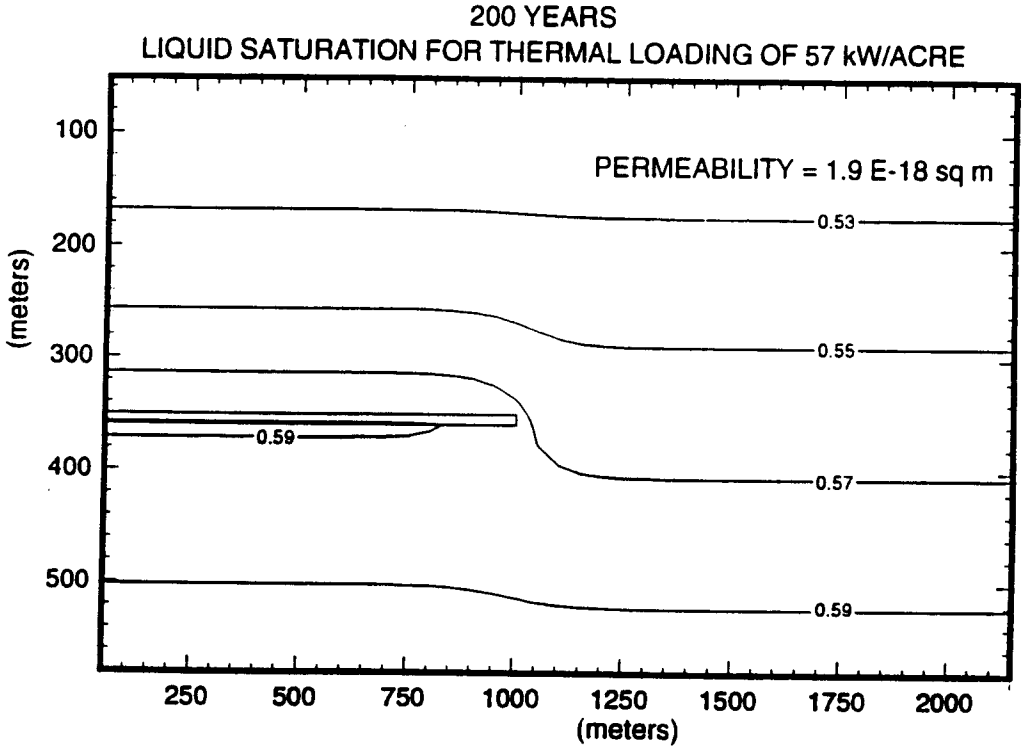

Figure 2-5. Liquid saturation at 200 years with an APD of 57 kW/acre and a permeability of 1.9 E-18 m²

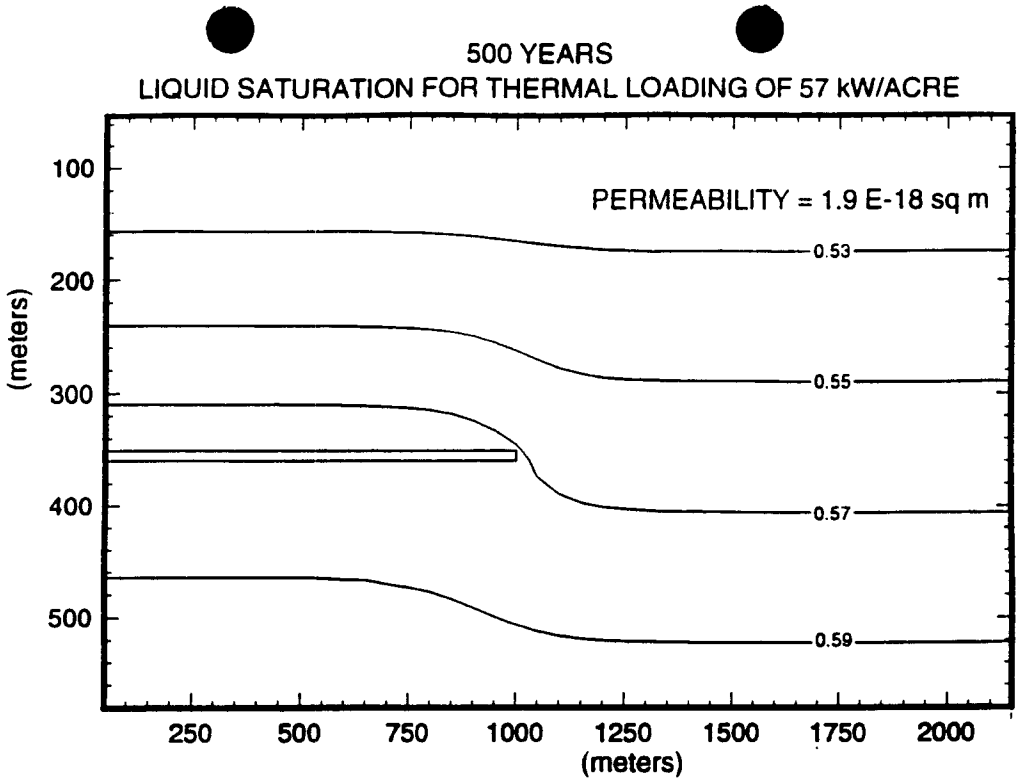

Figure 2-6. Liquid saturation at 500 years with an APD of 57 kW/acre and a permeability of 1.9 E-18 m²

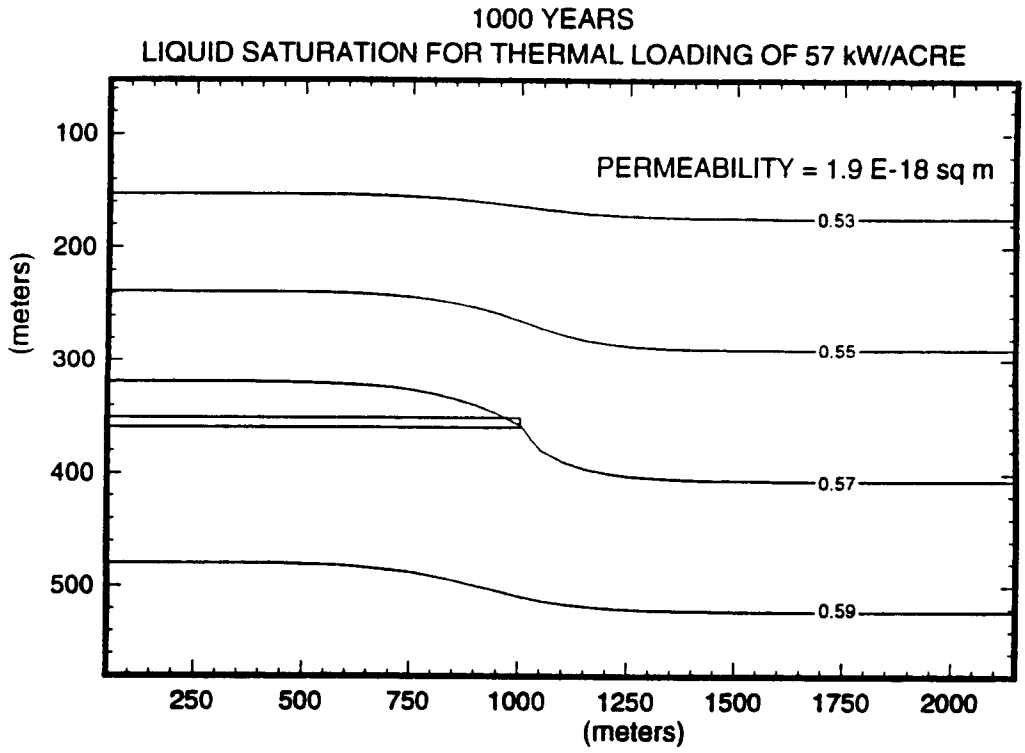

Figure 2-7. Liquid saturation at 1000 years with an APD of 57 kW/acre and a permeability of 1.9 E-18 m²

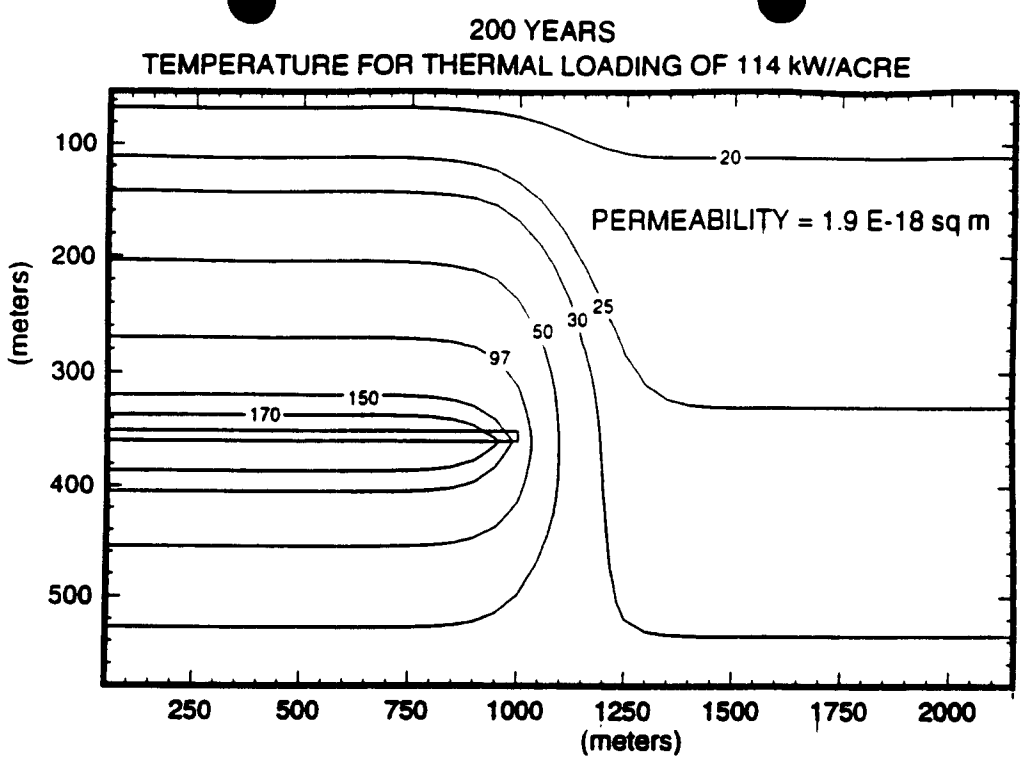

Figure 2-8. Temperature (°C) at 200 years with an APD of 114 kW/acre and a permeability of 1.9 E-18 m²

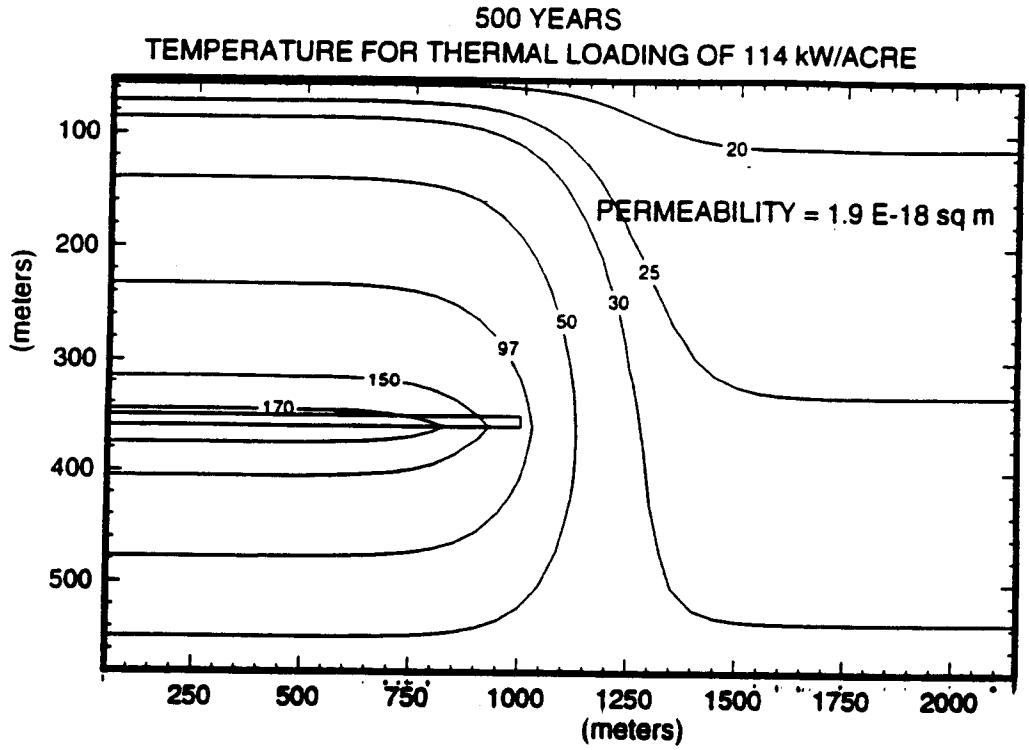

Figure 2-9. Temperature (°C) at 500 years with an APD of 114 kW/acre and a permeability of 1.9 E-18 m²

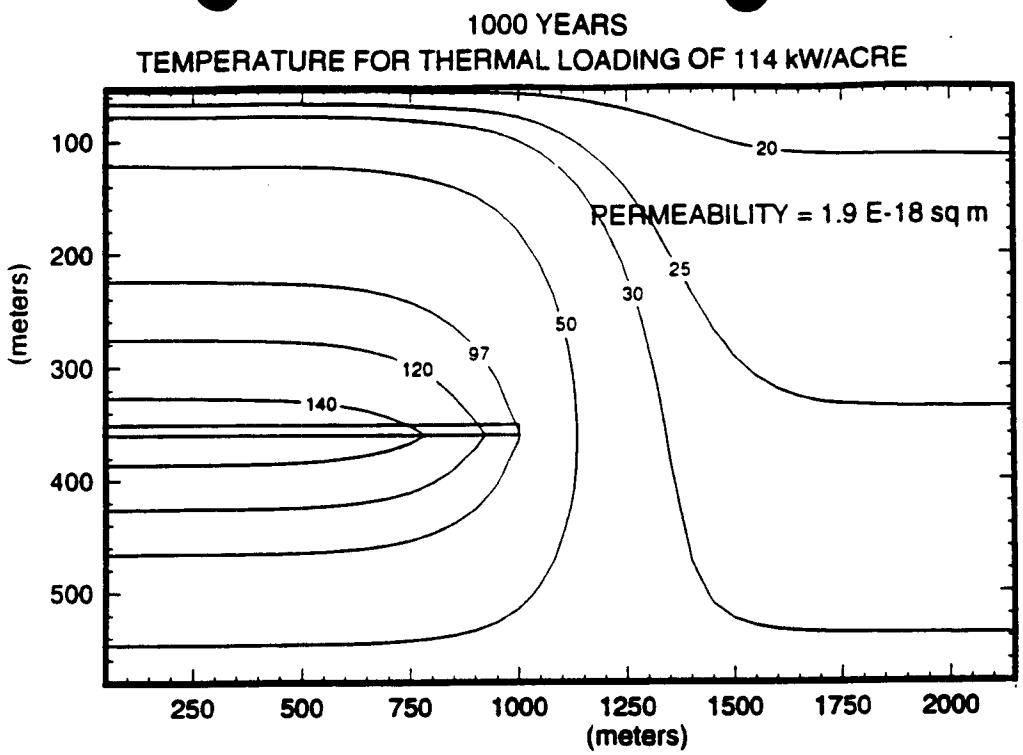

Figure 2-10. Temperature (°C) at 1000 years with an APD of 114 kW/acre and a permeability of 1.9 E-18 m²

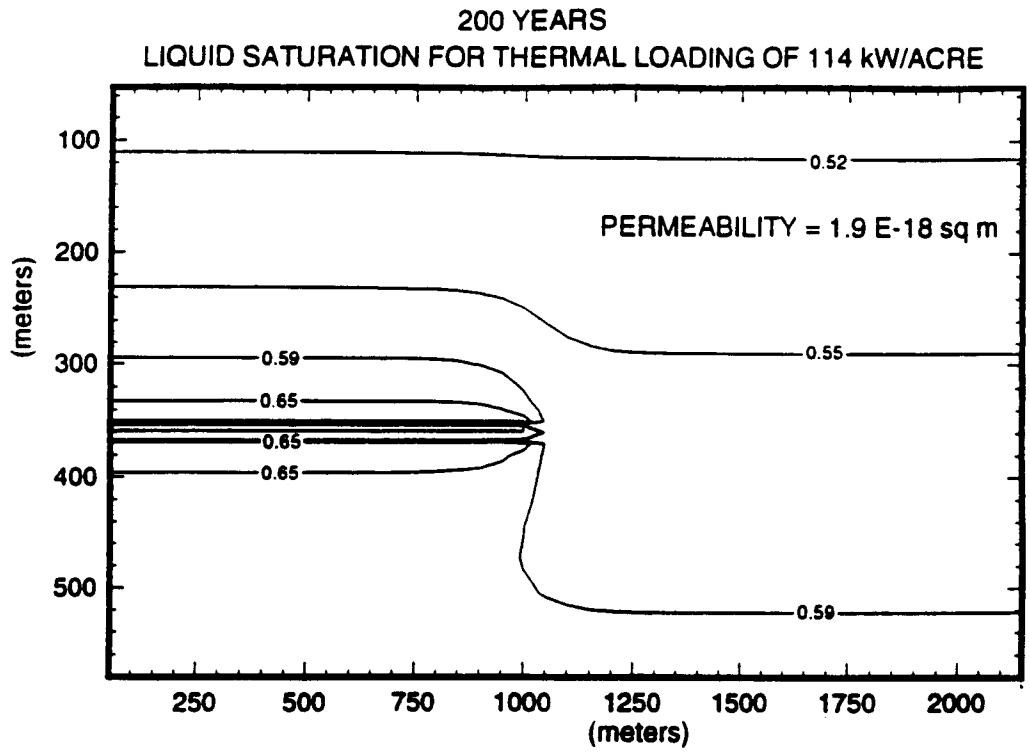

Figure 2-11. Liquid saturation at 200 years with an APD of 114 kW/acre and a permeability of 1.9 E-18 m²

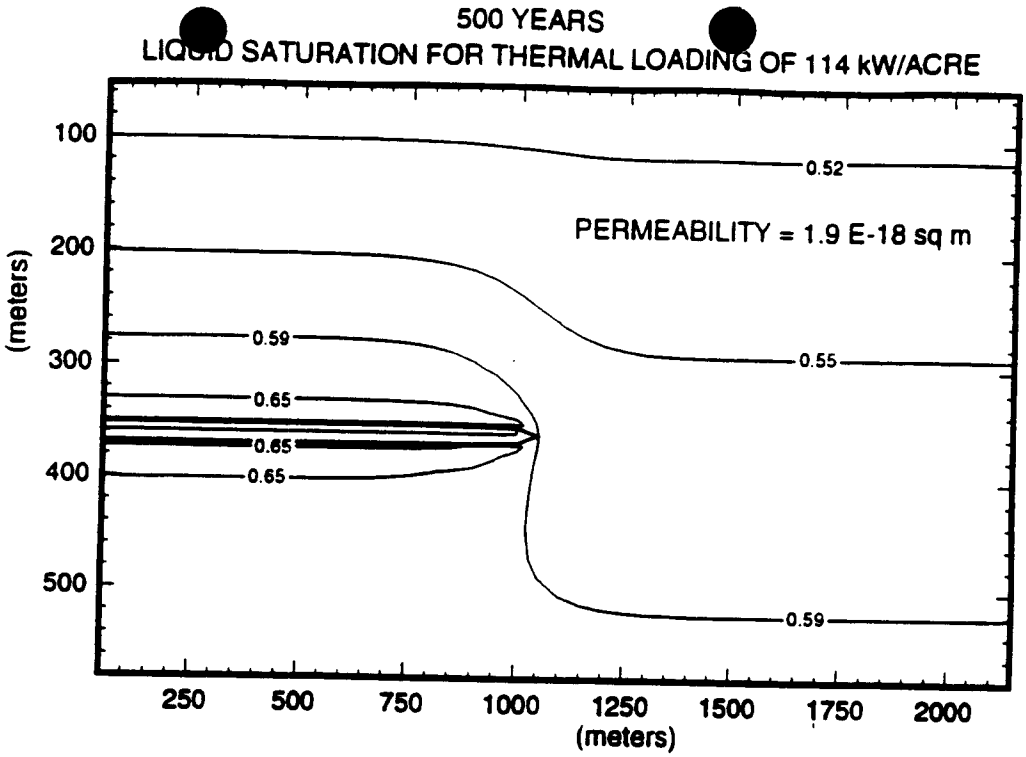

Figure 2-12. Liquid saturation at 500 years with an APD of 114 kW/acre and a permeability of 1.9 E-18 m²

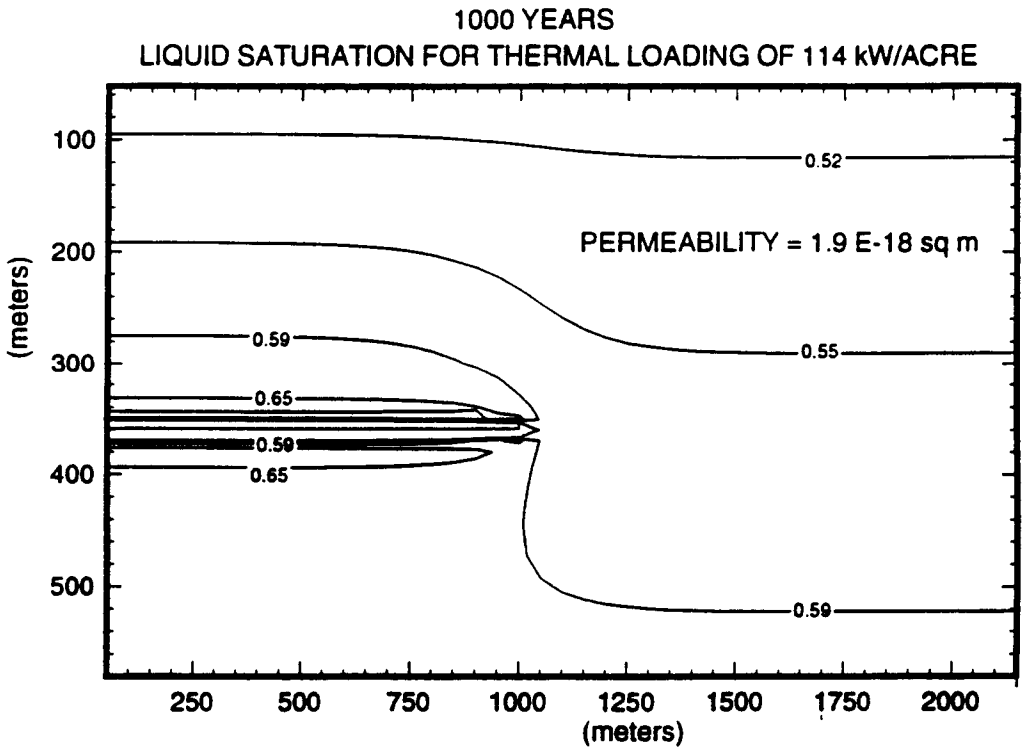

Figure 2-13. Liquid saturation at 1000 years with an APD of 114 kW/acre and a permeability of 1.9 E-18 m²

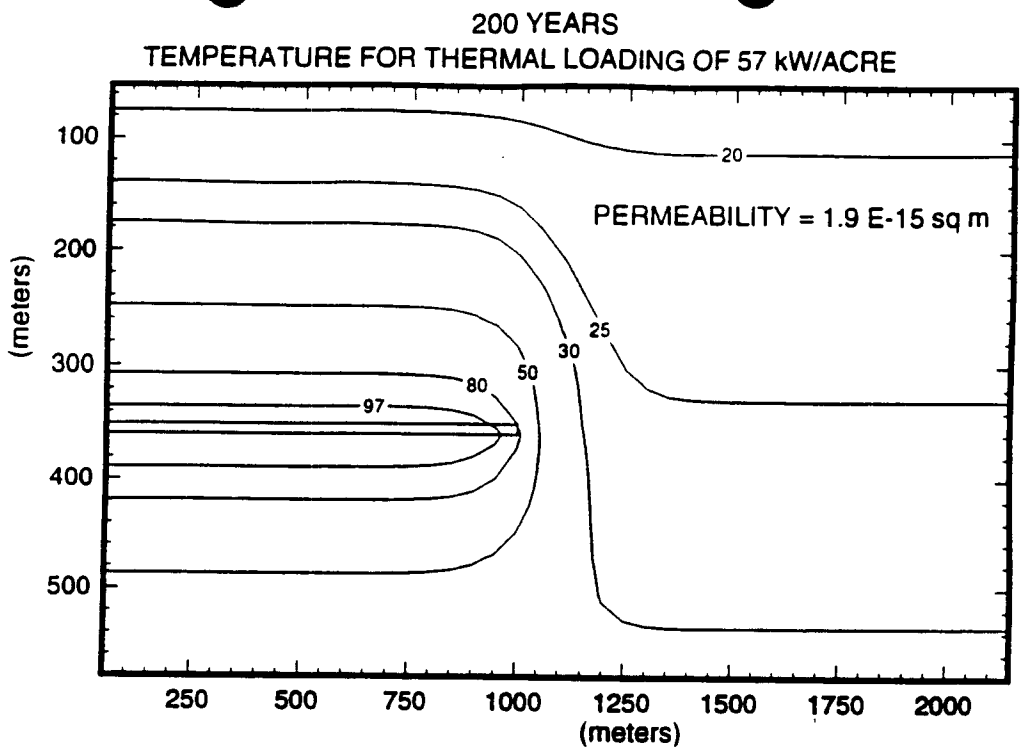

Figure 2-14. Temperature (°C) at 200 years with an APD of 57 kW/acre and a permeability of 1.9 E-15 m²

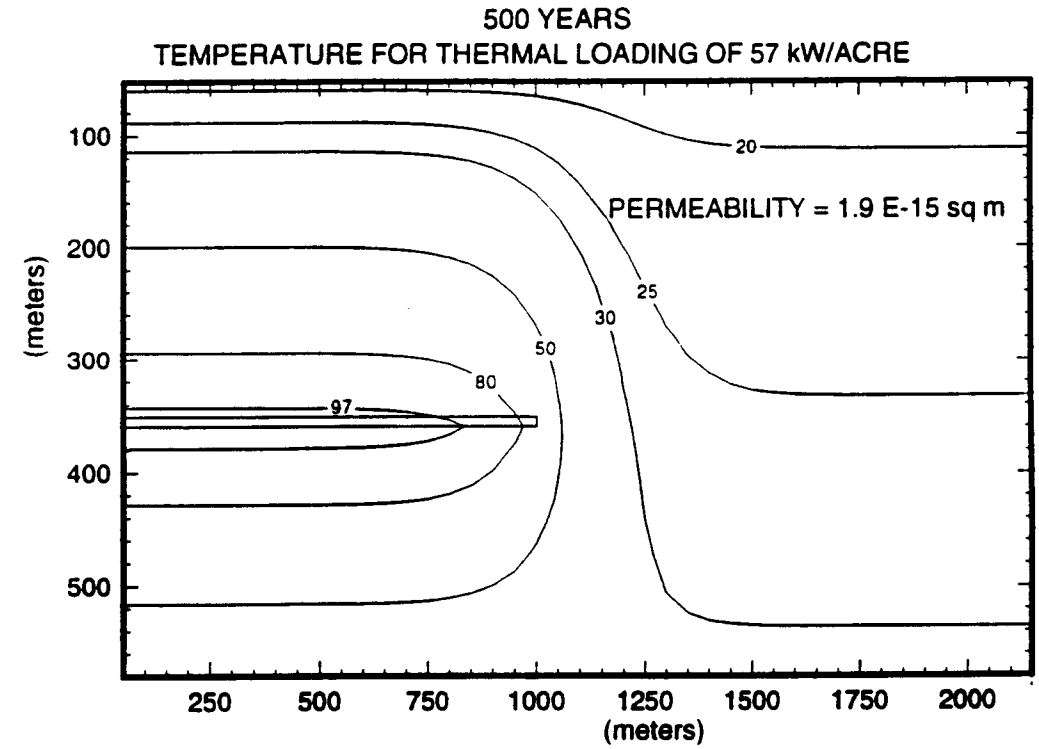

Figure 2-15. Temperature (°C) at 500 years with an APD of 57 kW/acre and a permeability of 1.9 E-15 m²

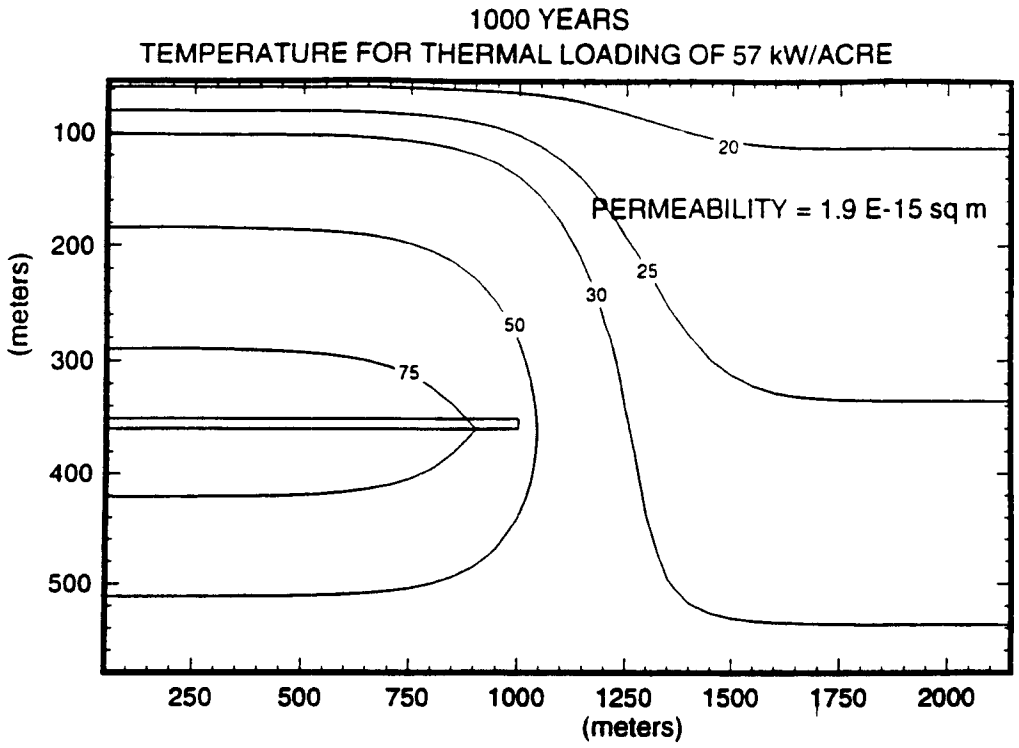

Figure 2-16. Temperature (°C) at 1000 years with an APD of 57 kW/acre and a permeability of 1.9 E-15 m²

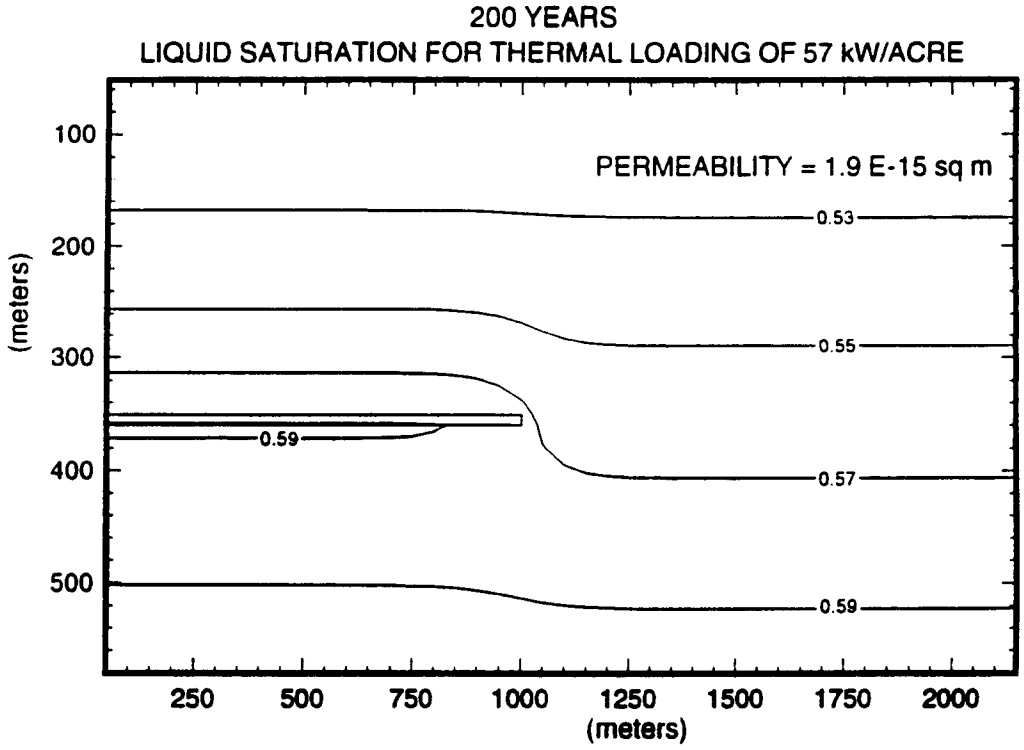

Figure 2-17. Liquid saturation at 200 years with an APD of 57 kW/acre and a permeability of 1.9 E-15 m²

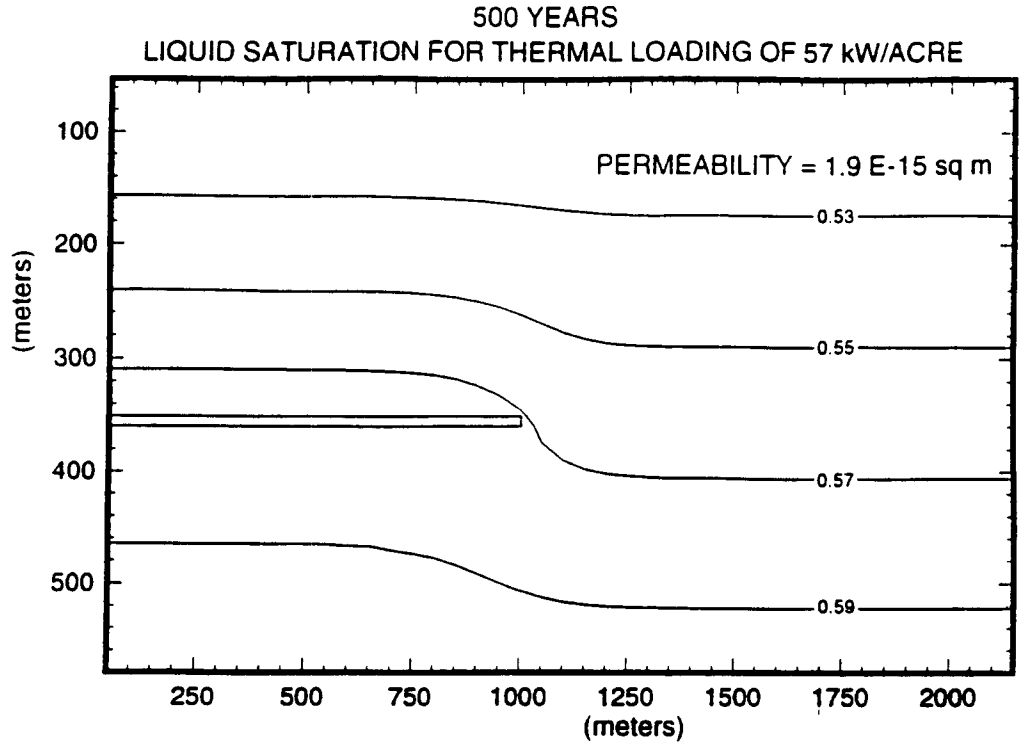

Figure 2-18. Liquid saturation at 500 years with an APD of 57 kW/acre and a permeability of 1.9 E-15 m²

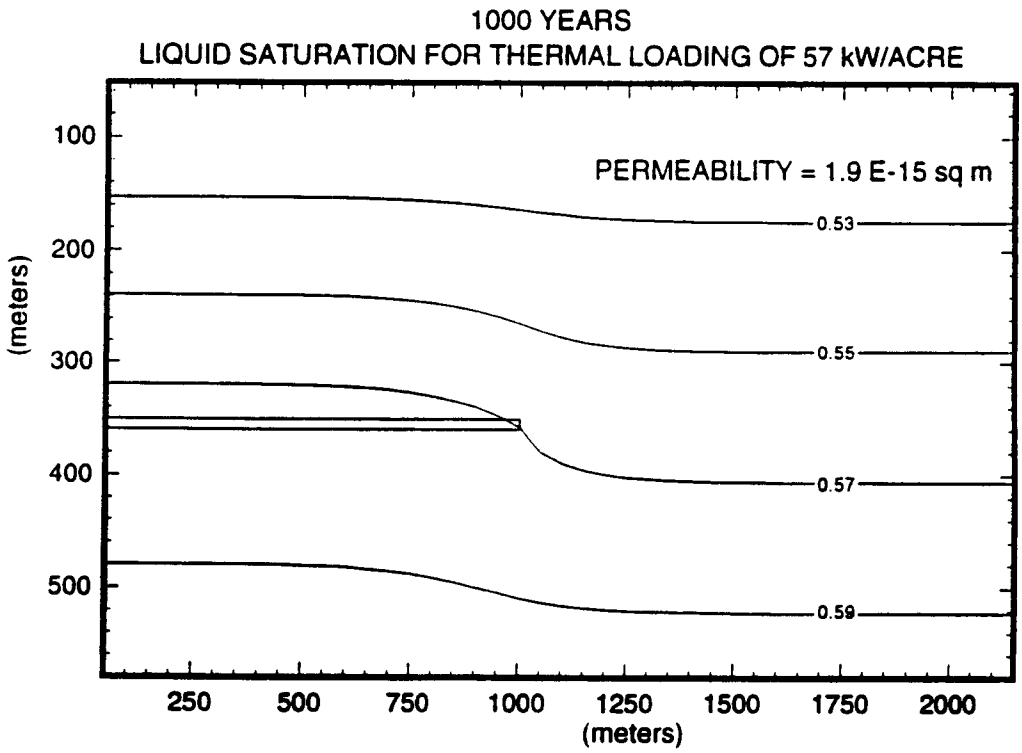

Figure 2-19. Liquid saturation at 1000 years with an APD of 57 kW/acre and a permeability of 1.9 E-15 m²

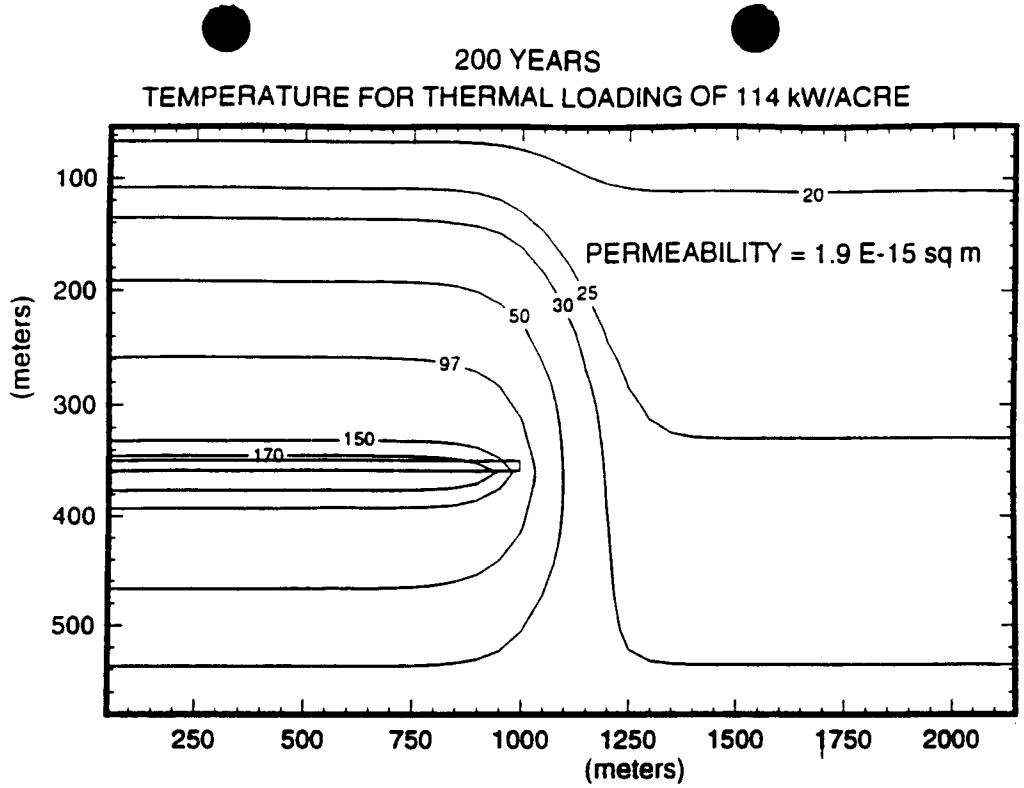

Figure 2-20. Temperature (°C) at 200 years with an APD of 114 kW/acre and a permeability of 1.9 E-15 m²

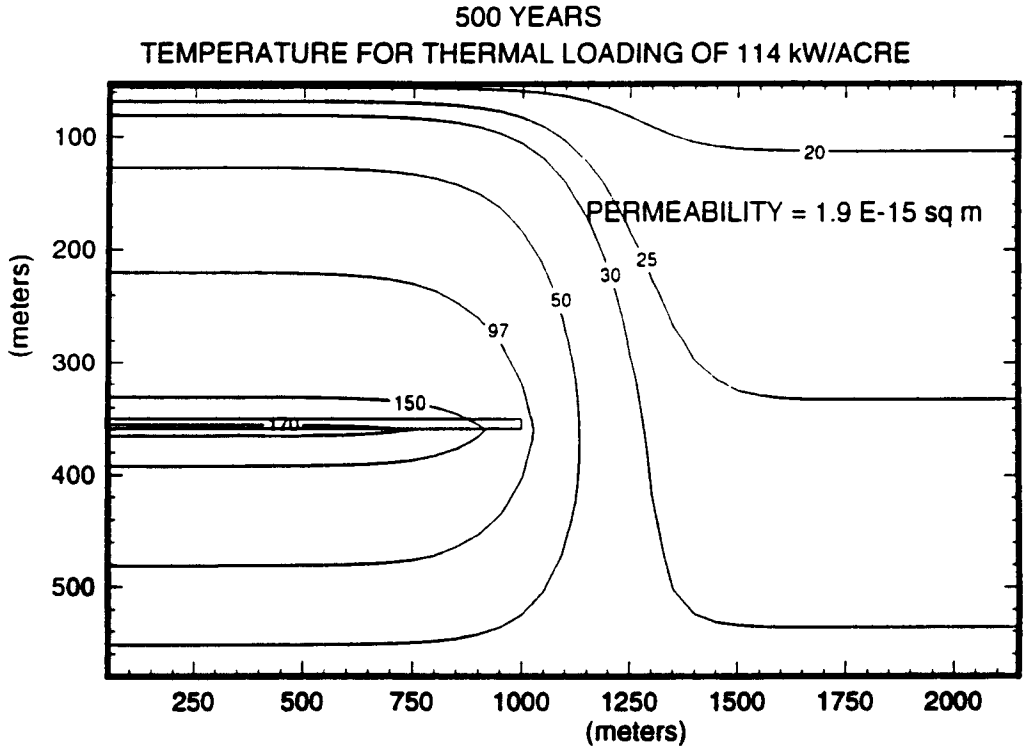

Figure 2-21. Temperature (°C) at 500 years with an APD of 114 kW/acre and a permeability of 1.9 E-15 m²

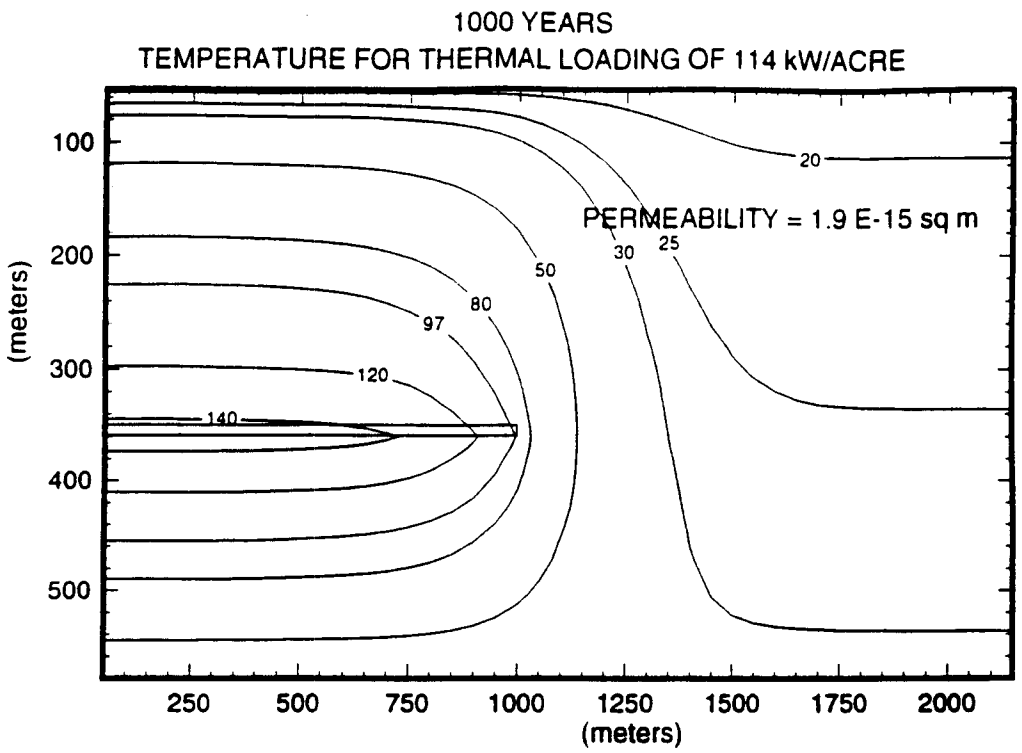

Figure 2-22. Temperature (°C) at 1000 years with an APD of 114 kW/acre and a permeability of 1.9 E-15 m²

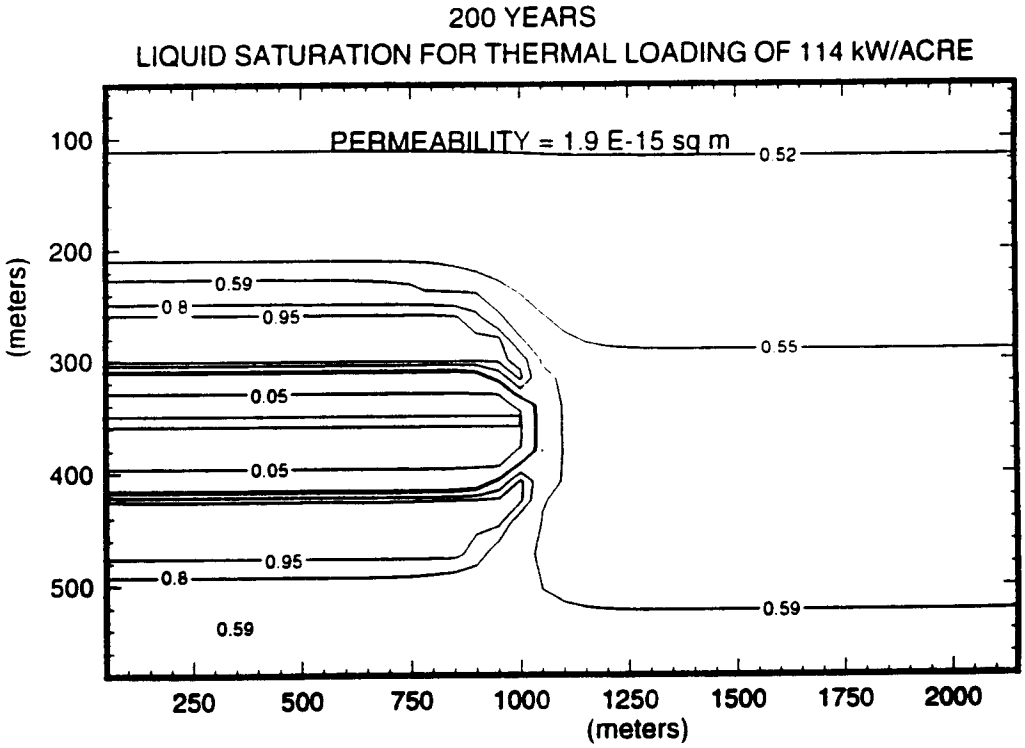

Figure 2-23. Liquid saturation at 200 years with an APD of 114 kW/acre and a permeability of 1.9 E-15 m²

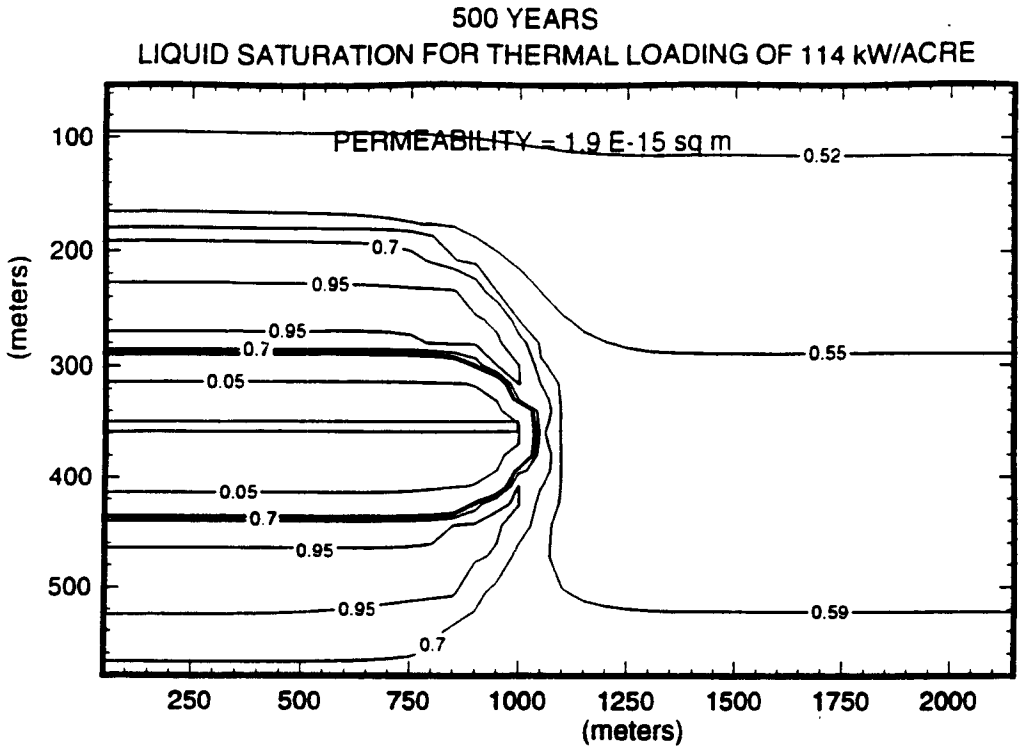

Figure 2-24. Liquid saturation at 500 years with an APD of 114 kW/acre and a permeability of 1.9 E-15 m²

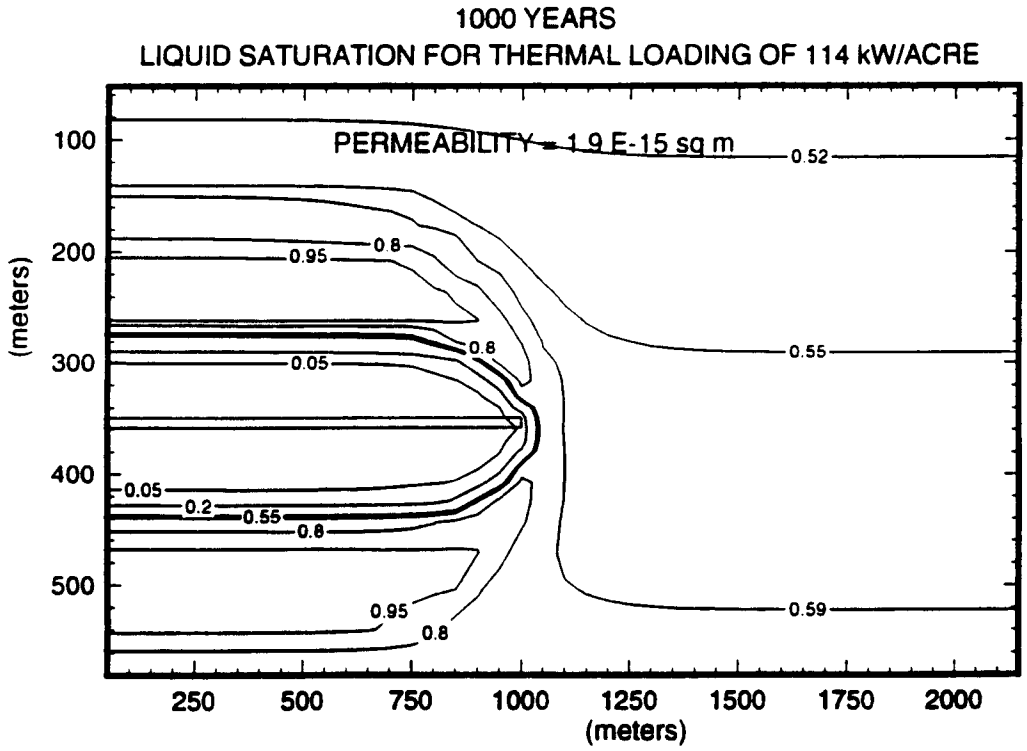

Figure 2-25. Liquid saturation at 1000 years with an APD of 114 kW/acre and a permeability of 1.9 E-15 m²

The temperature and liquid saturation regimes for an APD of 57 kW/acre in a model with a permeability of 1.9 E-18 m^2 are indistinguishable from the simulations predicated upon a model with a permeability of 1.9 E-15 m^2. This similarity is attributed to the observation that except for a zone close to the repository, the temperatures remained below boiling with the result that heat transfer occurred solely by conduction in both cases. However, for an APD of 114 kW/acre there were differences in temperatures between simulations based upon a permeability of 1.9 E-18 m^2 as compared to simulations assuming a permeability of 1.9 E-15 m^2, although the differences were not great. The basic trend of the thermal regime for both these cases appeared to be similar.

In general, at an APD of 114 kW/acre elevated temperatures were observed at greater distances from the repository for the test case with a high permeability relative to the test case with a low permeability. However, the core temperature at the repository was greater for the case with a lower permeability. The occurrence of convection in the test cases at an APD of 114 kW/acre with the greater permeability is suggested in the liquid saturation plots (Figures 2-22 to 2-25). Large dry zones enveloped by high saturation zones located above and below the repository are predicted for all three time intervals. Similar behavior is not observed in the simulations with less permeable media where minimal changes in saturation are observed.

For the purposes of this study, one measure of the extent of the disturbed zone is defined to be the contour where the temperature is 97 C, the boiling point of water at the repository level (Johnson and Montan, 1990). Whether increased temperatures in the repository region located in unsaturated regimes are deleterious to performance are debatable. Also note that boiling point will not be a suitable measure for saturated sites. A 97 C contour line has been included on the temperature figures. As illustrated, simulated temperatures for an APD of 57 kW/acre exceed the temperature for boiling (e.g., 97 C) only during early times and only within a short distance from the repository. The maximum distance where temperatures exceed 97 C is 20 meters above and 30 meters below the repository. As previously stated, there are no discernable differences between the simulations using different matrix permeabilities for an APD of 57 kW/acre.

The 97 C contours from simulations for an APD of 114 kW/acre were located at significantly greater distances from the repository. The extent of the 97 C contour was calculated to be 90 meters above and 105 meters below the repository for the media with higher permeability and 80 meters above and 95 meters below for the less permeable media, both at 200 years. Although the core temperature has decreased at later times, the extent of the 97 C contour increased to 125 meters above but decreased to 95 meters below the repository at 1000 years for the more permeable media. In the case of the less permeable media, the 97 C contour increased to 125 meters above the repository and 105 meters below the repository at 1000 years.

The lateral extent of the 97 C contour was less than the vertical extent in all cases. The 97 C contour did not extend beyond the outermost limit of the repository in any cases with an APD of 57 kW/acre nor during late time (e.g., 1000 years) with an APD loading of 114 kW/acre. During early times for both high and low permeabilities at an APD of 114 kW/acre the maximum extent of the 97 C contour beyond the limit of the repository was no greater than 40 meters.

The 97 C contour does not appear to be a conservative indicator for the extent of the disturbed zone in simulations of the more permeable material as illustrated in the plots of liquid saturation. In the simulations for an APD of 114 kW/acre, the extent of the zone with elevated saturation (i.e., 95 percent)

exceeds the extent of the 97 C contour by several tens of meters. Since significantly elevated saturations were not observed in the simulations based on the less permeable media, liquid saturation is not a reasonable indicator for the extent of the disturbed zone for less permeable media.

2.6 SUMMARY

A quantifiable measure of the extent of the disturbed zone of a HLW repository is required to determine the GWTT as currently written in 10 CFR Part 60. Numerical simulations have been conducted using VTOUGH (Pruess, 1987, and Nitao, 1988) to assess the extent of the disturbed zone in terms of the temperature and liquid saturation regimes at a geologic HLW repository. These simulations were performed for different thermal loadings and different assigned values of permeability.

Several observations can be made from this preliminary study. Increasing the thermal load of a repository from an APD of 57 to 114 kW/acre dramatically changes the temperature and liquid saturation regimes expected at a HLW repository. Temperatures at the repository exceed 140 C at 1000 years with an APD of 114 kW/acre as compared to temperatures no greater than 97 C for the same time with an APD of 57 kW/acre. Changes in liquid saturation were not as pronounced as changes in temperature. Liquid saturation at 1000 years for the higher APD exceeded 65 percent near the repository, while saturations were only slightly higher than the pre-existing level of about 57 percent observed at the lower APD.

Heuristic analysis of a model with a medium with high permeability (1.9 E-15 m^2) indicates that significant changes in liquid saturation could occur that would not be expected in a model with low permeability (1.9 E-18 m^2). The presence of highly saturated zones with associated dry-out zones above and below the repository persists beyond the time interval of interest in the GWTT rule (i.e., 1000 years).

Based upon these preliminary analyses, neither temperature nor liquid saturation can individually qualify as a conservative indicator of the disturbed zone. For example, the 97 C contour is not a good indicator of the extent of the disturbed zone. This is shown in simulations for a high APD and a high permeability. In this case, the extent of the zone (defined by the 95 percent saturation contour) exceeds the extent of the 97 C contour. Likewise, simulations predicated using a low permeability indicate that the extent of the 97 C contour exceeds the extent of the 95 percent contour. A more comprehensive indicator that includes both of these parameters possibly, in addition to other parameters, could provide better criteria to define the extent of the disturbed zone.

Efforts are ongoing to investigate the feasibility of an alternative parameter (or parameters) as an indicator of the extent of the disturbed zone. These studies will be performed in light of the fact that the disturbed zone could be defined to extend across the entire thickness of the unsaturated zone if the criteria includes a more rigid indicator (such as 1 or 5 C above ambient or the presence of buoyancy-driven gas flow). It is the objective of future studies to ascertain whether the disturbed zone is a quantitatively tenable concept.

3 MODEL COMPLEXITY AND GROUNDWATER TRAVEL TIME IN TRANSIENT UNSATURATED FLOW

3.1 STATEMENT OF THE PROBLEM

The central aim of this analysis was to examine the relationship between the distribution of groundwater travel times (GWTT) and mass fluxes, in a variably saturated medium, as a function of model complexity. As used here, model complexity refers to the conceptual representation of the heterogeneous hydraulic properties of the medium. The dual hydraulic behavior of a fractured-porous matrix was assumed to be described by the "double-hump curve" (Klavetter and Peters, 1986).

An initial effort was made to perform computer simulations of variably-saturated flow in a hydrostratigraphic description similar to that of the Yucca Mountain site. Applications of the PORFLOW code to model steady flow in that case were unsuccessful in producing convergent steady-state simulations. These problems did not appear to be resolved by simple grid refinement. Difficulties with obtaining convergent solutions for the steady-state case have been encountered by other researchers and is generally attributed to the strongly nonlinear nature of the governing equations.

Rather than devote significant effort to correct the problems with the simulation, it was decided to pursue a different hydrostratigraphic setting. Because of its data availability, the Las Cruces Trench Plot 2B site was selected. In addition, the focus of the analysis was narrowed to consider the relations between: (i) the distribution of travel times and model complexity; and (ii) the fastest particle trajectory and the model complexity.

A preliminary attempt was made to ascertain the effects on GWTT distributions of model complexity and the manner in which site characterization data are incorporated into numerical models. This study makes use of previously developed models of the Plot 2b experiment at the Las Cruces Trench site which have been reported on extensively in previous reports on the Center for Nuclear Waste Regulatory Analyses's (CNWRA) effort to develop a model validation methodology (Wittmeyer and Sagar, 1992). The Las Cruces Trench experiment's abundance of site characterization data, including extensive water content measurements obtained during the infiltration experiment, as well as water retention curves and saturated hydraulic conductivities for over 600 soil samples, makes it ideal for testing the effect of data on GWTT distributions. The following approach was followed to address this issue:

- Generate the hydraulic conductivity field by determining the soil hydraulic parameters by punctual kriging, or by assigning uniform properties on a layer-by-layer basis.
- Solve the steady-state variably saturated flow problem with no flow boundary conditions at the top and sides, and gravity drainage at the bottom.
- Use the results from the previous step as initial conditions for transient variably saturated flow problem with a consistent flux boundary condition at the top.
- Perform particle tracking computations with the flow fields obtained from the previous step.
- Plot and analyze pathline and travel times for each particle, and compare to analytical solutions.

3.2 MODEL DESCRIPTION

Three conceptual models were constructed of flow through a two-dimensional (2D) vertical transect at the Las Cruces Trench experiment. These models differ from each other only in terms of the manner in which the spatial structure of the soil hydraulic properties were described. The van Genuchten-Mualem model (van Genuchten, 1980) was used to describe the water retention characteristics and unsaturated hydraulic conductivity of the soil. For each of the three models, the parameters of the van Genuchten function were determined by fitting to the water retention data using a constrained nonlinear least squares procedure. The least complex model, designated Model A, consisted of nine horizontal layers, corresponding to the nine distinct soil horizons identified at the site, in which the soil hydraulic model parameters were assumed constant. Models B and C were more complex and consisted of 121 and 3621 rectangular zones, respectively. Within each rectangular zone, the soil hydraulic model parameters were determined by punctual kriging with an exponential semi-variogram. The soil hydraulic property zonation of Models B and C were based on 11 $\times$ 11 and 51 $\times$ 71 rectilinear blocks, respectively.

The variably saturated flow and solute and energy transport modeling program PORFLOW (Runchal and Sagar, 1992) was used to perform a series of transient simulations of unsaturated flow. PORFLOW is an integrated finite difference based code whose three-dimensional (3D) computational mesh is automatically constructed on a rectilinear grid. The computational mesh used for the 3621-zone model, is shown in Figure 3-1. It consisted of 81 nodes in the horizontal direction, 97 nodes in the vertical direction, and 3 nodes normal to the vertical plane. The mesh was increasingly refined towards the center and top of the domain to accommodate the large pressure head gradients expected to occur at early time directly below the strip source. Boundary conditions were everywhere defined to be no-flow, except at the bottom of the model and at the 1.2 m horizontal portion at the top where the strip source is located. To simulate gravity drainage, a negative pressure head gradient of unit magnitude was specified at the bottom of the domain. At the strip source, the boundary condition was prescribed flow type set equal to 1.82 cm/day during the first 150 days of simulation and zero thereafter. Initial conditions were obtained from steady state simulations with no flow boundary conditions specified at the top and sides, and gravity drainage specified at the bottom. Steady state initial conditions were used to minimize the effects of moisture redistribution below the wetting front. Each simulation was run for 500 days.

3.3 PARTICLE TRACKING

The 1.2 meter breadth of the strip source depicted at the top of Figure 3-1 was used to represent the lateral extent of the potential solute release zone. One hundred particles were positioned along the base of the strip source so that their spacing was uniform and released at time zero. Inasmuch as the approach used here assumed that the flow field was fully characterized by the spatial structure of the soil hydraulic data, the only source of uncertainty associated with the trajectory of a particle from the strip source to a specified compliance plane was caused by the uncertainty as to where along the strip the particle is released. A total of seven compliance boundaries (at depths of 50, 100, 200, 300, 400, 500, and 600 cm) was incorporated into the model. Figures 3-2, 3-3, and 3-4 show the pathlines traced by each of the 100 particles over the 500 day simulation period for Models A, B, and C, respectively. Note that since the flow regime was not steady, these pathlines are not streamlines and thus the particle trajectories may intersect one another. For all models, the particle trajectories were truncated when they intersected the compliance plane located 600 cm below the strip source. Increasing the model complexity

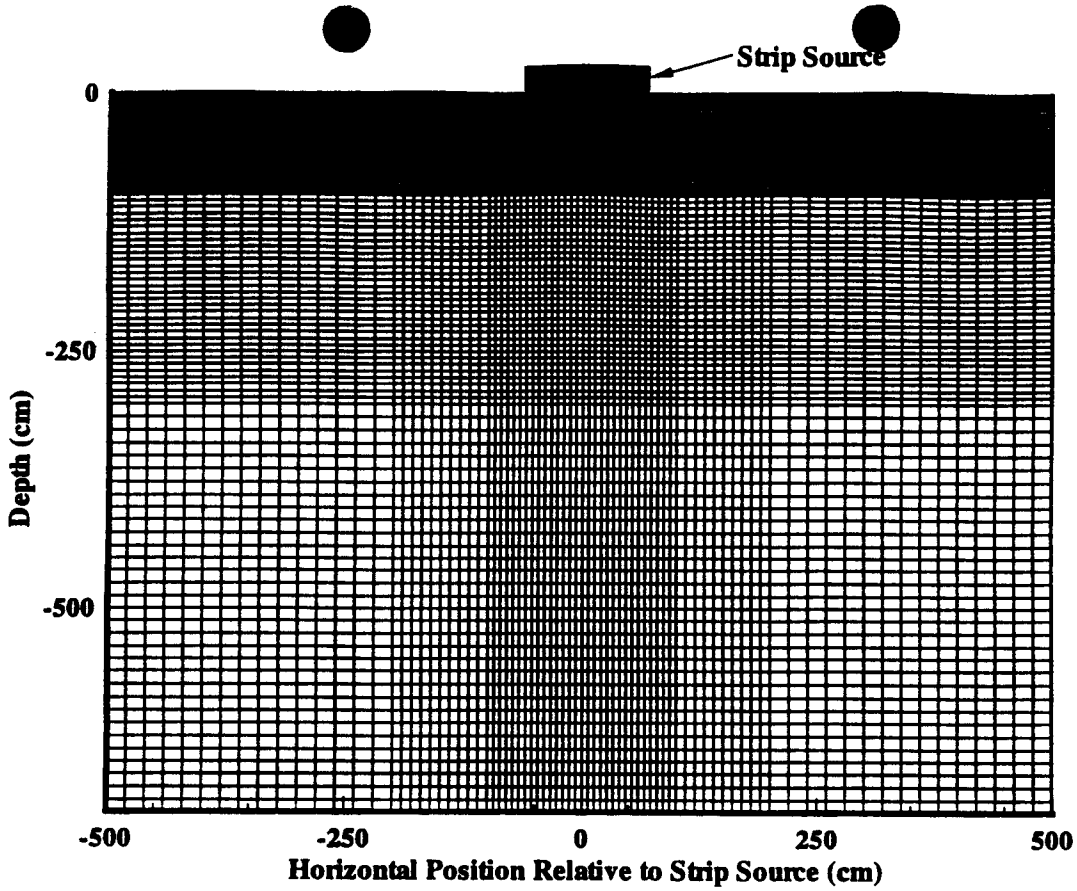

Figure 3-1. Finite difference mesh used in the 3621-zone model

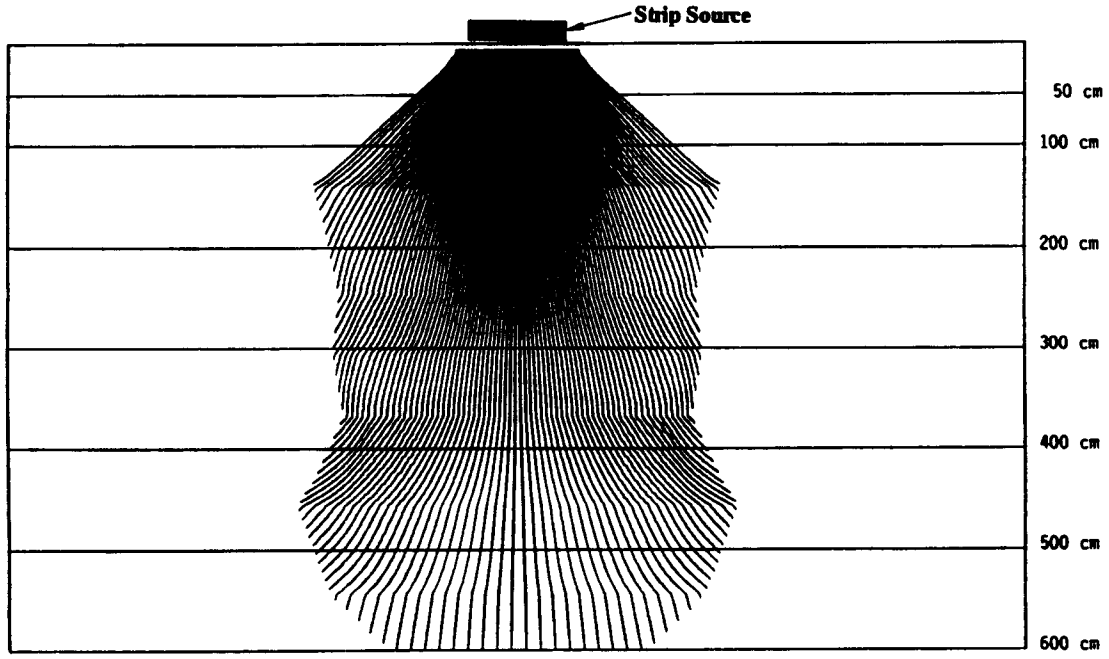

Figure 3-2. Pathlines of 100 particles for 500 days of simulation: Model A (nine horizontal layers of distinct hydraulic properties)

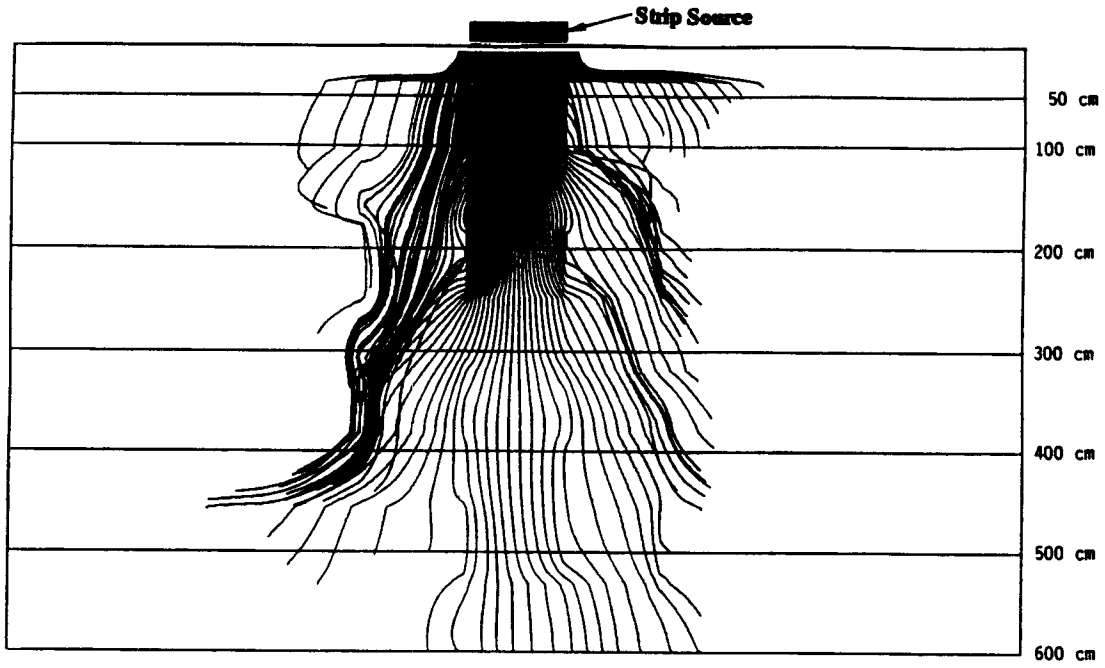

Figure 3-3. Pathlines of 100 particles for 500 days of simulation: Model B (121 zones of distinct hydraulic properties

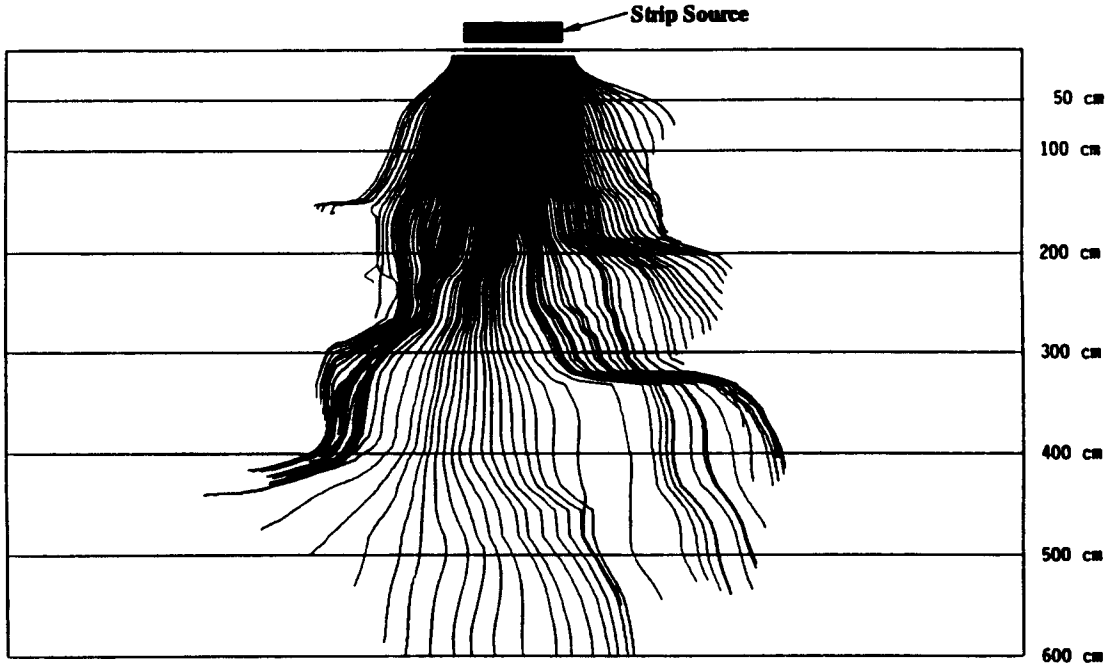

Figure 3-4. Pathlines of 100 particles for 500 days of simulation: Model C (3621 zones of distinct hydraulic properties)

clearly affects the pattern of the particle trajectories, with the layered soil model (Model A) showing the greatest uniformity in trajectories with no pathline intersections.

The trajectory of each particle is given by the kinematic relationship

$$V_l(t) = \frac{dX_l(t; X_0, t_0)}{dt} \tag{3-1}$$

where X_0 is the location of particle l at time t_0, V_l is the particle velocity, and X_l is the particle location. Owing solely to the uncertainty in the initial position of the fastest particle trajectory, the travel time from the source to any given compliance plane is uncertain. The particle locations, X_l, for $l = 1, \ldots, 100$, at times, $t = 1, 5, 10, 25, 50, 100, 150, 200, 300$, and 500 days are shown for Models A, B, and C in Figures 3-5, 3-6, and 3-7, respectively. For Model A, the snapshots of particle positions show great spatial uniformity, although the limbs of the particle fronts are bent as the wetting front advances through different soil layers. At early times ($t < 50$ days), Models B and C still present fairly well-formed, contiguous particle fronts in the center of the flow field. However, at all times on the lateral margins of the central portion of the flow field, and at later times in all regions of the flow field, the snapshots of particle positions for Models B and C reflect the effects of spatial heterogeneity in the velocity field.

3.4 GROUNDWATER TRAVEL TIMES

The travel time of a particle advected through a steady state, but nonuniform velocity field is readily computed from

$$\tau(X_l) = \int_{X_0}^{X_p} \frac{dx}{V(x)}, \tag{3-2}$$

where X_p is the position of the compliance plane, X_0 is the initial position of the particle and τ is the travel time. For transient, nonuniform velocity fields, the implicit dependence of particle position on time must be accounted for and Eq. (3-2) re-written

$$\tau(X_l) = \int_{X_0}^{X_p} \frac{dx}{V[x(t)]}. \tag{3-3}$$

The time at which the first of the 100 released particles reached a specified depth or compliance plane was determined by searching each of the particle trajectory files produced by PORFLOW. These first arrival times are shown in Figure 3-8 for all three models. The plots of first arrival times shown in this figure are surprisingly similar. For the first 300 cm of depth, Model C produced slightly shorter times and Model A slightly longer, while Model B's results were generally in between. At depths greater than 300 cm the results of first arrival times do not distinguish among the models on the basis of model complexity as defined here. Failure to observe (at greater depths) the tendency for the most complex models to produce the shortest travel times within the upper 300 cm may be due to the transient effects of the abrupt cutoff of infiltrating water after 150 days. One might expect that with the increase in the complexity of the model's structure the likelihood of fast paths through the flow field is increased and thus, under saturated steady flow conditions, the shortest travel times would occur in the most complex models. However, in unsaturated flow (especially under transient conditions) the moisture dependent anisotropy (Ababou, 1991) may yield more tortuous paths and, therefore, greater travel times.

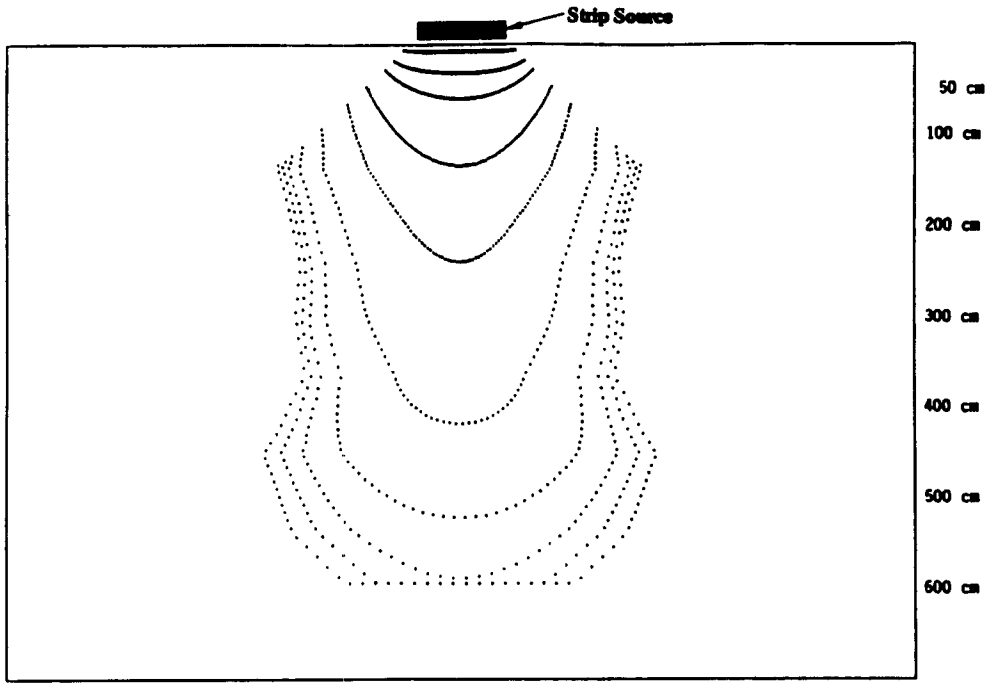

Figure 3-5. Particle locations at day 1, 5, 10, 25, 50, 100, 150, 200, 300, and 500 from top to bottom, respectively: Model A (nine horizontal layers of distinct hydraulic properties)

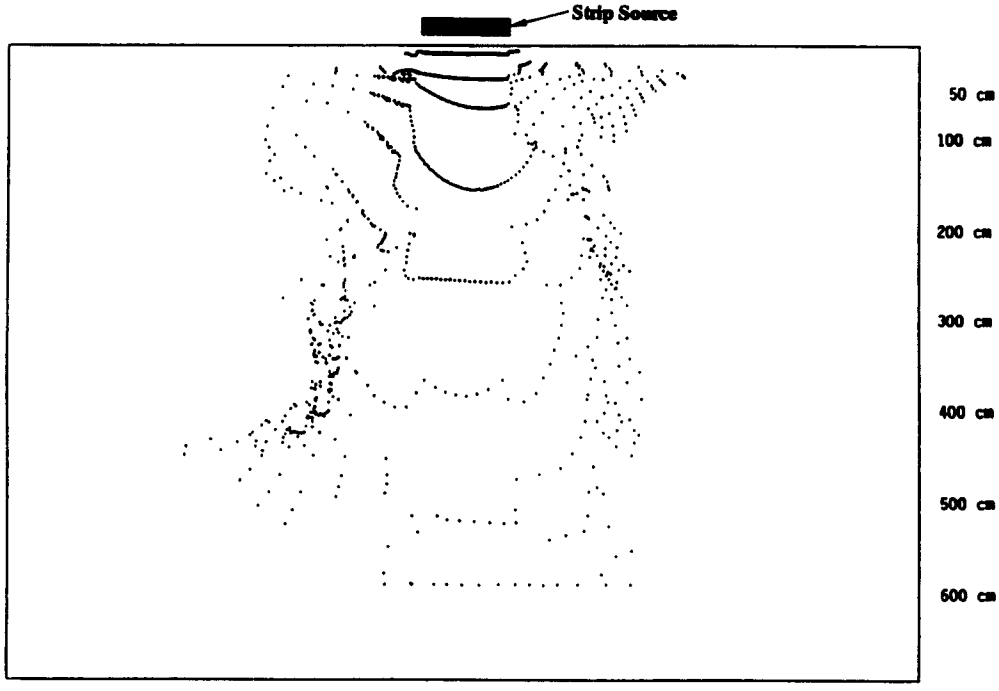

Figure 3-6. Particle locations at day 1, 50, 10, 25, 50, 100, 150, 200, 300, and 500 from top to bottom, respectively: Model B (121 zones of distinct hydraulic properties)

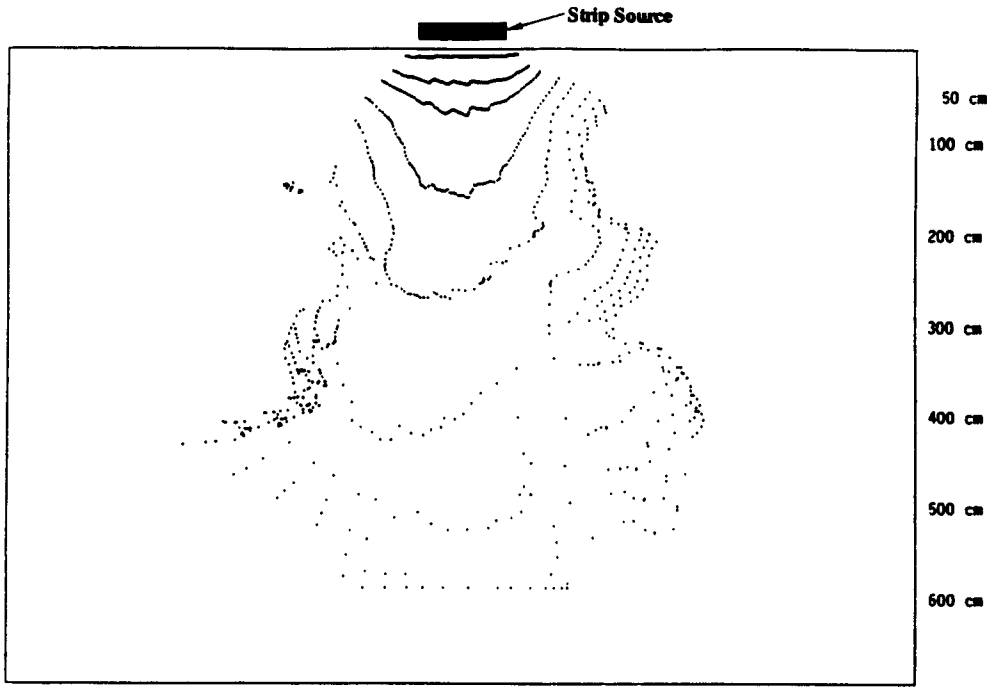

Figure 3-7. Particle locations at day 1, 5, 10, 25, 50, 100, 150, 200, 300, and 500 from top to bottom, respectively: Model C (3621 zones of distinct hydraulic properties)

3.5 DISCUSSION OF RESULTS

The variance of particle travel times to compliance planes located from depths 10 to 600 cm are shown for the three models in Figure 3-9. Note that variance is presented on a logarithmic scale to cover the eight orders of magnitude variation in this measure. Between depths of 200 to 400 cm, the variance of travel times for all models appears to reach a constant value between 2500 and 7000 days^2. As might be expected, the least complex model exhibits the smallest travel time variance in the uppermost 120 cm of the vertical domain. Moreover, the travel time variance for Model A shows a smooth, logarithmic increase in variance with depth within the first 120 cm. However, Model B shows greater travel time variance within the first 120 cm of depth than does Model C.

The degree of heterogeneity, inherent in each model, is directly affecting the dimensionality of the flow regime and thus, the travel time estimate. At greater depths, where the large scale variability of the domain is sampled, all three models yield approximately the same variance in travel time. However, at smaller depths the degree of heterogeneity, closely related to the tortuosity of the pathlines, renders Model C to correspond to a more uniform travel time distribution than Model B. Both, as expected, yield greater travel time variances than Model A. The fact that Model B is less complex than

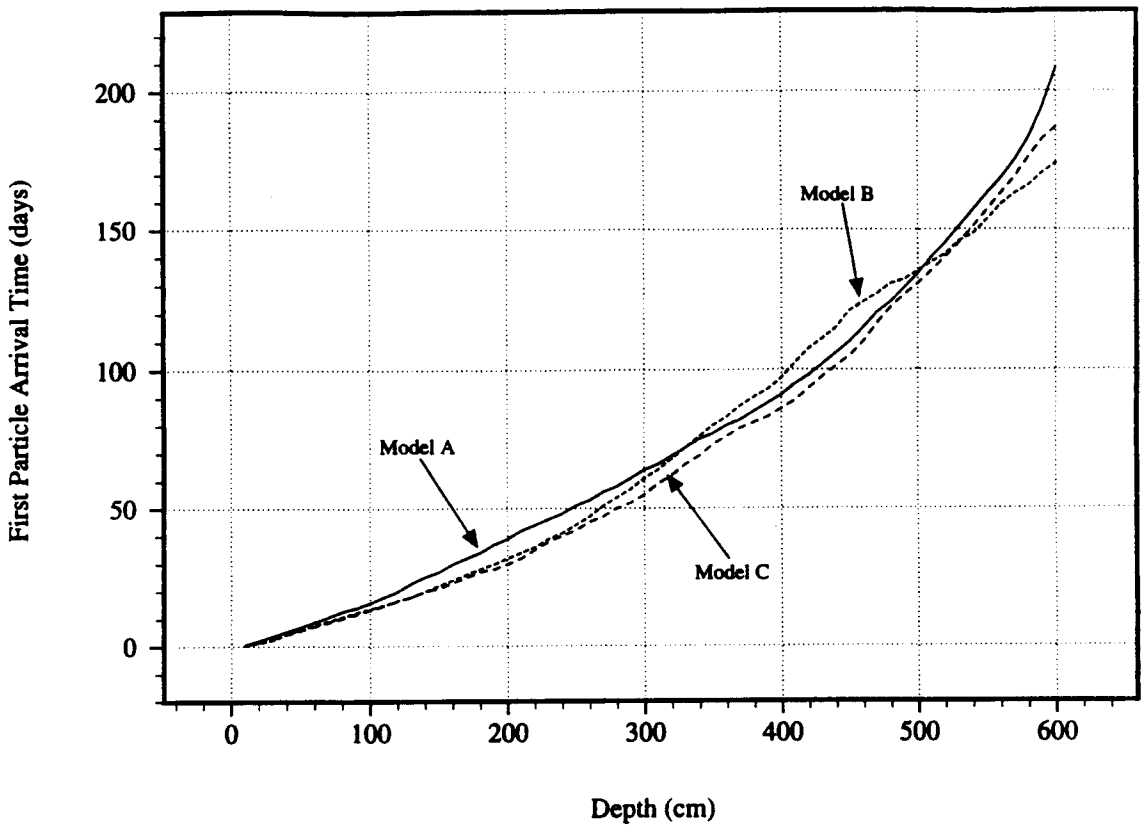

Figure 3-8. First particle arrival times with respect to depth

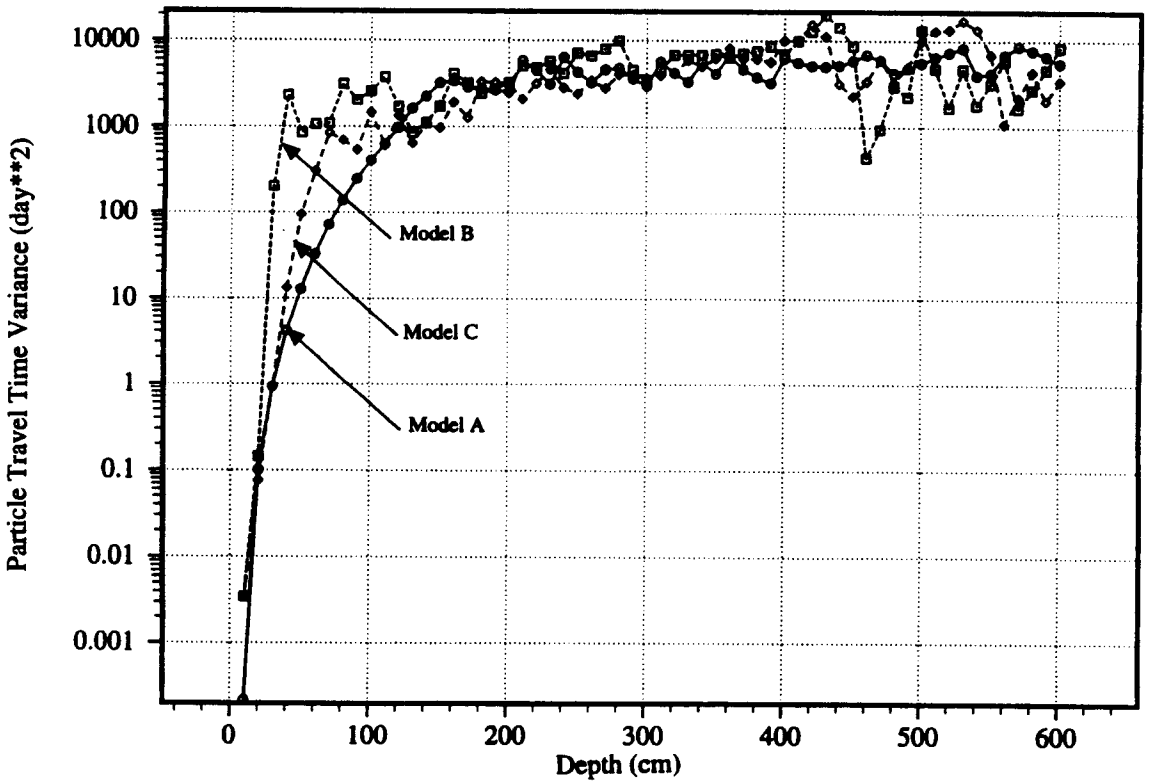

Figure 3-9. Travel time variance of arrival times at different depths

Model C, and yet leads to greater travel time variances, can be explained by the level of spatial variability this model exhibits at depths smaller than 120 cm. Indeed, the flow regime generated by each model may be seen from the plots of particle trajectories in Figures 3-2 through 3-4. In Figure 3-3 it is apparent that to a large degree the flow is more uniform within the 250 cm immediately below the strip source. It appears that model complexity, as defined in this study, does not consequentially predict the actual complexity of the local velocity field that is generated by the model. A more detailed analysis relating degree of heterogeneity, as a function of depth, to the variance in calculated travel times could provide the necessary means for making inferences regarding model complexity. This was not a part of this study.

The cumulative travel time distribution at any compliance point X_p and any time τ can be directly related to the spatial distribution of the particles by

$$G(\tau;X_p) = \int_{x_{1p}}^{\infty} \int_{x_{2p}}^{\infty} f(x_1,x_2;\tau)\, dx_1\, dx_2, \tag{3-4}$$

where $X=(x_1,x_2)$, and $f(x_1,x_2;t)$ is the probability density function (pdf) of the particle's position. Inasmuch as the compliance planes are parallel to the x_2 or horizontal axis, the compliance plane may be located by the single coordinate x_1, and the relevant pdf is simply the marginal pdf

$$f(x_1;\tau) = \int_{-\infty}^{\infty} f(x_1,x_2;\tau)\, dx_2. \tag{3-5}$$

The cumulative travel time distribution at the compliance plane specified by the point x_{1p} is

$$G(\tau;x_{1p}) = \int_{x_{1p}}^{\infty} f(x_1;\tau)\, dx_1, \tag{3-6}$$

Marginal vertical displacement pdf's are shown in Figures 3-10, 3-11, and 3-12 for Models A, B, and C, respectively, as functions of time. For all three models, the particles are very tightly grouped during the first day of simulation and, therefore, the marginal pdfs at day 1 approximate Dirac delta distributions. Although only 100 particles were used to generate these pdfs and the distributions are decidedly nonsmooth, it is still apparent that the shapes of the marginal pdfs are best preserved through time by Model A.

For steady state, saturated flow, the pdf for a single particle can be shown (Dagan, 1989) to be given by the Gaussian distribution

$$f(x_p;\tau) = \left(\frac{1}{2\pi\Sigma_{11}}\right)^{1/2} \exp\left[\frac{-(x_p - V\tau)^2}{2\Sigma_{11}}\right] \tag{3-7}$$

where Σ_{11} is the variance of the particle position, V is the deterministic seepage velocity, τ is time, and the product $V\tau$ is the mean particle position at time τ. Although the flow regimes simulated by the three models do not meet the assumptions specified for the derivation of Eq. (3-7) [e.g., Eq. (3-7) is based on steady, saturated flow, and the present problem is transient, unsaturated flow], Gaussian or near-Gaussian behavior might be expected to occur before the movement of the wetting front ceases. Equation (3-7) can be modified for time dependent spatial variance, and re-written as

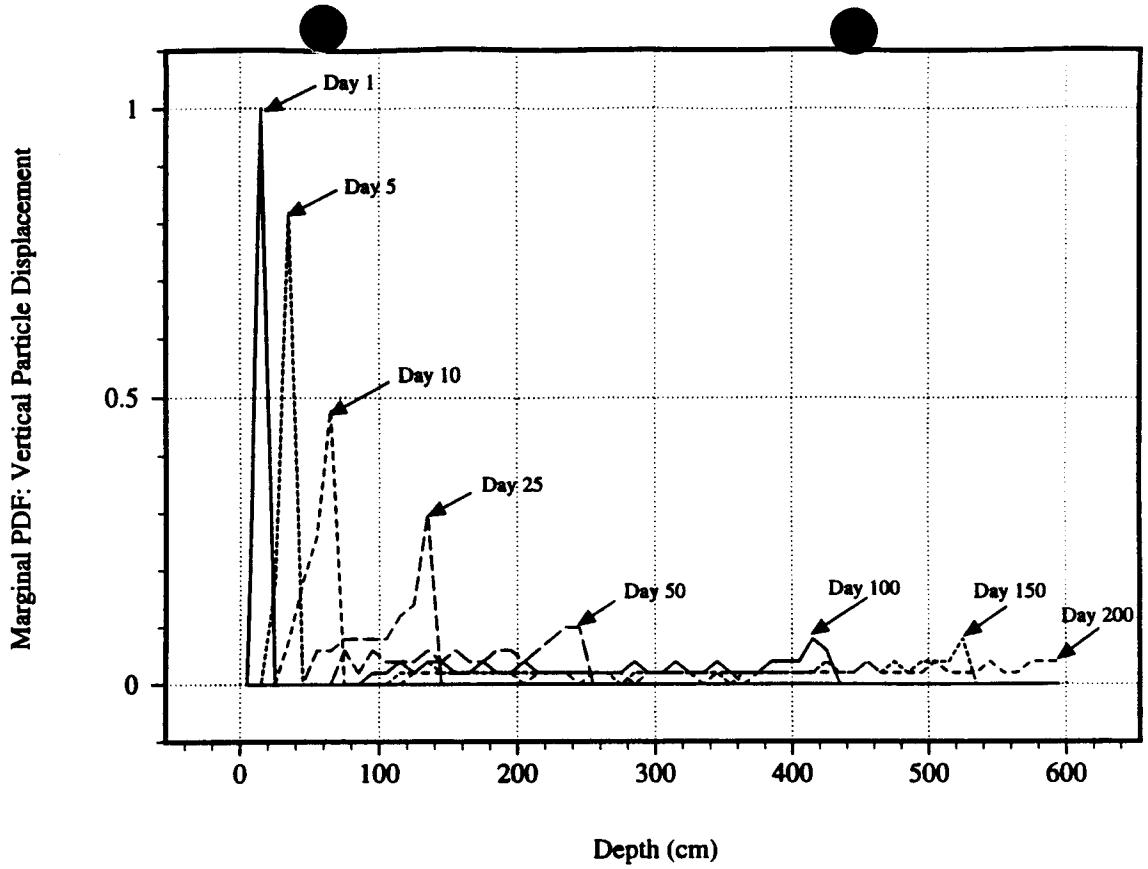

Figure 3-10. Marginal travel time PDF: Model A (nine horizontal layers of distinct hydraulic properties)

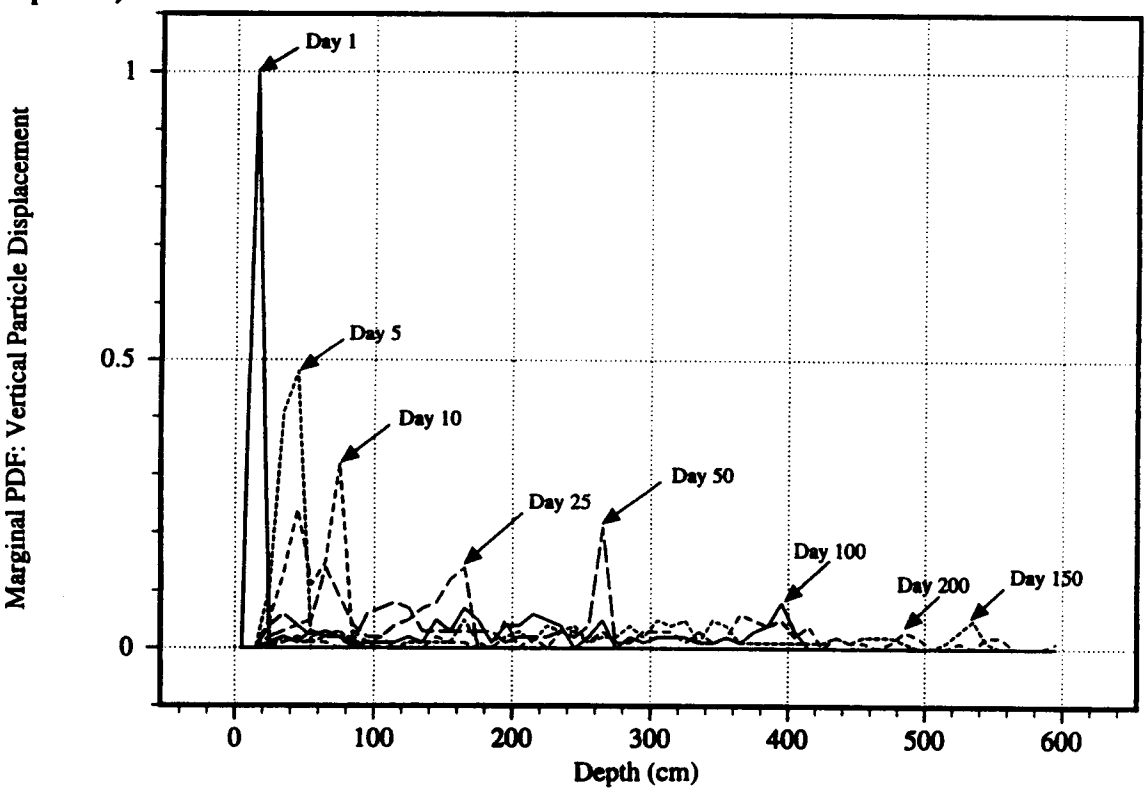

Figure 3-11. Marginal travel time PDF: Model B (121 zones of distinct hydraulic properties)

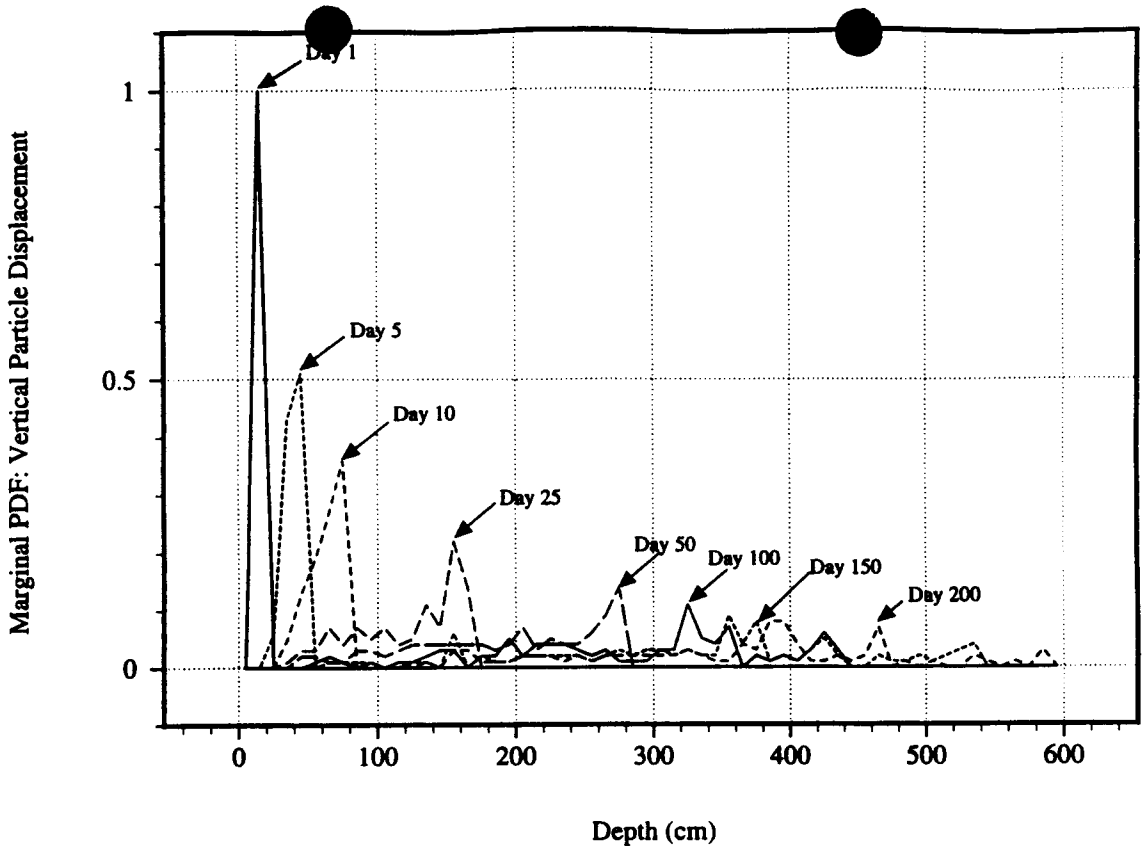

Figure 3-12. Marginal travel time PDF: Model C (3621 zones of distinct hydraulic properties)

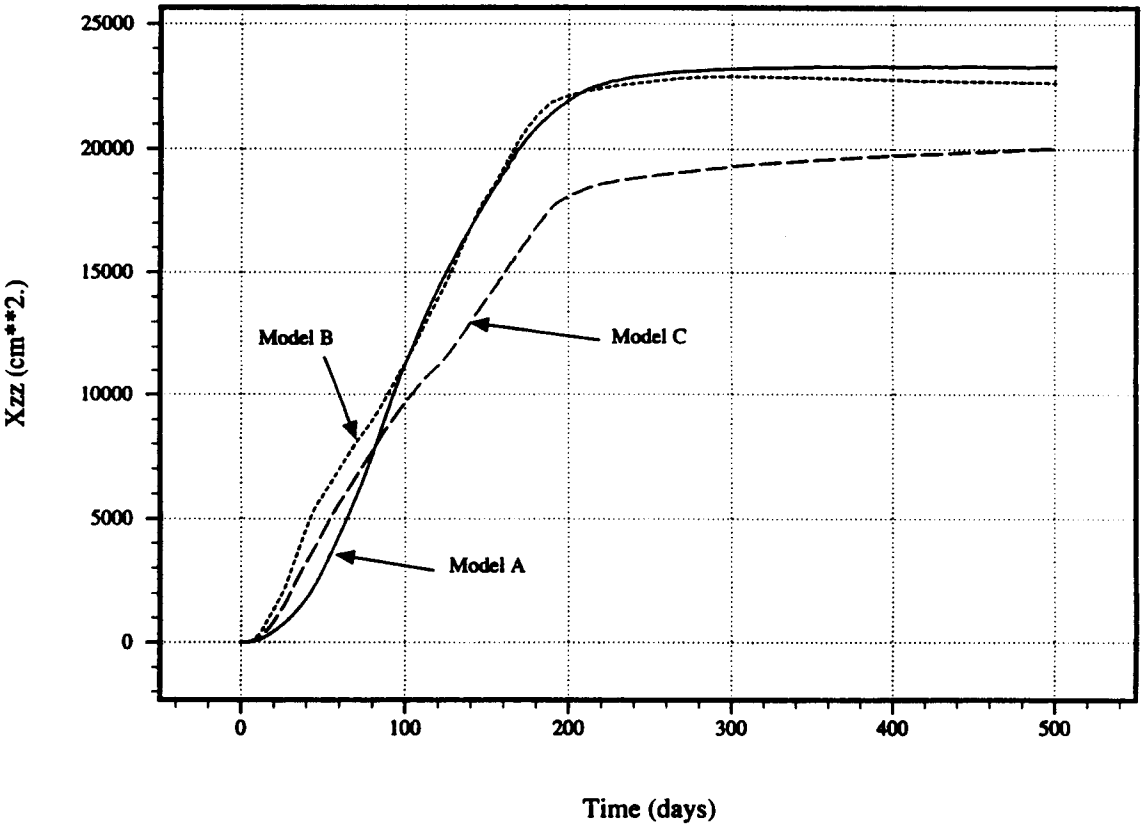

Figure 3-13. Estimated variance of the particle position in the vertical direction

$$f(x_p;\tau) = \left(\frac{1}{2\pi\Sigma_{11}}\right)^{1/2} \exp\left\{\frac{-[x_p-\mu(\tau)]^2}{2\Sigma_{11}}\right\} \tag{3-8}$$

where $\mu(\tau)$ is the mean particle position at time τ.

The estimated variance of the particle position in the vertical direction, Σ_{11}, and in the horizontal direction, Σ_{22}, are shown as functions of time in Figures 3-13 and 3-14, respectively. As might be expected based on the marginal pdf plots in Figures 3-10 through 3-12, the vertical variance of the particle's position is smallest for the most complex model, Model C. Although the horizontal variance of the particle's position is not needed for subsequent computations, it is nonetheless of interest to observe from Figure 3-14 that Model C produces the largest degree of lateral spreading. Both Σ_{11} and Σ_{22} appear to increase linearly with time during the first 180 days of the simulation for all three models. Vertical spreading of the particles (Σ_{11}) remains nearly constant following cessation of infiltration (at 150 days), while horizontal spreading continues to increase, albeit at a reduced rate, due to lateral redistribution of water.

If it is assumed that Eq. (3-8) describes the vertical spatial distribution of particles, then by substituting Eq. (3-8) into Eq. (3-6) the travel time cumulative distribution function (CDF) can be estimated and compared to the actual travel time CDF. Substitution of Eq. (3-8) into Eq. (3-6) yields

$$G(\tau;x_{1p}) = \int_{x_{1p}}^{\infty} \left(\frac{1}{2\pi\Sigma_{11}}\right)^{1/2} \exp\left\{\frac{-[x_1-\mu(\tau)]^2}{2\Sigma_{11}}\right\} dx_1. \tag{3-9}$$

The solution to Eq. (3-9) is given by

$$G(\tau;x_{1p}) = \frac{1}{2}\,\mathrm{erfc}\left\{\frac{x_{1p}-\mu(\tau)}{[2\Sigma_{11}]^{1/2}}\right\}. \tag{3-10}$$

Figures 3-15 through 3-21 show the computed and theoretical travel time CDFs at compliance planes located at 50, 100, 200, 300, 400, 500, and 600 cm depth for all three models. The CDFs based on the Gaussian particle spatial distribution assumption are similar to the computed travel time CDFs at shallow depths for Models A and C. The particle travel time CDFs for Model B show non-Gaussian behavior at all of the measured compliance planes at all times. The inflection in the computed travel time CDF for Model B which occurs at approximately 20 days at 50 cm depth, 70 days for 200 cm depth, and 120 days at 300 cm depth reflects the lateral bifurcation of the particle trajectories which occurs within the 250 cm region immediately below the strip source (see Figure 3-3). This bifurcation of the trajectories is probably caused by the blocky, non-smooth structure of Model B's parameter zonation.

Because only 100 particles were tracked through the flow field, it is difficult to elicit quantitative conclusions about the differences in the travel time CDFs for the three models at the far left tail of the distribution, which is the portion of greatest importance for regulatory issues. However, it is possible to examine and compare the computed and Gaussian travel time CDFs at a relatively high cumulative probability of 10 percent. In Tables 3-1 through 3-3, the computed and Gaussian tenth percentile travel times to five compliance planes are listed for Models A, B, and C, respectively. Similar to what was seen when the fastest travel times were compared, the more complex models produced the fastest computed tenth percentile travel times, at least up to the compliance plane at 300 cm depth. However,

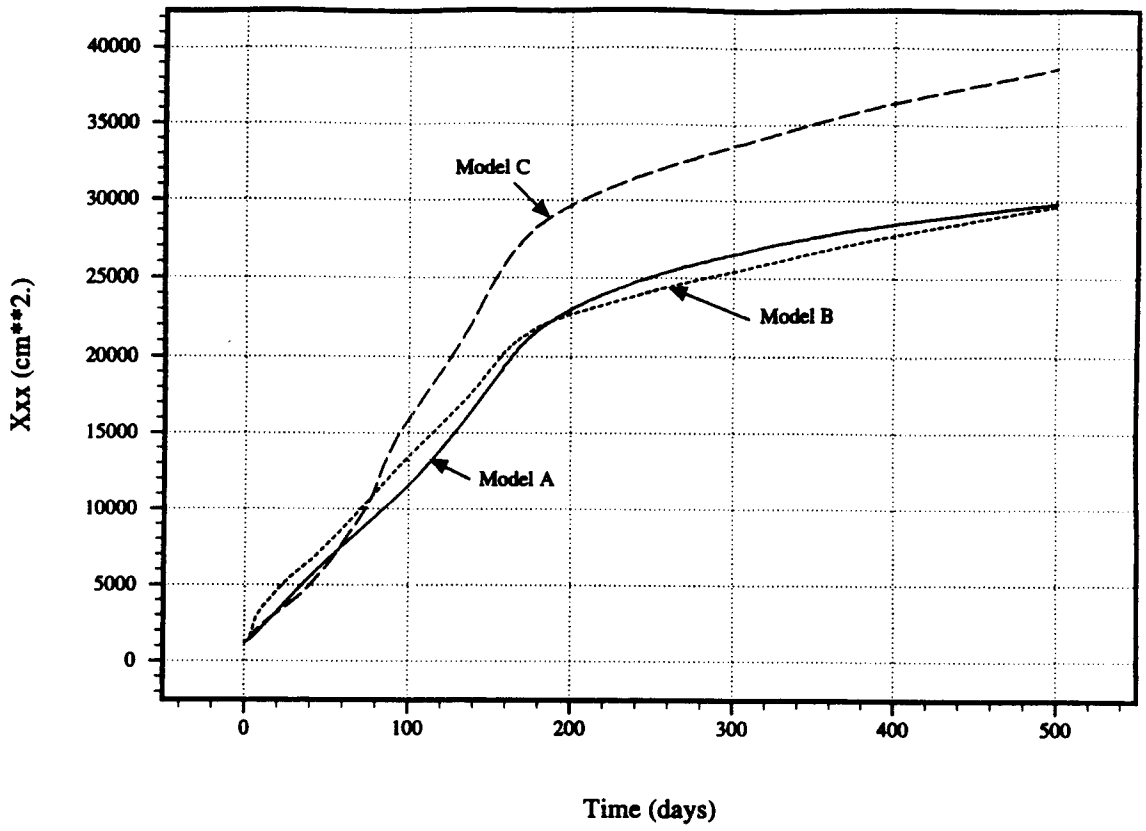

Figure 3-14. Estimated variance of the particle position in the horizontal direction

at the 400 cm deep compliance plane, the tenth percentile travel time, computed with Model B, is 10 days greater than that of Model A.

Although the assumption that the marginal pdf for the vertical position of a particle is Gaussian is not well supported, it is interesting to note that the tenth percentile travel times which were estimated based on this assumption are remarkably close to the computed travel times. For the tenth percentile travel time the Gaussian model tends to underpredict the travel times at the shallow compliance planes and overpredict travel times at the deeper compliance planes. The close agreement of the computed and Gaussian tenth percentile travel times must not be seen to imply that the Gaussian model provides a useful tool for predicting GWTT distributions for transient, unsaturated flow. However, it is noted that the time-dependent mean particle position and vertical location variance used in the Gaussian model were determined from the actual trajectories of the 100 particles. In order for predictive models to be useful in computations of GWTT distributions they must also provide a basis to estimate the time-dependent mean particle location and variance using directly measured quantities. While developments in stochastic continuum models of flow and transport in saturated porous media have produced useful predictive models which relate the statistical structure of hydraulic conductivity to that of the velocity field and thereby to the statistical structure of the particle trajectories, the added complexity of variable saturation may limit the applicability of this method.

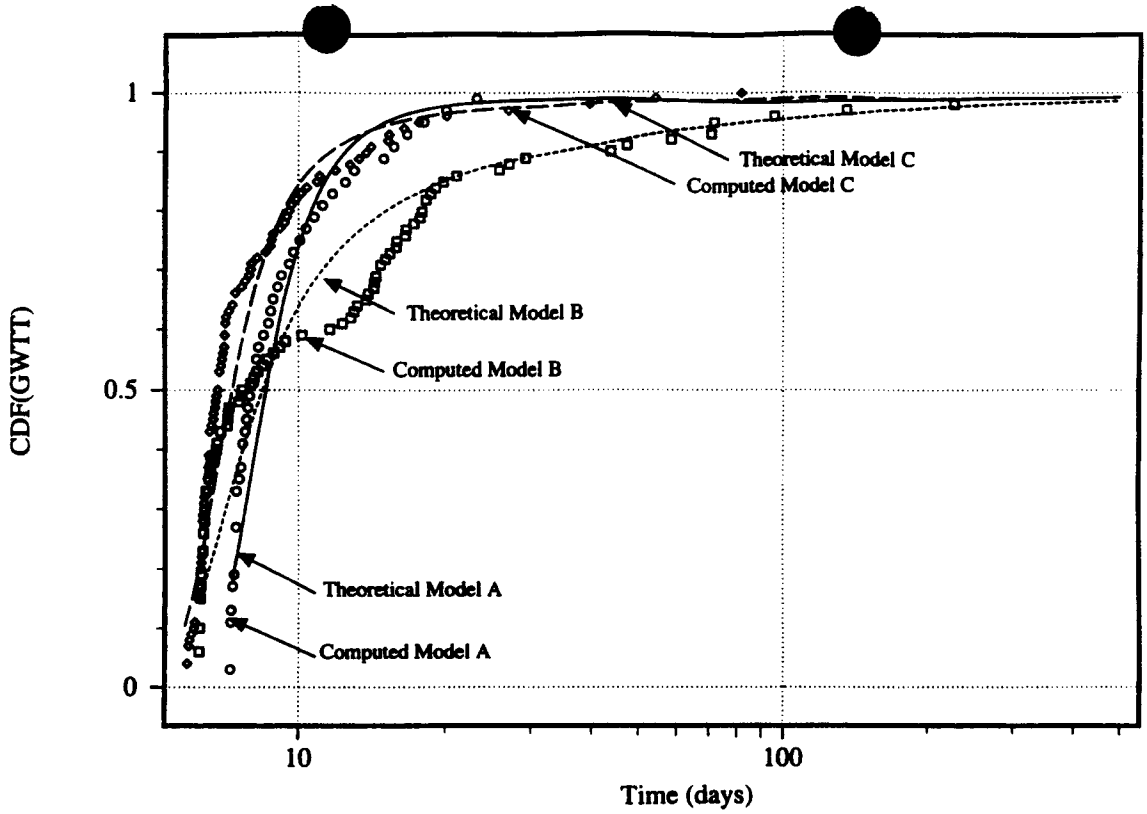

Figure 3-15. Comparison of theoretical (lines) and conceptual (symbols) travel time CDFs for a 50 cm compliance boundary

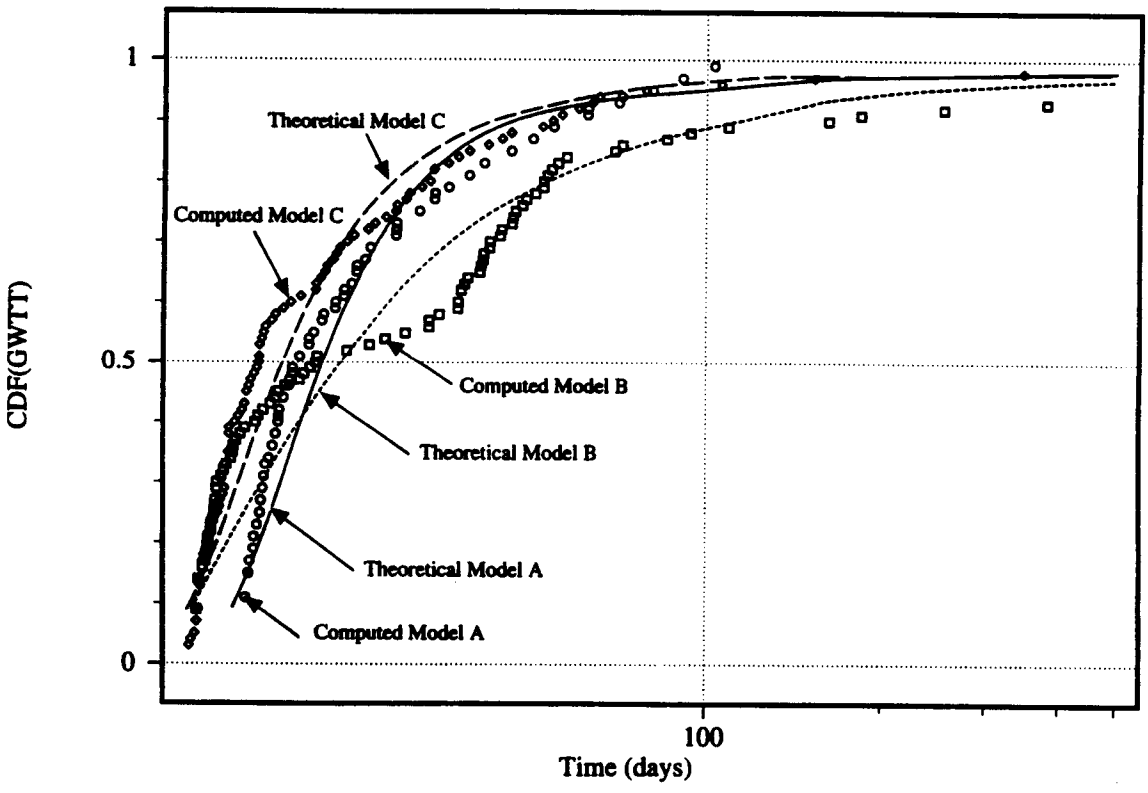

Figure 3-16. Comparison of theoretical (lines) and conceptual (symbols) travel time CDFs for a 100 cm compliance boundary

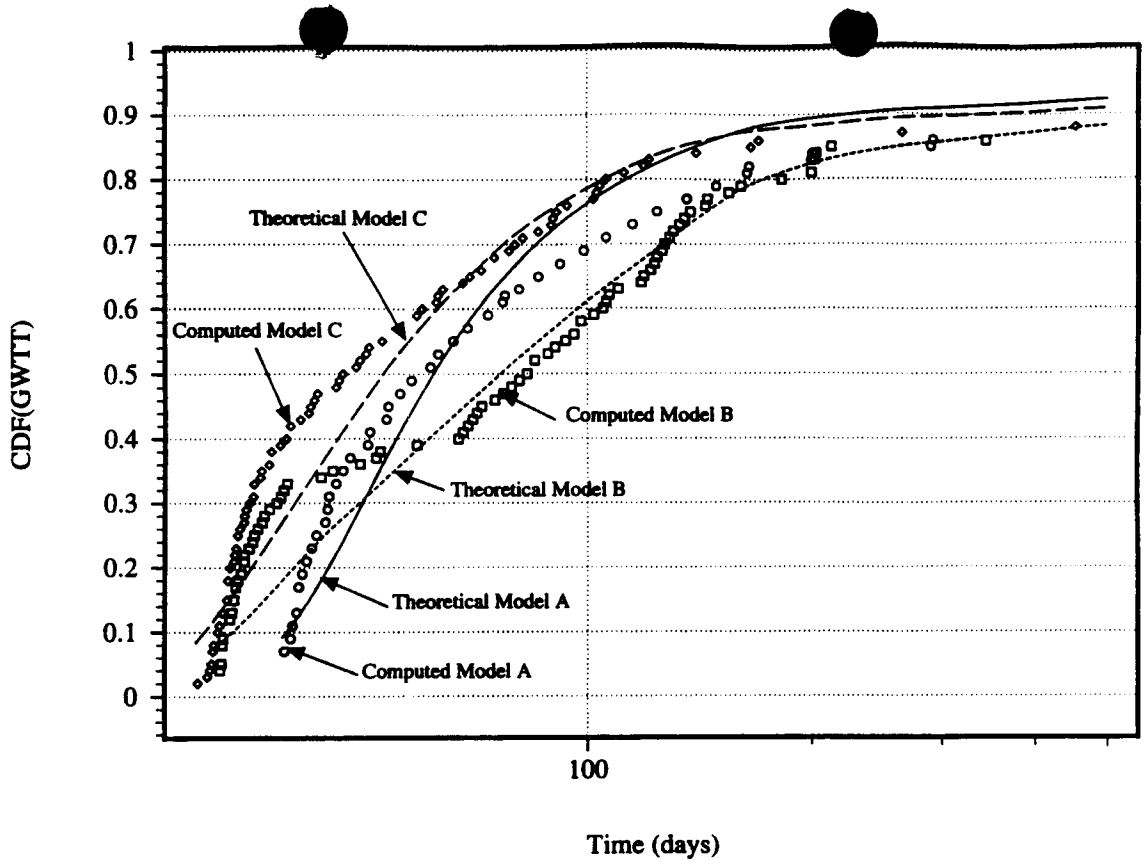

Figure 3-17. Comparison of theoretical (lines) and conceptual (symbols) travel time CDFs for a 200 cm compliance boundary

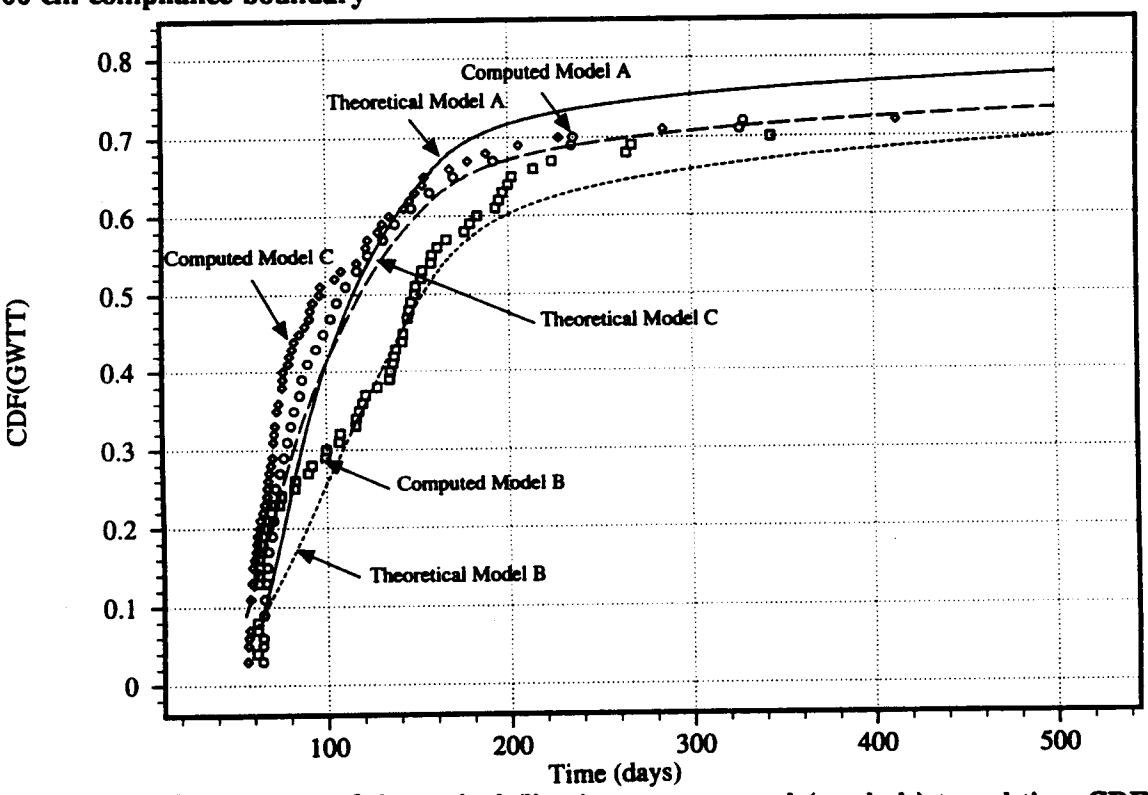

Figure 3-18. Comparison of theoretical (lines) and conceptual (symbols) travel time CDFs for a 300 cm compliance boundary

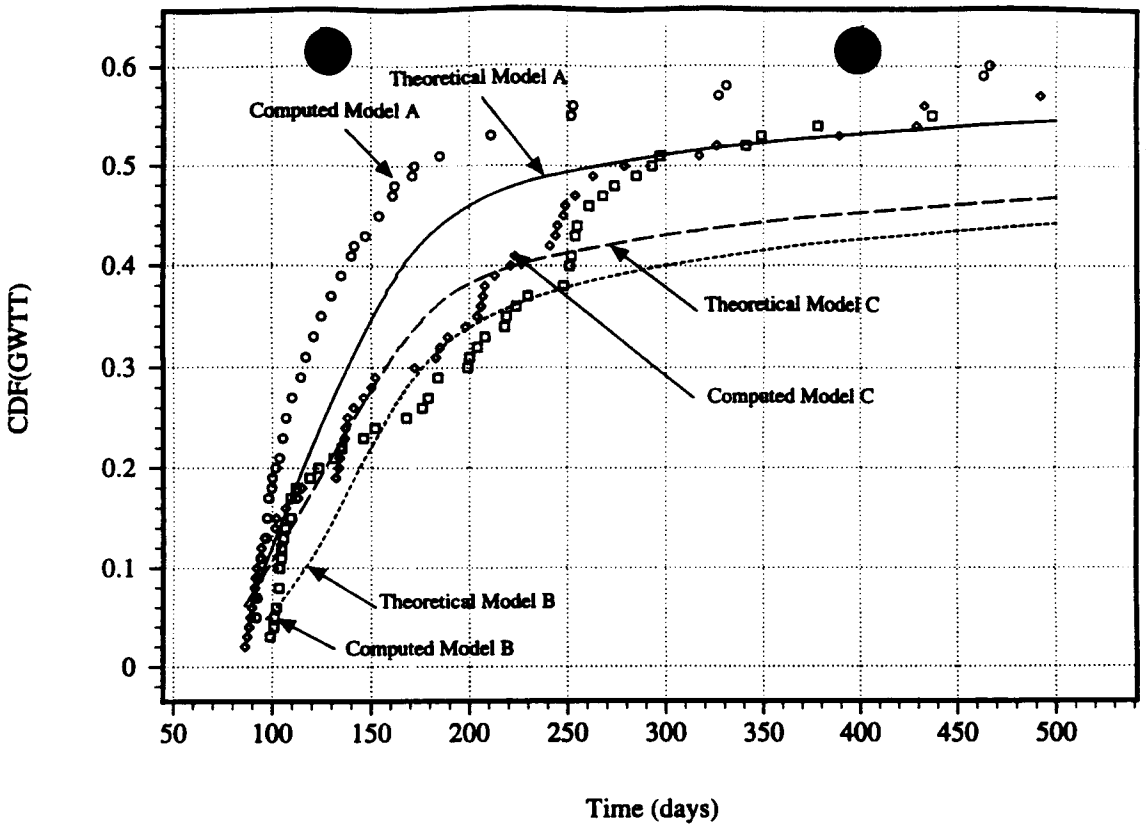

Figure 3-19. Comparison of theoretical (lines) and conceptual (symbols) travel time CDFs for a 400 cm compliance boundary

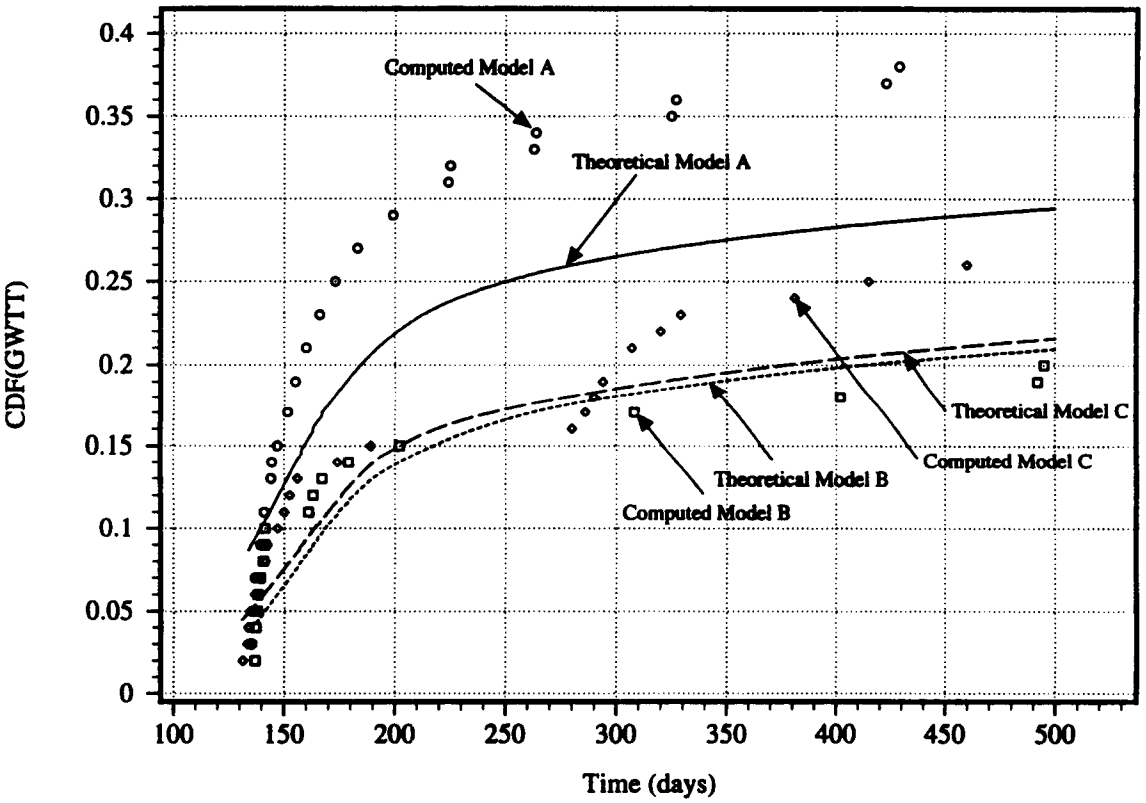

Figure 3-20. Comparison of theoretical (lines) and conceptual (symbols) travel time CDFs for a 500 cm compliance boundary

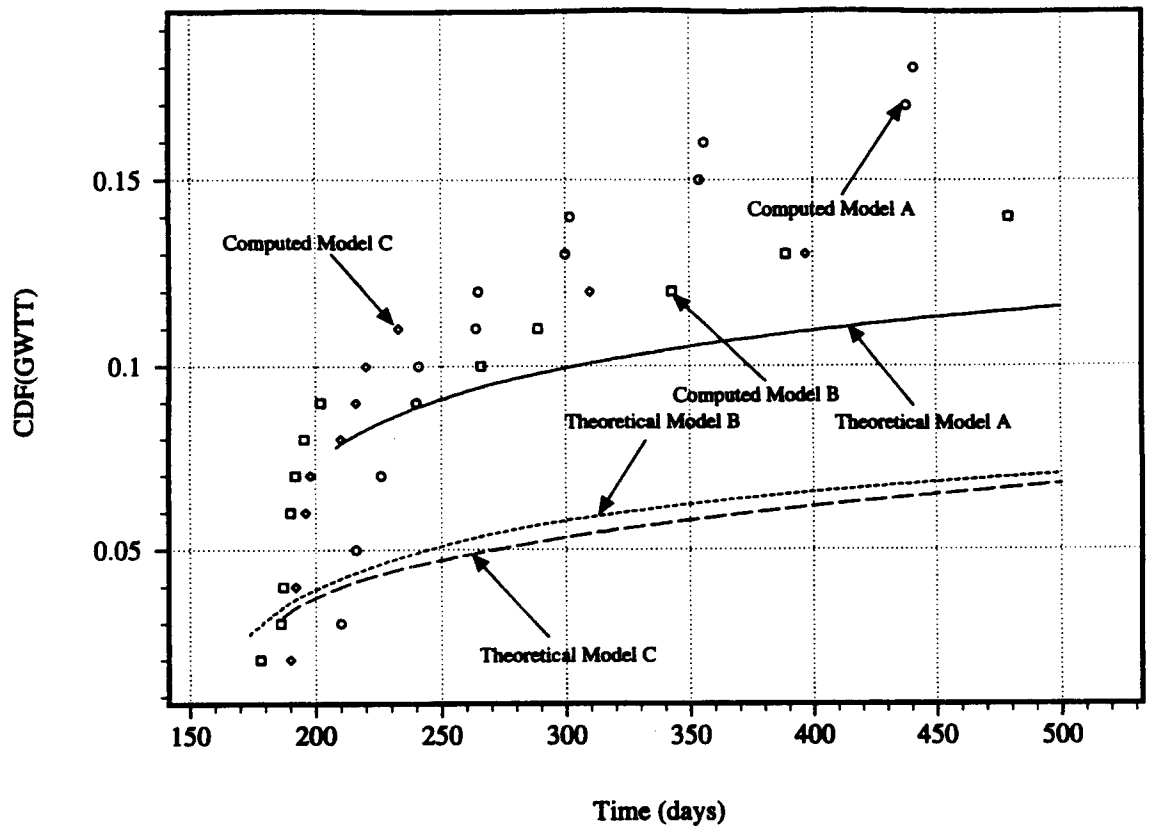

Figure 3-21. Comparison of theoretical (lines) and conceptual (symbols) travel time CDFs for a 600 cm compliance boundary

3.6 SUMMARY

This section summarizes a study of the relationship between model complexity, (spatial variability of the soil hydraulic properties), on the travel time of particles departing from uniformly spaced locations along a strip source, through a variably saturated, transient flow regime. Model structure clearly has an effect on the first arrival time and the distribution of travel times, although simply categorizing a model by its number of distinct parameters zones does not help to predict which model produces the fastest travel time or the greatest travel time variance. Travel time distributions result from the spatial distribution of particle trajectories which are, in turn, the result of the spatial variability of the seepage velocity field. For saturated flow, the relationship between hydraulic conductivity and Darcy velocity implies that models which have a larger number of hydraulic property zones will generally produce more spatially complex velocity fields and thereby affect the distribution of travel times. For unsaturated flow, the relationship between the number of distinct parameter zones and the complexity of the resulting velocity field is not so obvious. Unsaturated phenomena such as moisture dependent anisotropy or fingering will, under certain conditions, reduce the effective dimensionality of the flow system and thus sever the link between model complexity and flow field complexity.

Table 3-1. Model A: Tenth percentile travel time

Plane (cm)	50	100	200	300	400
$\tau_{computed}$ (days)	7.2	16.7	40.1	65.2	93.5
$\tau_{gaussian}$ (days)	6.9	16.0	39.5	65.7	95.7

Table 3-2. Model B: Tenth percentile travel time

Plane (cm)	50	100	200	300	400
$\tau_{computed}$ (days)	6.3	13.8	32.7	61.8	103.5
$\tau_{gaussian}$ (days)	6.0	13.7	33.4	67.0	117

Table 3-3. Model C: Tenth percentile travel time

Plane (cm)	50	100	200	300	400
$\tau_{computed}$ (days)	6.1	13.9	32.0	57.5	92.0
$\tau_{gaussian}$ (days)	5.8	13.5	30.7	56.5	97.7

Computational tools are being developed at the CNWRA which may allow large-scale, Monte Carlo simulation of transient flow in unsaturated flow regimes and the subsequent development of high resolution travel time CDFs. Continued development of stochastic continuum methods may also provide analytical tools which can be used to predict travel time distributions in unsaturated regimes based on the statistical structure of the unsaturated hydraulic conductivity and moisture retention functions. Additionally, solute transport computations may provide the link between GWTT and concentration, a parameter which is easily associated with risk assessment. Simulations of this type, especially in fractured media, will be helpful in assessing the applicability of GWTT as a regulatory measure of performance.

4 PROBABILISTIC CALCULATIONS OF GROUNDWATER TRAVEL TIME IN SATURATED POROUS MEDIA WITH STOCHASTIC HETEROGENEITIES

4.1 STATEMENT OF THE PROBLEM

One of the primary difficulties in determining a unique "fastest path of likely radionuclide travel" is the presence of heterogeneities in naturally occurring geologic media. The simplest type of geologic heterogeneities is represented by stratigraphic layers. Depending upon the formational history, the layer boundaries are sometimes sharp but these boundaries are mostly transitional and fuzzy. In the layered representation of geologic media, each layer is generally assumed to be homogeneous within itself. However, that is rarely true. A higher level of complexity is introduced in the conceptual model when relevant properties in any of the layers are assumed to vary in space. The representation of such spatial variations is highly dependent upon the scale of modeling — variations being present at all scales. An even higher level of complexity is introduced when special features such as fractures, faults, cavities, vugs, etc. are considered in developing conceptual models. Such features are special because even when their physical dimensions are small (compared to the total domain), they can significantly affect control over the flow field and hence flow paths and travel times. There is not much controversy in that flow paths, and travel times associated with them, are dependent upon how heterogeneities are represented and the scale at which they are represented. When heterogeneities are represented at a gross scale, it is possible to miss a flow tube which is carrying a small quantity of water, but bounds the fastest possible path. Such a path may be resolved only when small-scale heterogeneities are fully represented.

Conceptualization of hydrogeology is the first step in the process of estimating the groundwater travel time (GWTT). At the broadest level, one has two choices: (i) to divide the domain into well defined geologic zones, each zone having unique and deterministic properties; or (ii) to obtain a stochastic conceptualization of the site. The latter choice is the subject of this study. In contrast to representing the property of a zone by a deterministic value, in the stochastic representation, the property is assumed to be a random variable with an associated probability distribution. The probability distribution may represent either actual variation of the property within the zone, or it can be a measure of the uncertainty in that property, or both. A correlated three-dimensional (3D) stochastic field is the most complete representation for a random process.

The method for calculating the GWTT presented in this chapter is based on the representation of the hydraulic conductivity as a spatially correlated stochastic field. An ensemble of hydraulic conductivity realizations is obtained using a sampling method known as the Nearest Neighbor Model (NNM). The NNM method was first employed by Smith and Freeze (1979a,b), but was provided improved theoretical basis and extended to perform conditional simulations by Bagtzoglou and Ababou.[1] A brief explanation of this method will be provided later in this chapter. For each realization of the hydraulic conductivity in the ensemble, the saturated steady-state groundwater flow equation is solved. The velocity field thus obtained is then used to estimate GWTT along particular paths by releasing a large number of water particles at various starting points. This way, path variability is sampled through the realization ensemble space and also through the independent particle "flights" within a specific flow field

[1]Bagtzoglou, A.C., and R. Ababou. 1992. "Generation and conditioning of multi-dimensional Gauss-Markov random fields" (in preparation).

realization. The uncertainty in predicted GWTT due to parameter variability is assessed for a data set which may be roughly considered to be characteristic of the Yucca Mountain saturated zone. However, a GWTT analysis for the Yucca Mountain site will require a much greater level of site-specific data analysis than was performed in this study.

4.2 TECHNICAL APPROACH

To study the implications of calculating GWTT in a saturated medium whose heterogeneities were described in a stochastic manner, the following steps were followed:

- Generate statistically equivalent (equally likely), yet independent, realizations of a hydraulic conductivity field which is assumed to be a second order stationary Gauss-Markov process.
- Solve the saturated, steady-state groundwater flow equation for a set of fixed and known boundary conditions for each realization of hydraulic conductivity field. For each realization, obtain a velocity field.
- Estimate GWTT for each realization of velocity field by advecting a large number of water particles of infinitesimal mass.
- Estimate statistics of GWTT for a large collection of particles of infinitesimal mass within a velocity field realization and across the ensemble of velocity fields.

4.2.1 Generation of Spatially Correlated Random Fields

In this exercise, the hydraulic conductivity field was assumed to be a spatially correlated, second-order stationary field. The common assumption of lognormality of the marginal distribution of the hydraulic conductivity was also made. Together, these two assumptions imply that the geometric mean of hydraulic conductivity is constant over the entire region, and also that a correlation length based on relative distance (in contrast to distance from a fixed location) between two space locations can be defined and is also constant. Several schemes can be used to generate an ensemble of equally likely hydraulic conductivity fields. These include, in addition to simple uncorrelated random sampling, the Turning Bands Method (Tompson et al., 1989), various stratified sampling methods including the more popular Latin Hypercube Method (Iman et al., 1980), and the NNM. The NNM is particularly suited to the sampling of stationary Gauss-Markov fields and is used in this exercise. A brief outline of the method is provided below.

In general, a 3D, stationary Gauss-Markov, zero-mean, stochastic process, $Y(\mathbf{X})$, satisfies the following linear partial differential equation with homogeneous boundary conditions.

$$(\nabla^2 - \alpha^2)\, Y(\mathbf{X}) = \sigma_0\, U(\mathbf{X}) \qquad (4\text{-}1)$$

In Eq. (4-1), α and σ_o are parameters related to the variance and correlation length of Y, and U is a Brownian process. The random field, $Y(\mathbf{X})$, has the following characteristics

$$R_{YY}(\xi) = \sigma_Y^2 \, exp(-\alpha|\xi|)$$
$$\sigma_Y^2 = \frac{\pi}{\alpha}\,\sigma_o^2 \qquad (4\text{-}2)$$
$$\lambda_Y^3 = \frac{\pi}{\alpha^3}$$

where λ_Y is the correlation length and σ_Y^2 is the variance of the random field $Y(\underline{X})$. In the context of this work, $Y(\underline{X})$ is the log-conductivity field. As can be seen from Eq. (4-2), parameters α and σ_o are related to the physical properties of $Y(\underline{X})$.

In a 3D domain, discretization of Eq. (4-1) yields

$$Y_{i,j,k} = a\left(Y_{i-1,j,k} + Y_{i,j-1,k} + Y_{i,j,k-1} + Y_{i+1,j,k} + Y_{i,j+1,k} + Y_{i,j,k+1}\right) + b\,\hat{U}_{i,j,k} \qquad (4\text{-}3)$$

where $\hat{U}_{i,j,k}$ is a white (uncorrelated) random field with unit variance. Coefficients a and b in Eq. (4-3) are functions of the properties of the field to be generated (λ_Y, σ_Y) and the grid size $(\Delta_x, \Delta_y, \Delta_z)$. From Eq. (4-3), it is clear that the sample value of Y in a grid block is a function of values of Y in its immediate neighborhood; hence the name Nearest Neighbor Model. The advantage of the NNM lies in the ease with which Eq. (4-3) can be implemented on hypercube topology based parallel computer architectures. Moreover, conditioning is performed in a very convenient way by treating the data points as internal boundary conditions. In this study, a code named Connection Machine Nearest Neighbor Model (CMNNM) was developed for the massively parallel CM-200 computer. Extremely high computational speeds were achieved through the use of CMNNM. Figure 4-1 depicts a typical realization for $Y(\underline{X})$ corresponding to a $\sigma_Y = 2$. The detailed structure in the random field is apparent.

4.2.2 Obtaining Hydraulic Head and Velocity Fields

For a 3D problem, the steady-state, saturated groundwater flow equation (without source/sink terms) is

$$\frac{\partial}{\partial x}\left[K(x,y,z)\frac{\partial h}{\partial x}\right] + \frac{\partial}{\partial y}\left[K(x,y,z)\frac{\partial h}{\partial y}\right] + \frac{\partial}{\partial z}\left[K(x,y,z)\frac{\partial h}{\partial z}\right] = 0 \qquad (4\text{-}4)$$

where h is the hydraulic head, and K is the spatially varying hydraulic conductivity. Equation (4-4) is discretized by a block-centered central difference scheme [similar to the one used for Eq. (4-1)], with constant grid spacing. This discretization scheme leads to a hepta-diagonal banded system of algebraic equations, which is solved by the diagonally preconditioned conjugate gradient method (DPCG) described in Bagtzoglou and others (1992a) and references therein. A description of the numerical code used, some benchmark tests, and its application to saturated/unsaturated flow problems can be found in Bagtzoglou and others (1992b).

Once the hydraulic head solution was obtained, the water flux vector field was estimated by using Darcy's Law and forward differencing for hydraulic head gradient calculation. Figure 4-2 shows a 3D hydraulic head field corresponding to the hydraulic conductivity field presented in Figure 4-1 and

Figure 4-1. Three-dimensional hydraulic conductivity field generated by the NNM process. Red indicates values above the mean, whereas blue indicates values below the mean.

Figure 4-2. Three-dimensional hydraulic head field corresponding to the hydraulic conductivity field presented in Figure 4-1. Mean flow is from the area in red to the area in blue.

assuming two Dirichlet boundaries and no flow across all others. Even though the direction of flow is predominantly in one direction (to be expected because of the boundary conditions imposed), the effect of heterogeneity was apparent at the local scale.

4.2.3 Groundwater Travel Time Calculation

Once the water flux vector field was obtained, GWTT calculations are performed by advecting through the flow domain a large number of infinitesimally small water particles. The computer code SLIM-2.4 (Tompson et al., 1987), a highly vectorized particle tracking code, was used for this purpose. The structure of SLIM-2.4 was modified to accommodate repeated flow field realizations.

The number of particles exiting the flow domain through an arbitrary, but specified, compliance boundary was monitored. Thus, cumulative distribution functions (CDF) for GWTT were readily obtained. The modified SLIM-2.4 computer code also calculated probability density functions (PDF) of particle locations and their associated statistics over the realization ensemble space. This allows one to make inferences in regards to the most probable destination of a particle originating at a specified location in space. A description of the methodology implemented to transform particle locations to PDF can be found in Bagtzoglou and others (1992c).

4.3 COMPUTATIONAL DETAILS

4.3.1 Description of Computational Domain

The physical domain has dimensions 5,000 × 2,500 × 2,500 meters in the X, Y, and Z directions, respectively. The computational grid consisted of 55,800 nodes arranged in a 62 × 30 × 30 lattice. The computational grid spacing was uniform along all three directions, $\Delta_x=\Delta_y=\Delta_z=81.97$ meters. Figure 4-3 illustrates a X-Y projection of the 3D grid. Even though the saturated thickness of interest at Yucca Mountain is most probably less than 1,000 meters, the depth of the domain was chosen to be 2,500 meters so that it spans at least ten correlation lengths vertically. Furthermore, the particle pulse was released in the middle of the domain (depth-wise) as shown in Figure 4-4. Thus, the maximum vertical distance a specific particle may travel was no more than 1,250 meters. Details on the exact size and location of the particle release region will be given later. The lateral boundary conditions were no-flow (Y = 0 and Y = 2,500 meters; Z = 0 and Z = 2,500 meters) and constant head (X = 0 and X = 5,000 meters). Similarly, for the GWTT calculation through particle tracking, the no-flow boundaries are considered as reflecting whereas the constant head conditions were considered as absorbing boundaries.

4.3.2 Description of Parameter Values

The spatially correlated Gauss-Markov random hydraulic conductivity fields are generated using the NNM. The following values of parameters were used:

- The geometric mean of the saturated hydraulic conductivity is $K_G = 5.8 \times 10^{-8}$ m/sec = 5×10^{-3} m/day. This value may be representative of the saturated zone (at large-scale) at the Yucca Mountain and is calculated from the transmissivity values found in Rice (1984). It is a very rough approximation but for illustration of the method, is considered to be adequate. Furthermore, it lies in the range of values reported by Peters and others (1984)

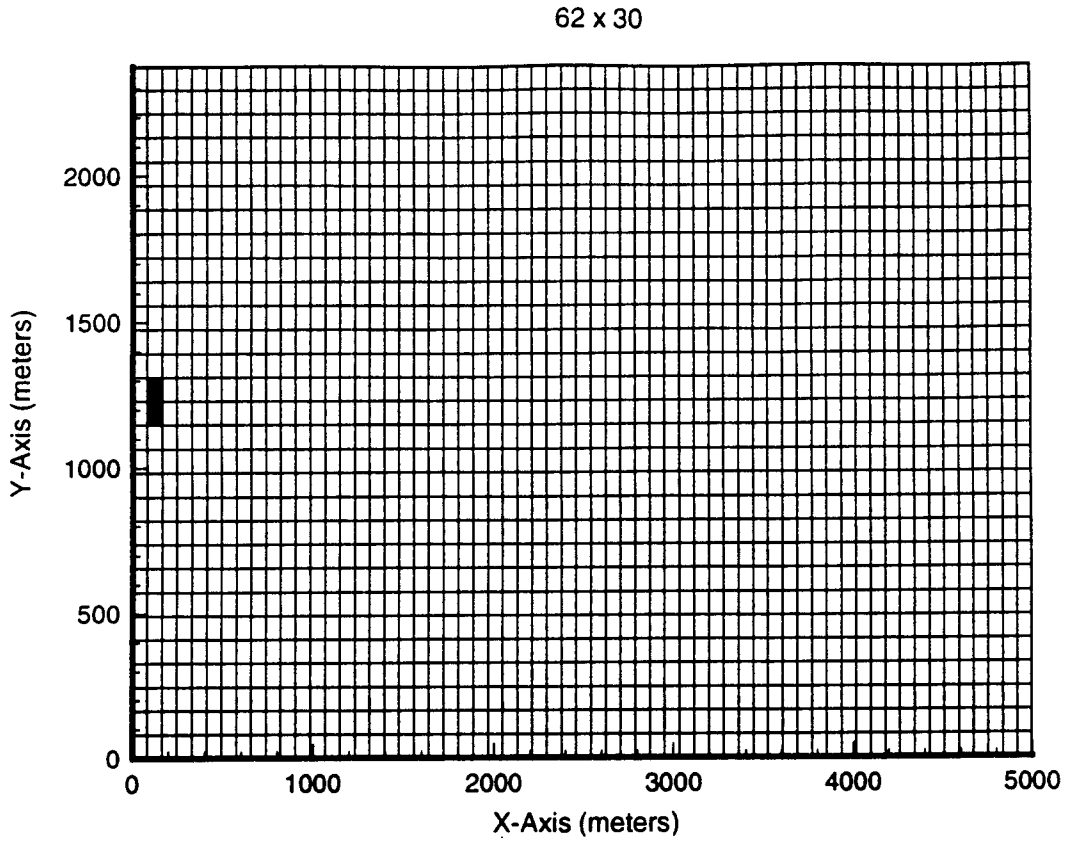

Figure 4-3. X-Y projection of the 3D grid used in the simulations. Area marked as black corresponds to the particle release region.

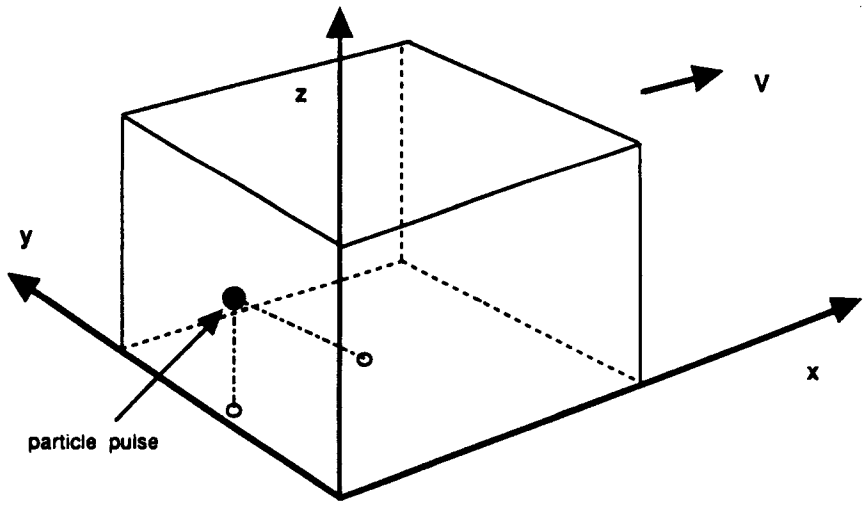

Figure 4-4. Schematic showing the relative location of the particle pulse release region. Note that the particle pulse is shown as a point for illustration purposes only.

for the Prow Pass (PPw) and Bullfrog (BFw) saturated welded units ($K_s = 1.5 \times 10^{-4}$ to 1.2×10^{-3} m/day).

- The regional hydraulic head gradient used in this work is 0.027. This value is reported by Ahola and Sagar (1992) who conducted regional groundwater flow simulations of the Yucca Mountain site. It is a relatively high value, characteristic of the northern part of the site, but is used here for illustration.

- In our simulations, the porosity is assumed to be constant in space. A value of $\phi = 0.25$, characteristic of the PPw and BFw (Peters et al., 1984) units, is chosen.

- The hydraulic conductivity fields are generated using a constant, isotropic correlation length $\lambda_Y = 245.9$ meters. This value ensures that the characteristic length of the domain, L_i in the i-th coordinate direction, is much larger than the corresponding correlation length of the stochastic hydraulic conductivity field in the same direction. Thus, $L_x \approx 20.3\lambda_Y$, $L_y = L_z \approx 10.2\lambda_Y$. By doing so, variability in the random fields has sufficient room to develop in space without being restricted by boundary effects (Thompson et al., 1987). Similarly, detailed local behavior will be observed since a fine computational resolution $\Delta_x = \Delta_y = \Delta_z = \lambda_Y/3$ is used. This is consistent with suggestions by Ababou and others (1989). It is also on the conservative side, since longer correlation lengths increase the probability of preferential pathways being encountered. This would lead to faster GWTT estimates [U.S. Nuclear Regulatory Commission (NRC), 1990].

- The standard deviation of the log-conductivity field is varied at $\sigma_Y = 0.225$ and $\sigma_Y = 0.90$. One may compare these to the range of values (0.59 to 0.87) obtained, in the geostatistical analyses performed on core data collected at Yucca Mountain (U.S. NRC, 1990). These values are also consistent with observations made by Wang (1992) who studied the variation in the saturated hydraulic conductivity of tuffaceous media.

- Two sets of simulations are conducted, each corresponding to the two levels of heterogeneity in the hydraulic conductivity fields. Twenty Monte Carlo realizations of hydraulic conductivity fields are generated for each set. Realistically, realizations on the order of few hundreds will probably have to be analyzed to obtain reasonable statistics of the GWTT. Only twenty are used in this exercise for illustration.

Within each realization, 10,000 water particles were released and tracked in a transient mode. The time step used in these simulations was $\Delta t = 3{,}650$ days yielding a maximal Courant number $C_o = 0.1624 < 1.0$, ensuring that no overshooting occurs. The particles are released at random over a parallelepiped region $\Delta_x \times 2\Delta_y \times 2\Delta_z$ in dimensions, as shown in Figure 4-3. By doing so, a large part of the variability in the flow fields was sampled through 200,000 (20 velocity field realizations $\times$ 10,000 particles per realization) independent particle "flights". Moreover, since the dimensions of the release area, perpendicular to the mean flow, were at the scale of the correlation length, the ergodic hypothesis for particle paths could be assumed to hold (Dagan, 1982).

4.4 DISCUSSION OF RESULTS

Figures 4-5 and 4-6 present a statistical analysis of the 3D hydraulic conductivity and water flux fields with $\sigma_Y = 0.90$, $\sigma_Y = 0.225$. These figures serve as a verification of the random hydraulic conductivity field generator. Both mean and standard deviation match closely the specified values. Furthermore, even though the normality hypothesis was not tested rigorously, it is apparent that the NNM generator reproduced the desired distribution. The histogram of the calculated flux vector magnitude is shown in Figures 4-5b and 4-6b. It is interesting to note the histogram shape for the magnitude of the water specific discharge vector which appears to be approximately lognormal also. This is consistent with observations made by Papp (1992). From the two levels of heterogeneity (i.e., variance of hydraulic conductivity) used in this study the following tentative relationship can be observed

$$\sigma_{\log V} \approx \frac{2}{3} \sigma_{\log K} \tag{4-5}$$

where V is the magnitude of the flux vector. The smaller variance of the log(V) field compared to the log(K) field is indicative of the dampening (smoothing) nature of the flow in porous media. The actual amount of dampening, however, may also depend upon the mean value of hydraulic conductivity and hydraulic gradient. This interesting idea was not investigated further in this study.

A typical realization of the hydraulic conductivity field is shown in Figure 4-7. It exemplifies the randomness of the fields used in these simulations. This particular figure corresponds to a X-Y plane at the middle of the 3D domain (Z = 1,250 m). Figures 4-8 and 4-9 present results from the groundwater flow simulation at steady-state conditions. Again, these are two-dimensional (2D) plots of data extracted from 3D fields at a plane cutting the release region. In Figure 4-8 the hydraulic head variation is shown. Note that the actual units of head in the legend are in kilometers. Figure 4-9 depicts the flow field corresponding to one of the 20 realizations conducted with $\sigma_Y = 0.90$. Also, presented in the same figure are three streamlines emanating from the center and the edges of the particle release region. Thus, an approximate bound of the area to be swept by the particles is obtained.

Results from the particle tracking simulation are shown in Figure 4-10. This is a plot of particle projections on X-Y and X-Z planes at three different times, t = 1,000, 10,000, and 20,000 years. One should note that the portion of the domain that is actually traversed by the particle cloud is a small percentage of the total domain, and is consistent with the approximate bound shown earlier in Figure 4-9. However, it is evident that a good portion of the domain variability is sampled in the direction of flow, for example, six correlation lengths at t = 10,000 years.

The effect of repeated realizations can be studied with the help of 3D particle-grid projection functions. This allows transformation of particle spatial coordinates to probability density functions (PDF) according to (Dagan, 1982)

$$f_x(\boldsymbol{X}, t; \boldsymbol{X}_o, t_0 = 0) = \frac{\phi}{M} < C(\boldsymbol{X}, t) > \tag{4-6}$$

where $f_x(\mathbf{X}, t, \mathbf{X}_o, t_0 = 0)$ is the probability for a particle, originally released at $\mathbf{X}_o$ at time t = 0, to end up within a small volume dV surrounding X at time t; ϕ is the porosity; M is the total mass released in the flow domain; and $< C(\mathbf{X}, t) >$ is the expected value of the concentration (or particle density) for

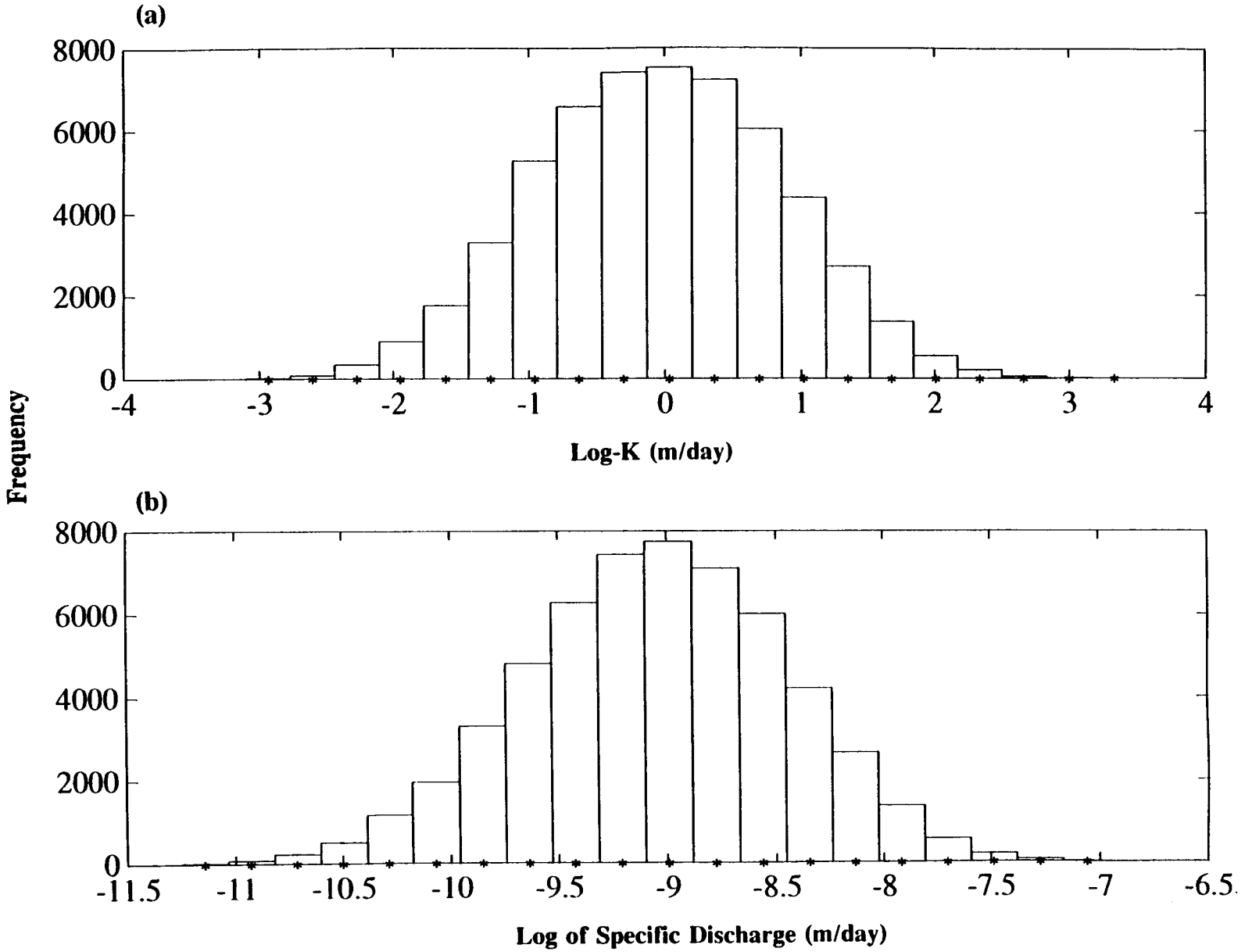

Figure 4-5. Histogram analysis of single realization results for σ_Y = 0.90. a) Logarithm of stochastically generated hydraulic conductivity. b) Logarithm of calculated specific discharge magnitude.

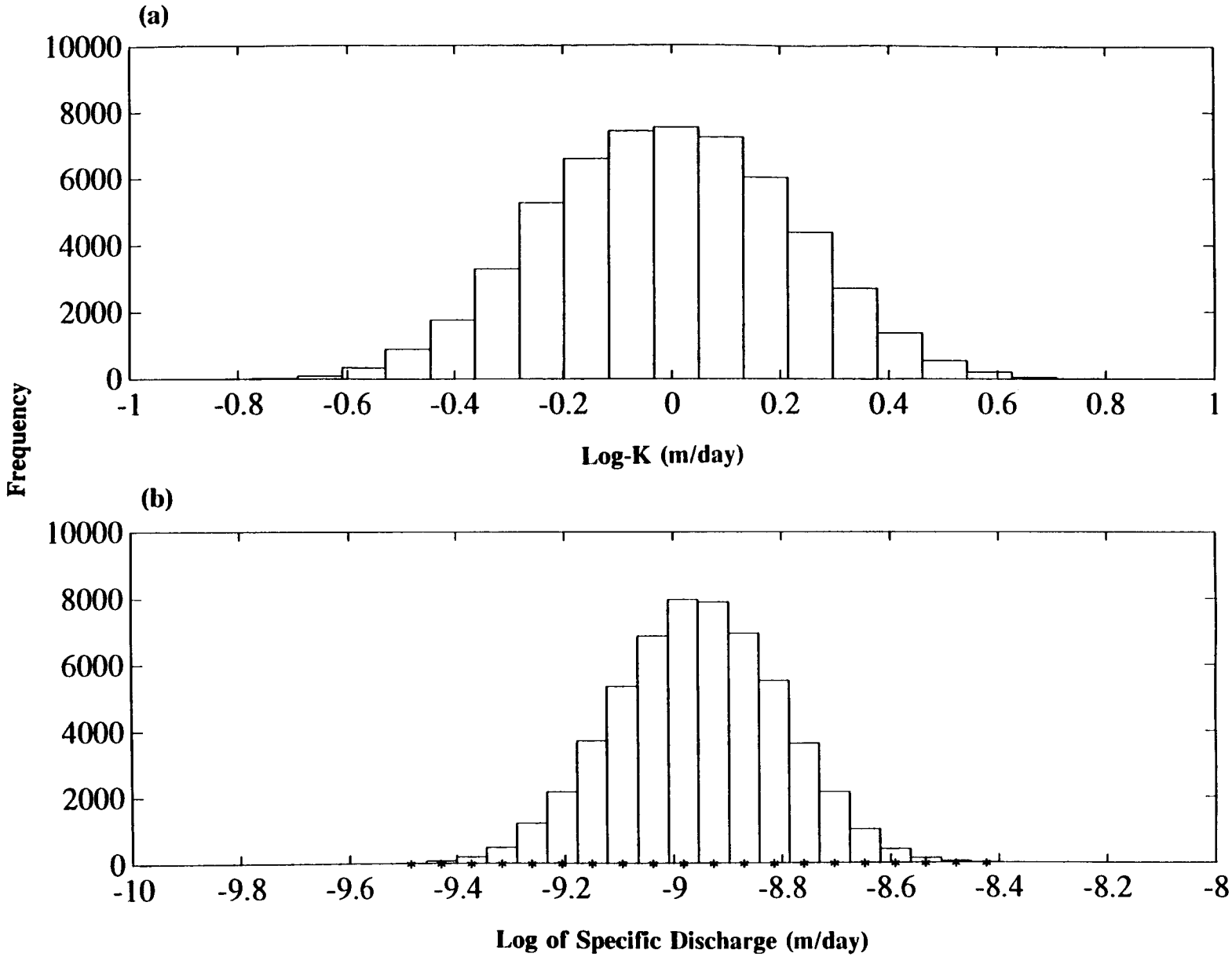

Figure 4-6. Histogram analysis of single realization results for σ_Y = 0.225. a) Logarithm of stochastically generated hydraulic conductivity. b) Logarithm of calculated specific discharge magnitude.

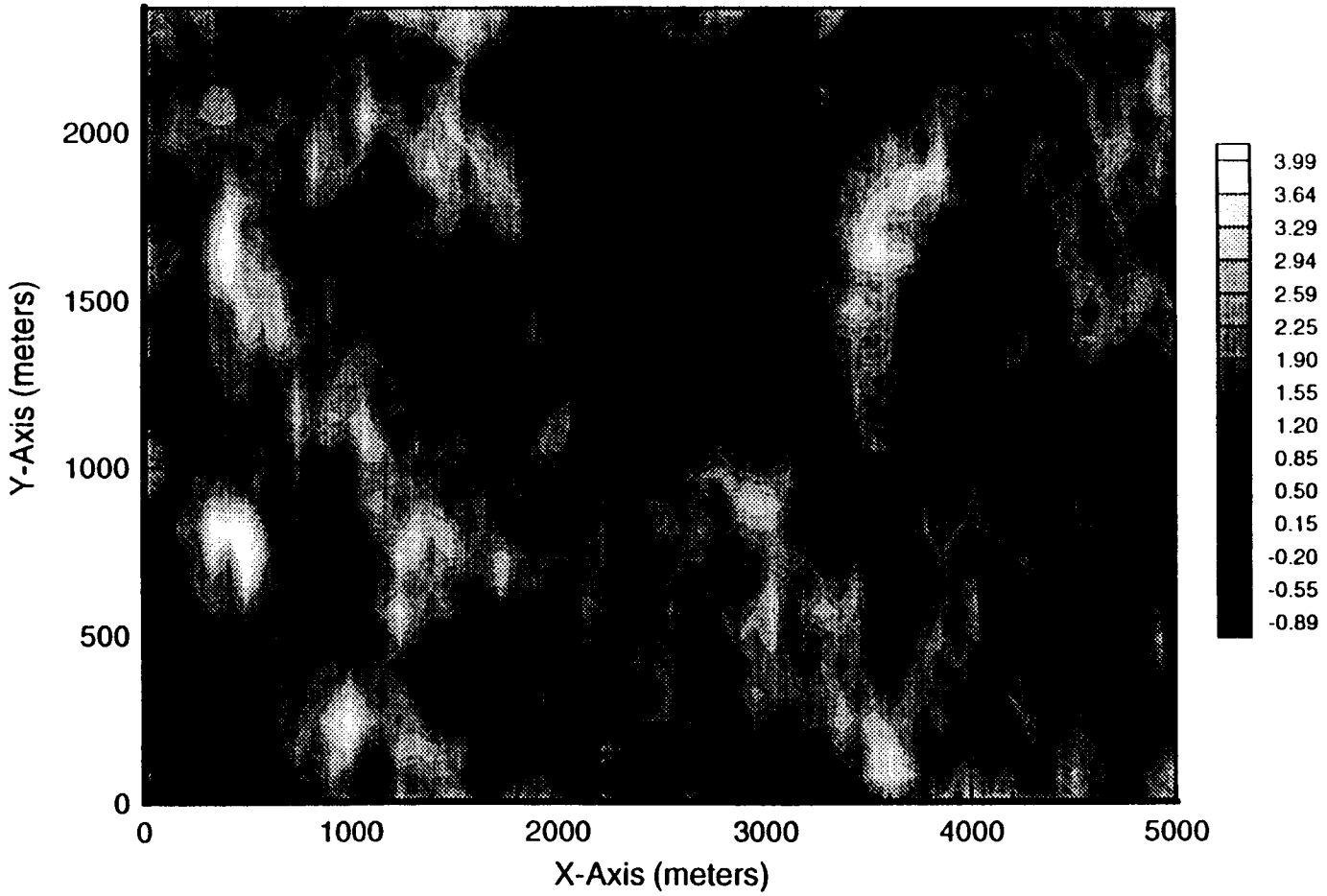

Figure 4-7. Typical realization for the logarithm of hydraulic conductivity (meters per day) for σ_Y = 0.90. Plot is on a horizontal plane at Z = 1,250 m.

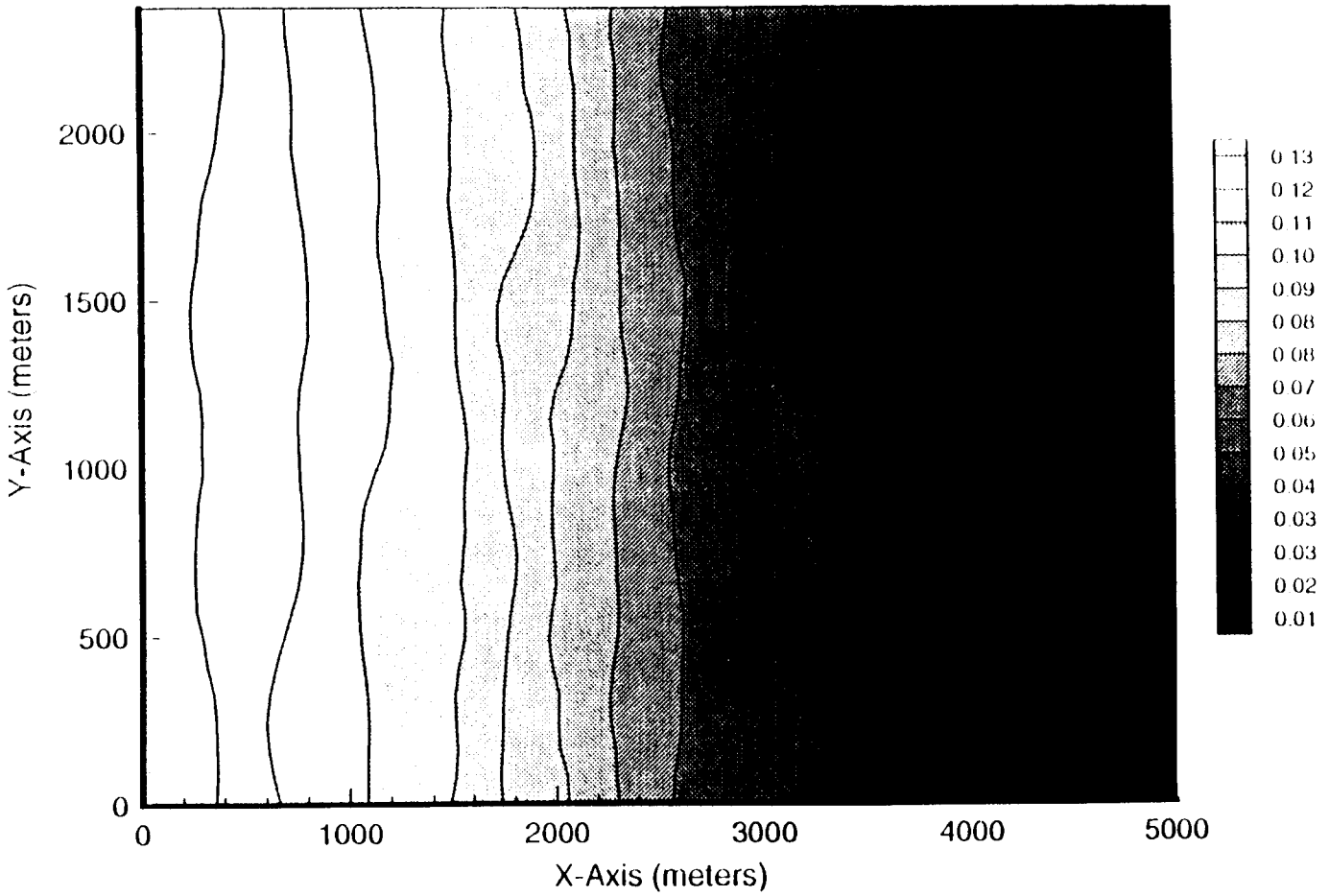

Figure 4-8. Typical realization for the hydraulic head field (in kilometers) for σ_Y = 0.90. Plot is on a horizontal plane at Z = 1,250 m.

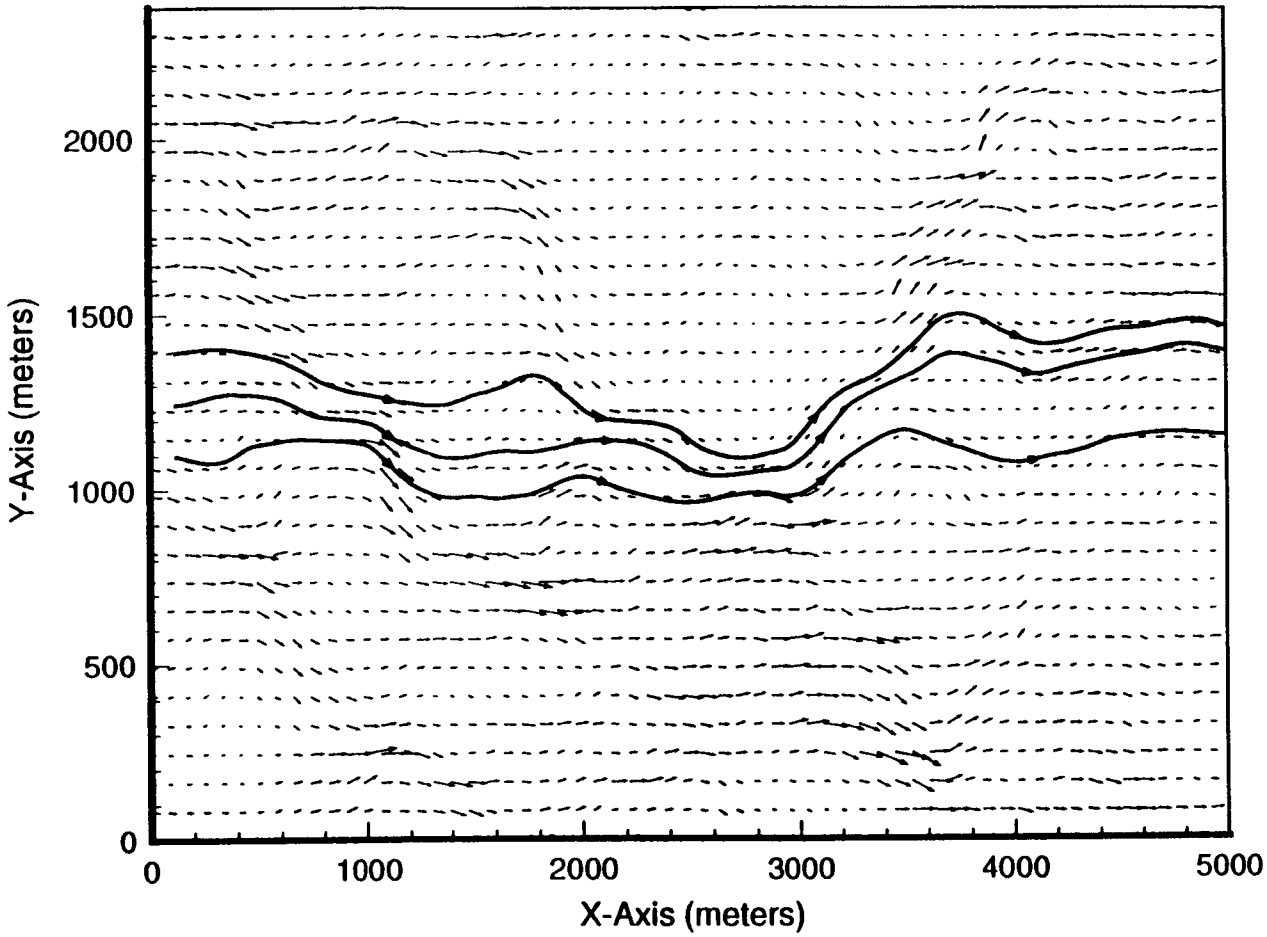

Figure 4-9. Typical realization of the flow field and streamlines for σ_Y = 0.90. Plot is on a horizontal plane at Z = 1,250 m.

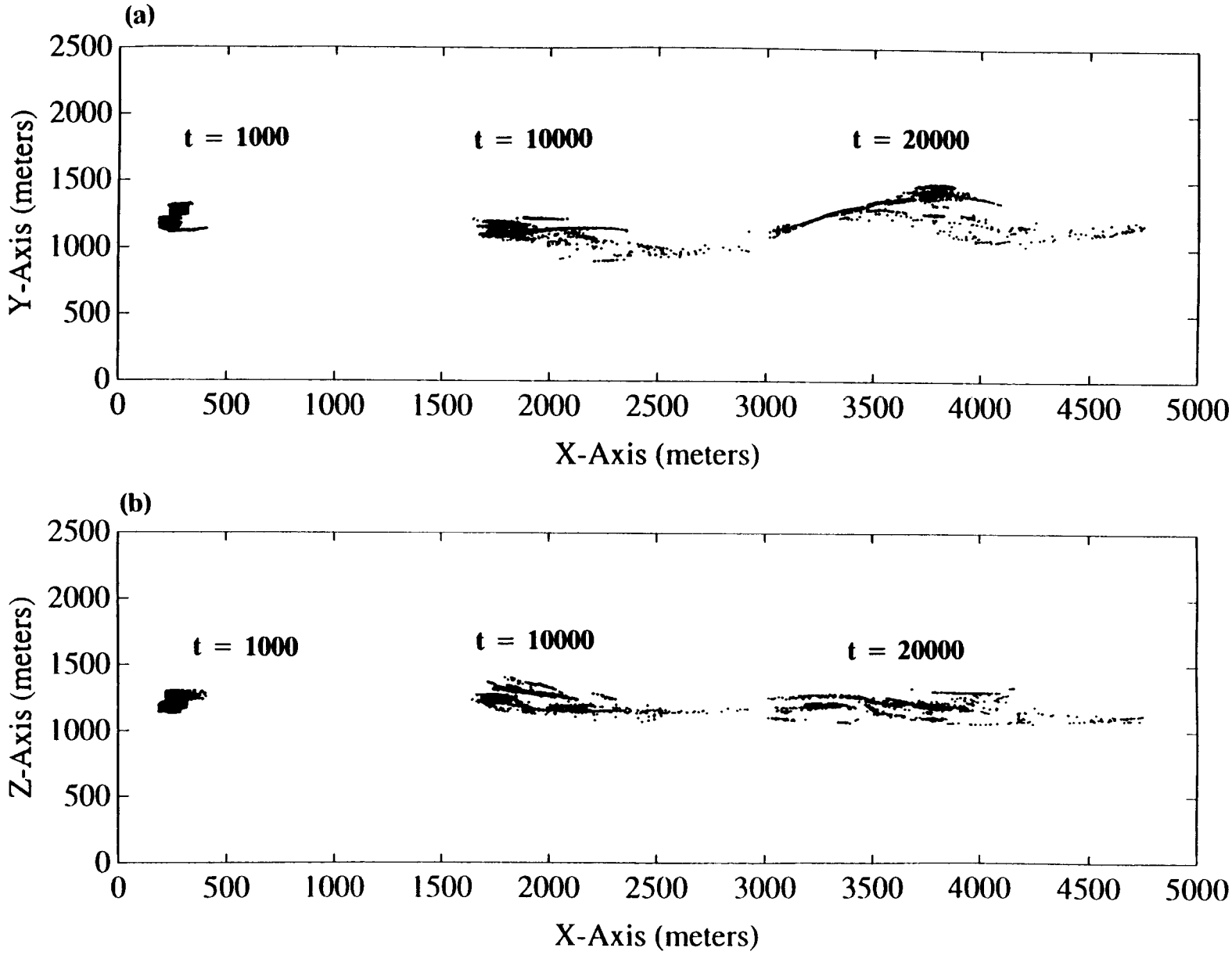

Figure 4-10. Results of particle tracking for a typical flow field realization for $\sigma_Y = 0.90$ at three different times (in years). a) X-Y projection of particles. b) X-Z projection of particles.

a series of random hydraulic conductivity field realizations. Details of this development can be found in Bagtzoglou and others (1991). Figure 4-11 corresponds to the particle cloud snapshots of Figure 4-10 and depicts a X-Y plane (Z = 1,250 m) representation of the particle location probabilities. It does not involve any repeated realizations of the hydraulic conductivity field, however, and as such will serve only for explanatory purposes. In the particular realization depicted in Figure 4-11, a particle released at t = 0 from within the release region has a probability of 5.59 percent of being found within the small marked area. To calculate the probability of finding a particle in a specified volume, the following integral must be calculated

$$P(X \in V) = \int_V f_x\,(X, t = T)\, dV \qquad (4\text{-}7)$$

In Eq. (4-7), dV denotes the volume of interest and since in the example presented, the release area is fixed, the dependence of f_x on X_o, 0 is not indicated. In the specific example at hand, this probability is approximately 18 percent. One should also keep in mind that the surface integral of the entire PDF field is not 100 percent, since that would happen only if the integration were to be performed over the entire volume of the domain.

Figure 4-12 shows results for the mean of 20 realizations at the same plane discussed before. The extra spread of the particle tracks is due to the velocity field variability across the realizations. Again, if one wanted to evaluate the probability of a particle being found within a certain area (or volume) of interest, integration according to Eq. (4-7) would have to be performed. Figure 4-12 depicts two notable features. First, the most probable (approximately 0.81 percent probability) location of a particle after 20,000 years is at X = 4,200 m; Y = 1,400 m; Z = 1,250 m which is well within the compliance boundary (defined arbitrarily to be located at 5,000 meters from the particle release region). Second, the interruption of the probability contours by the 5,000 meter boundary suggests that there is a non-zero probability of some of the particles having exited the compliance boundary in 20,000 years. For the particular example shown, this probability is estimated to be less than 1 percent.

Particle arrivals at the compliance boundary X = 5,000 m for both levels of porous medium heterogeneity were also analyzed. In Figure 4-13, the number of particles arriving at the compliance boundary is plotted against their arrival time for the case of $\sigma_Y = 0.90$. The plot in Figure 4-13a corresponds to a single velocity realization. The noise in this curve is indicative of the porous medium variability in this specific realization. This particular velocity field realization corresponds to the fastest GWTT estimate (among all realizations for this level of heterogeneity). One should note in Figure 4-13a that at discrete times (Δt = 10 years), parcels of particles arrive. The number of particles crossing the compliance boundary at any given time can be used as a weighing factor in GWTT statistics calculations. For example, in the realization of Figure 4-13a, the earliest particle arrival possible is 15,000 years, the mean particle arrival is 18,815 years, and the standard deviation of particle arrivals is 1,085 years. In Figure 4-13b, the mean breakthrough curve of all 20 realizations is depicted. Again, similar to the observations made on Figure 4-12, the spread of this curve is a direct result of flow variability sampled over the hydraulic conductivity realizations. For the example shown here, the earliest arrival possible is unaffected by this averaging, whereas the mean particle arrival and the standard deviation of particle arrivals are now calculated to be 28,260 and 8,500 years, respectively. Figure 4-14 presents results of the analysis conducted for the case $\sigma_Y = 0.225$. There are two characteristic differences illustrated between Figures 4-13 and 4-14. First, the noise present in the breakthrough curves (both in the single fastest GWTT realization and in the mean of all realizations) is drastically reduced. Second, the GWTT

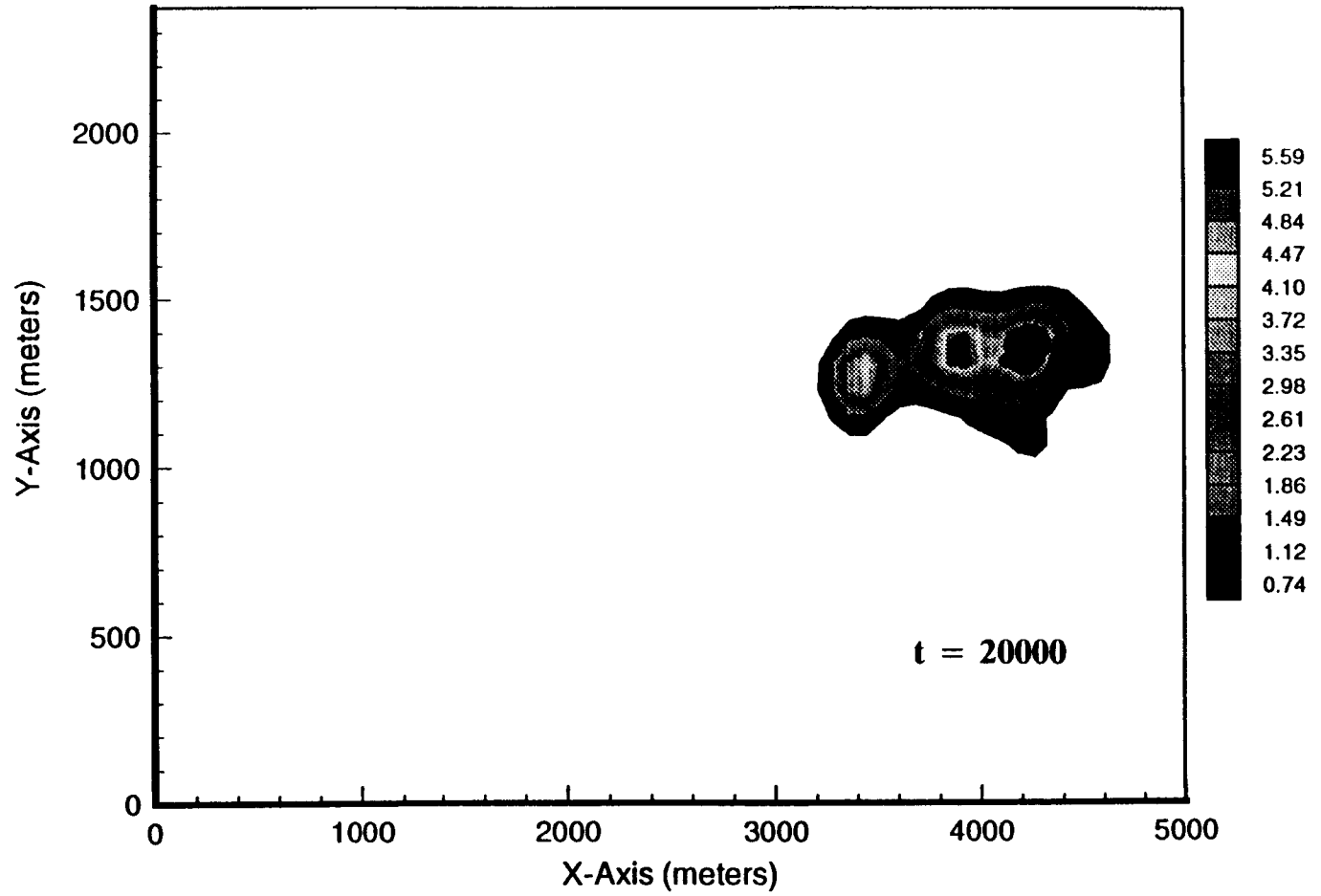

Figure 4-11. Probability density function field (percent) of particle destination at 20,000 years for a single realization of flow field with σ_Y = 0.90. Simulation involves 10,000 particles being tracked. Plot is on a horizontal plane at Z = 1,250 m.

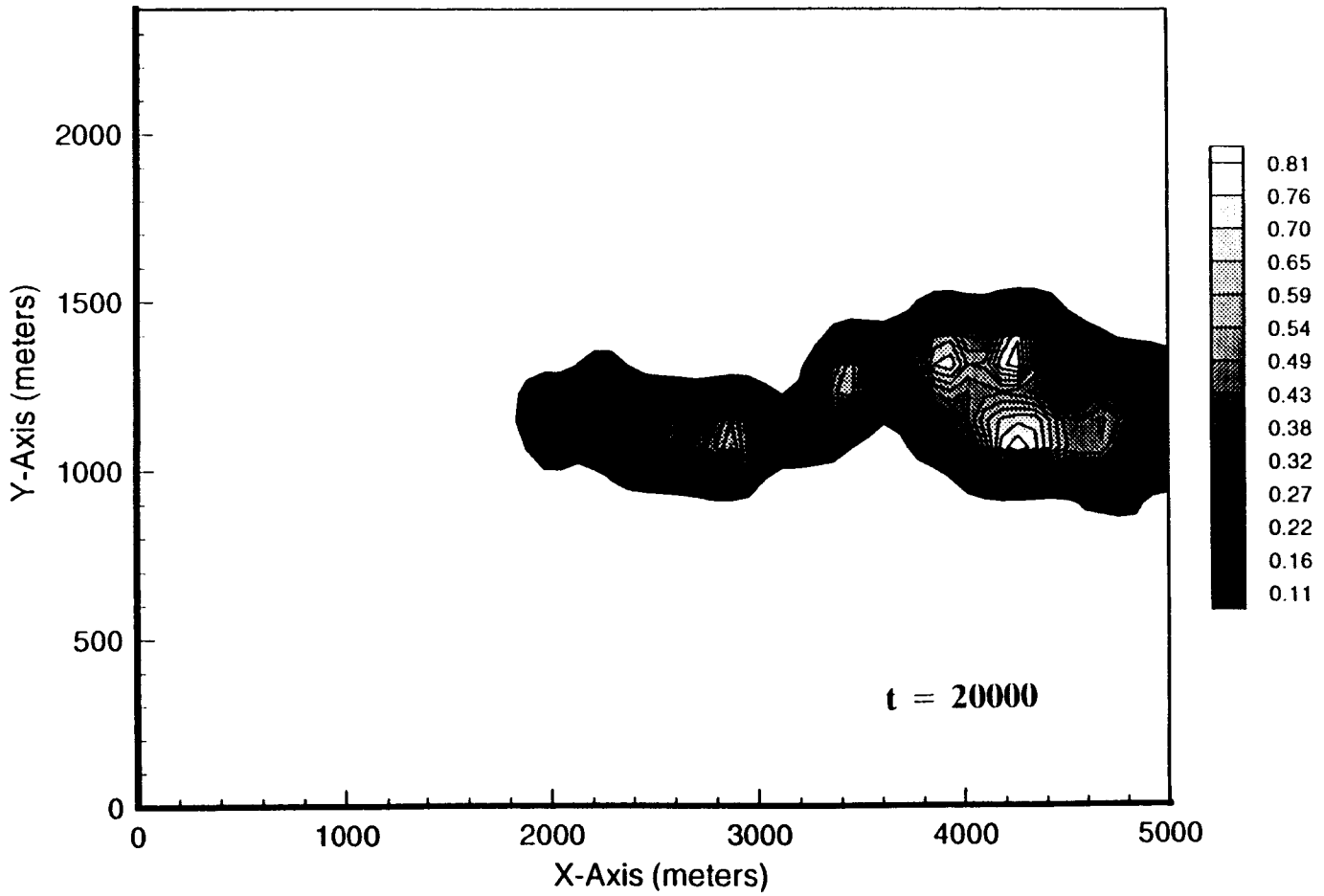

Figure 4-12. Mean of 20 repeated realizations, with 10,000 particles per realization, for probability density function field (percent) of particle destination at t = 20,000 years for σ_Y = 0.90. Plot is on a horizontal plane at Z = 1,250 m.

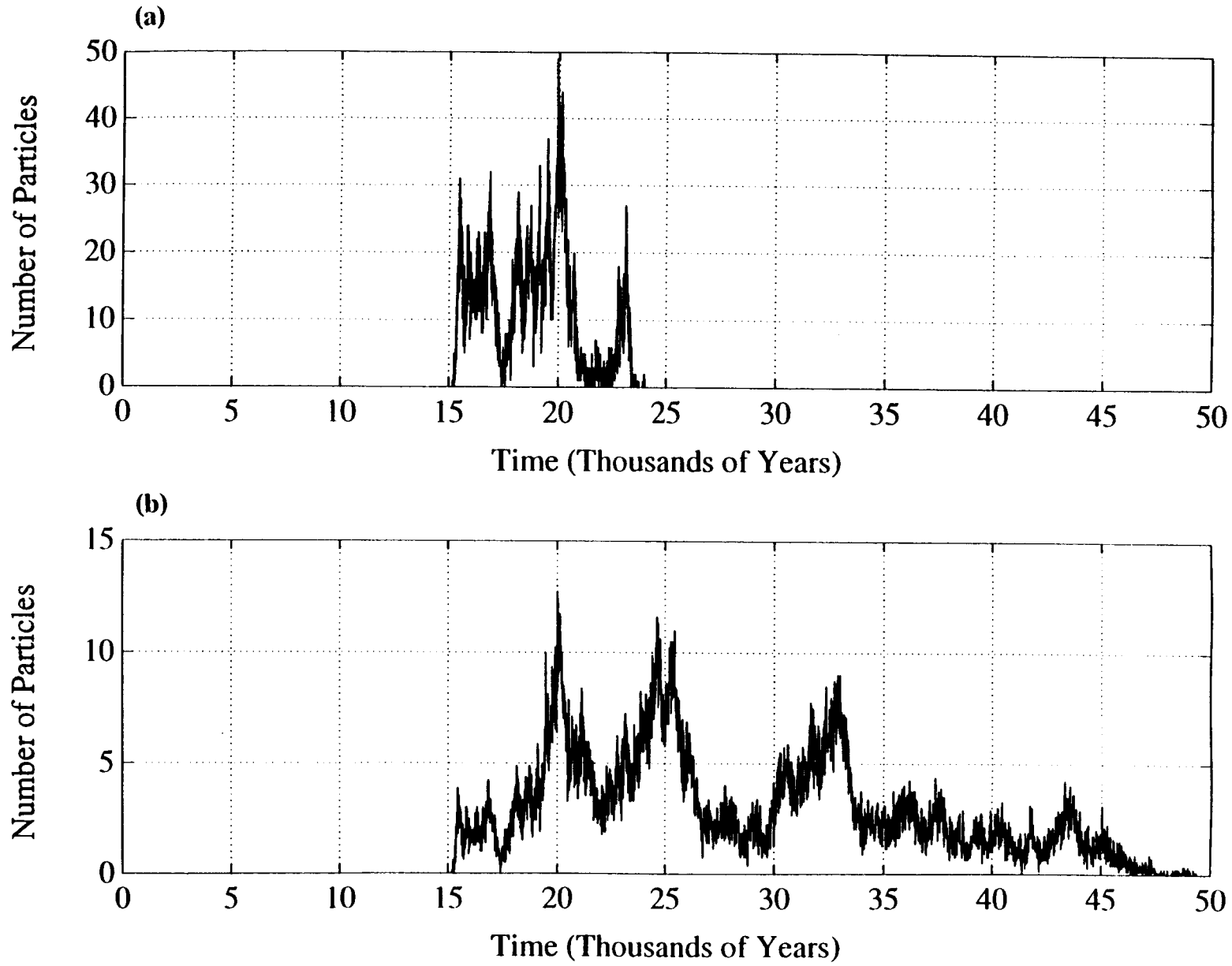

Figure 4-13. Particle breakthrough curve at the compliance boundary X = 5,000 m for σ_Y = 0.90. a) Realization corresponding to earliest arrival possible. b) Mean of 20 realizations.

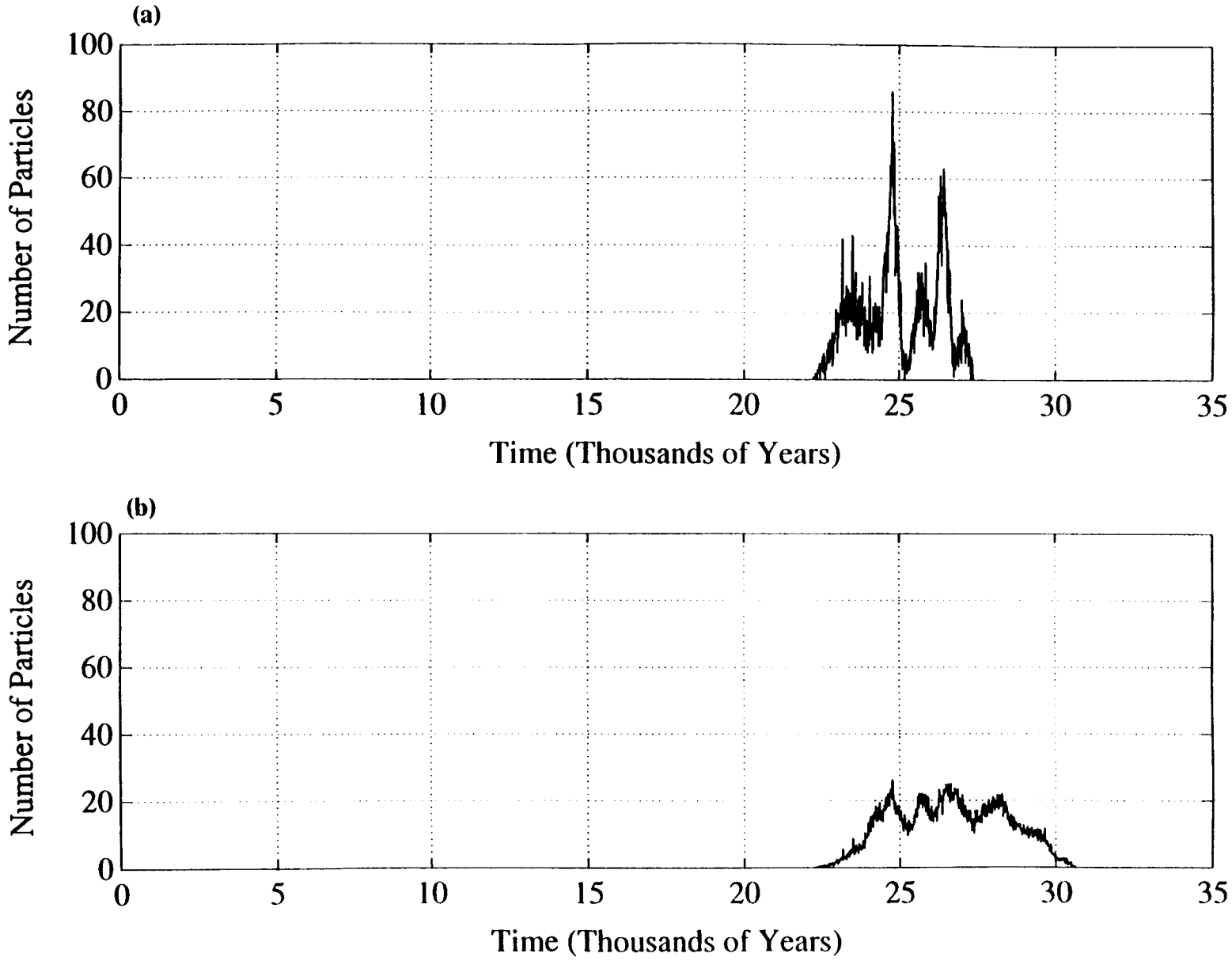

Figure 4-14. Particle breakthrough curve at the compliance boundary X = 5,000 m for σ_Y = 0.225. a) Realization corresponding to earliest arrival possible. b) Mean of 20 realizations.

is substantially increased by approximately 8,000 years.

In Figures 4-15 and 4-16, a comprehensive summary of the particle arrival analysis is presented for the levels of heterogeneity studied in this work. These plots depict the cumulative distribution function (CDF) for travel time in dimensionless form. The CDF corresponding to the mean of all realizations spans the interval between the earliest and latest arrivals in a smooth, almost sigmoidal, curve. Even though the normality hypothesis was not tested rigorously, it was assumed for subsequent analyses that the mean distribution of particle arrivals is normal. It is characteristic that for both levels of heterogeneity, the CDF of the mean of all realizations is very useful in making inferences about GWTT, since it preserves the earliest-latest arrivals and also incorporates all the intermediate variability. For example, Figure 4-15 indicates that 16 percent of the particle arrivals occur before 20,000 years, while 84 percent arrive before 37,000 years. Similar observations can be readily made with Figure 4-16 corresponding to the lower degree of heterogeneity.

Further analysis of the variation of the earliest particle arrival, over the realization ensemble space under the same level of heterogeneity, resulted in the GWTT statistics presented in Table 4-1. These values are comparable to the results by Andrews and others (1989). In their analysis of GWTT uncertainty at the Deaf Smith County bedded salt site in Texas, a $\sigma_{logt} = 0.255$ was obtained for a medium characterized by $\sigma_Y = 0.64$, $\mu_{logt} = 5.83$, and $\lambda_Y = 650$ m.

A plot of μ_{logt} versus σ_Y is presented in Figure 4-17. Note that for $\sigma_Y = 0.0$ the GWTT is calculated to be 25,370 years, taking into account $K_G = 5 \times 10^{-3}$ m/day, J = 0.027, n = 0.25, and a travel distance equal to 5,000 m. The standard deviation σ_{logt} is shown as error bars superimposed on the same plot. It is worthwhile noticing that as the heterogeneity increases, the mean earliest arrival possible decreases. At the same time, the standard deviation of travel time increases and approaches a plateau after approximately a value of $\sigma_Y = 1.00$. These results indicate the loss in predictive power as the heterogeneity of the porous medium increases. To demonstrate this, a plot of the reliability index (Harr, 1987)

$$\beta_{logt} = \frac{\mu_{logt}}{\sigma_{logt}} \tag{4-8}$$

as a function of the heterogeneity is depicted in Figure 4-18. It is clear that absolutely certain GWTT predictions can be made only for a perfectly homogeneous medium (and perfectly known boundary conditions). As the degree of heterogeneity increases, the reliability (or confidence) in GWTT predictions significantly degenerates. It should be kept in mind that the reliability index values shown in Figure 4-18 are only relative to the homogeneous medium case.

4.5 SUMMARY

Effective use of stochastic theory based approaches can provide the necessary framework to perform probabilistic calculations of GWTT. This study employed the NNM process for stochastic generation of spatially correlated hydraulic conductivity fields. Repeated realizations of conductivity and flow fields are obtained and used for Monte Carlo advective transport of a large (10,000) collection of water particles. Two levels of porous media heterogeneity [$\sigma_Y = (0.225, 0.90)$] were studied in order to assess its effect on GWTT. Based on these exploratory calculations, it is concluded that GWTT over the "fastest path" is a decreasing function of porous medium heterogeneity.

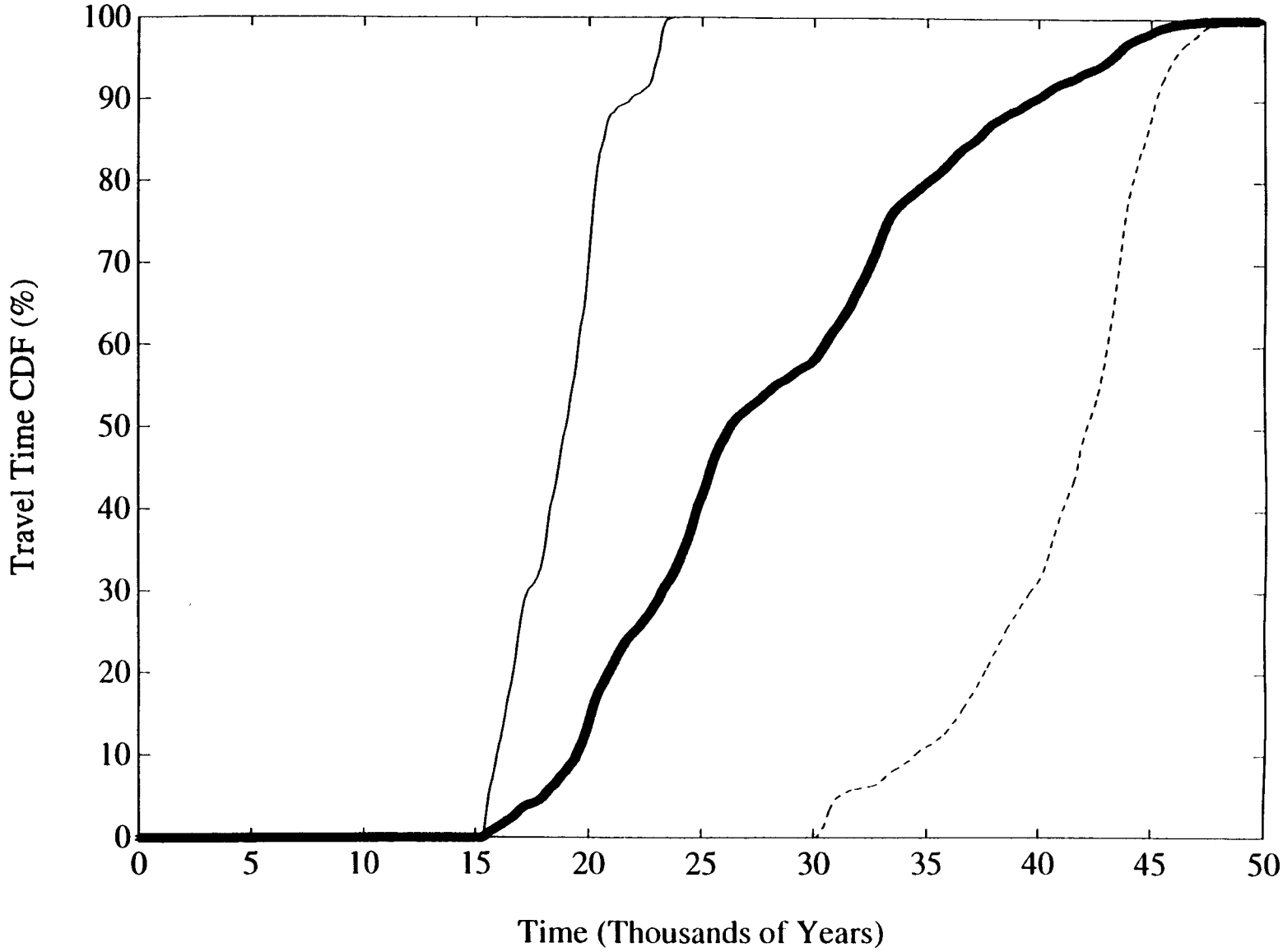

Figure 4-15. Cumulative distribution function for travel time for σ_Y = 0.90. Thick solid line: Mean of 20 realizations. Solid line: Realization corresponding to earliest arrival possible. Dashed line: Realization corresponding to latest arrival possible.

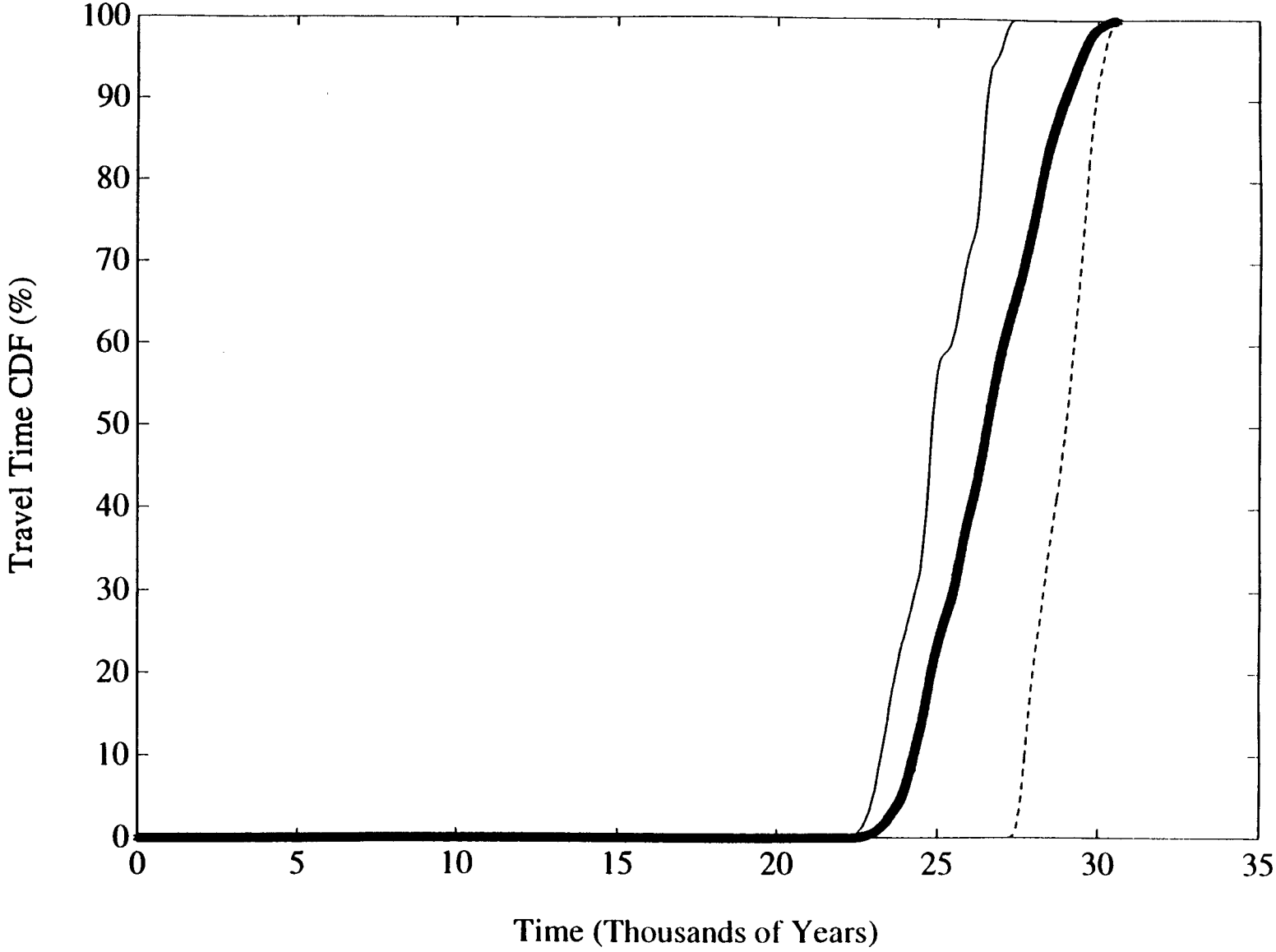

Figure 4-16. Cumulative distribution function for travel time for σ_Y = 0.225. Thick solid line: Mean of 20 realizations. Solid line: Realization corresponding to earliest arrival possible. Dashed line: Realization corresponding to latest arrival possible.

Table 4-1. Statistics of earliest particle arrivals for two levels of heterogeneity

	$\mu_{\log t}$	$\sigma_{\log t}$	P[GWTT ≤ 1,000 yrs]
$\sigma_Y = 0.225$	10.116	0.0695	≈ 0%
$\sigma_Y = 0.900$	9.863	0.1856	≈ 0%

Pertinent questions stemming from this work include:

- Is the earliest particle arrival a meaningful regulatory measure of performance?
- Could a percentile-based GWTT provide a realistic alternative?
- What would be the effects of media anisotropy on GWTT calculations?
- Would the results be significantly different if a larger number of realizations was used?
- Does the number of independent particle "flights" within a realization reduce the necessary number of realizations required?

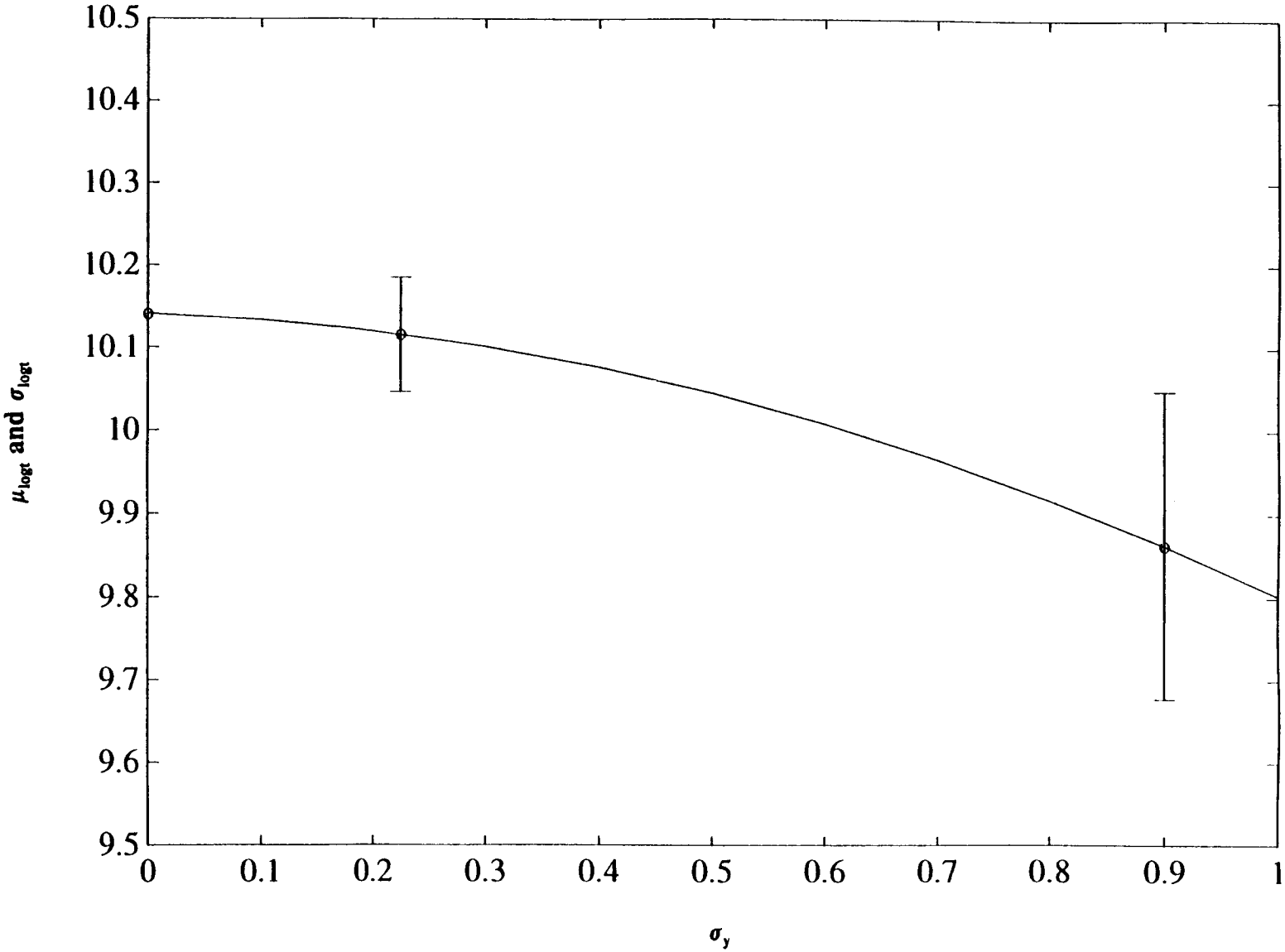

Figure 4-17. Plot of μ_{logt} versus σ_Y. Error bars reflect σ_{logt}.

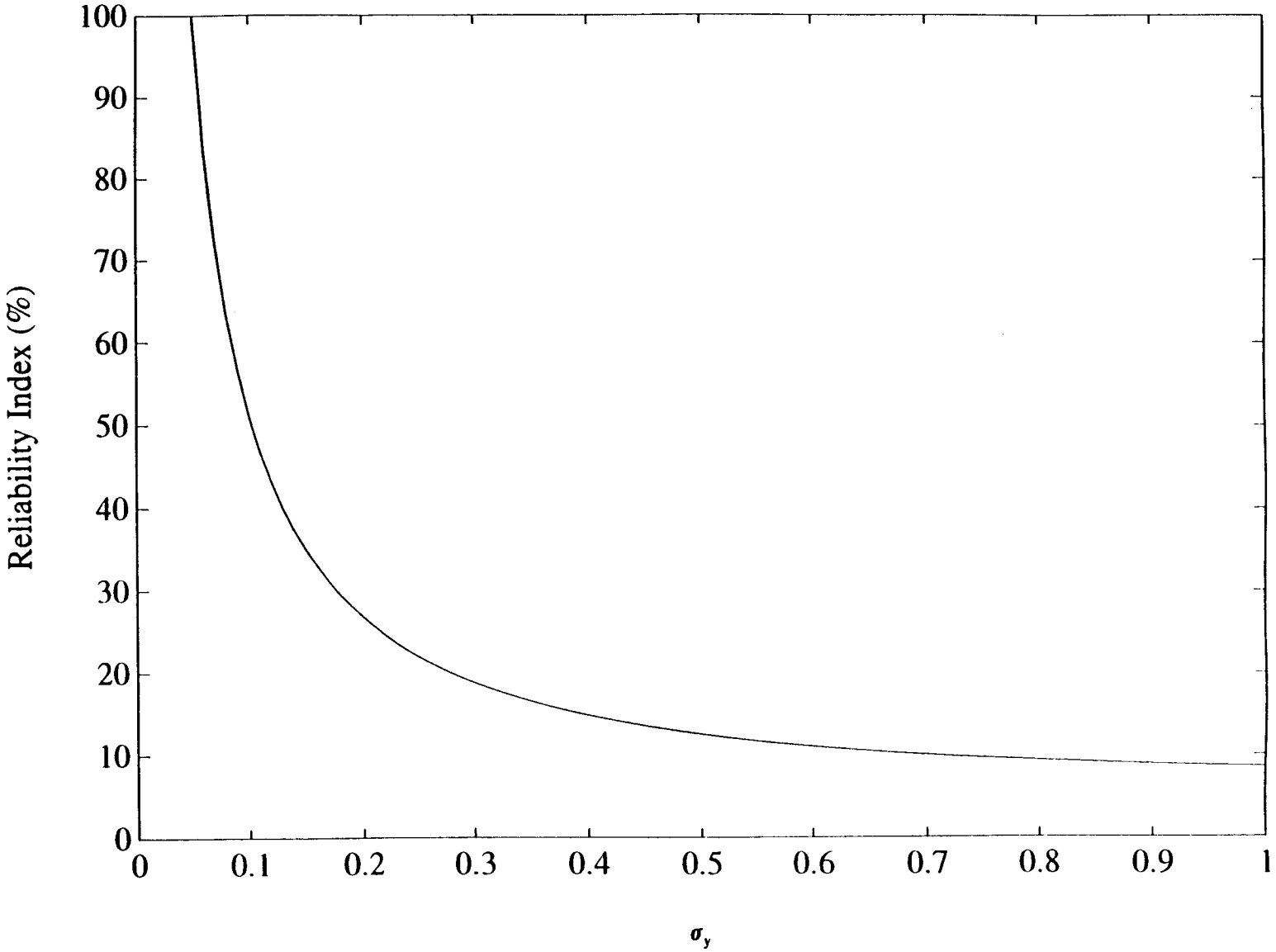

Figure 4-18. Plot of reliability index β as a function of level of heterogeneity σ_Y

5 SUMMARY

5.1 DISCUSSION

At present, there is no consensus as to whether groundwater travel time (GWTT) is an appropriate or sufficient performance measure for the geologic setting, particularly for unsaturated rock masses. Moreover, there is no clear understanding as to how the GWTT objective is to be implemented in a computational sense. A spectrum of alternatives to resolve the GWTT dilemma has been delineated in a document prepared for the Nuclear Regulatory Commission (NRC) by the Center for Nuclear Waste Regulatory Analyses (CNWRA) (Green and Sagar, 1992). An attempt was made in that document to list all reasonable options without assessing their relative strengths and weaknesses.

As the next step, a series of computational analyses has been conducted to provide quantitative insight into which general approaches are feasible and deserve further scrutiny. In order to provide this insight, analyses have been performed to investigate three aspects of the GWTT. In particular, these analyses were conducted to: (i) analyze the extent of the disturbed zone in response to different bounding conditions; (ii) assess the effects which model complexity and the incorporation of site characterization data into numerical models have upon GWTT distributions; and (iii) determine groundwater path variability through a stochastically-generated heterogeneous medium and assess its effects on GWTT.

Pertinent observations were made in the course of performing these computational analyses. These findings hopefully contribute to the identification promising options for implementation of the GWTT requirement. Additionally, lessons learned in the conduct of these analyses provide insight into what future directions might be pursued to determine how GWTT may be made a more meaningful performance measure.

5.2 CONCLUSIONS

Key observations made in analyzing the disturbed zone in response to different thermal loadings include the following:

- Increasing the average power density (APD) from 57 to 114 kW/acre changes the temperature and liquid saturation regimes predicted in the vicinity of a HLW repository. For example, an APD of 114 kW/acre resulted in temperatures greater than 140 C and liquid saturations in excess of 95 percent at 1000 years. Whereas, for an APD of 57 kW/acre, temperatures did not exceed 97 C, nor were significant saturation changes observed.

- Simulations performed with a relatively high permeability (1.9 E-15 m^2) indicate that significant changes in liquid saturation could occur that would not be expected in a model with lower permeability (1.9 E-18 m^2). The presence of zones of high saturation (>95 percent) and associated dry-out zones above and below the repository could persist beyond the 1000-year time interval of interest in the GWTT.

- Based upon preliminary analyses, neither temperature nor liquid saturation can individually qualify as a conservative indicator of the disturbed zone. Simulations were conducted where significant temperature changes (>97 C) were observed, but liquid saturation was relatively

unchanged. Where liquid saturation changes were greater (i.e., >95 percent, or < 5 percent), temperatures were observed to be moderate (i.e., < 95 C).

Interim results gained from analyses conducted on model complexity include the following:

- Model structure has a clear effect on the calculated first arrival time and the distribution of travel times in simulations of saturated media.

- For unsaturated flow regimes, there is no obvious relation between the complexity of the model and the complexity of the resulting velocity fields. Unsaturated phenomena such as moisture dependent anisotropy or fingering are thought to mask the relationship between model complexity and the resulting velocity field.

Observations resulting from the analyses of probabilistic calculations of GWTT through saturated stochastically generated heterogeneous media are as follows:

- Stochastic methods can provide for the efficient generation of spatially correlated hydraulic conductivity fields, useful in GWTT calculations using Monte Carlo methods.

- Based on analyses at two levels of porous media heterogeneity, it was concluded that GWTT over the "fastest path," and its associated reliability, is a decreasing function of porous medium heterogeneity.

Several technical questions relevant to the GWTT regulation were raised in the conduct of these analyses. These include the following:

- Should the concept of a disturbed zone be included in the consideration of GWTT as a performance measure?

- Can some combination of temperature and liquid saturation be used to define the extent of the disturbed zone or are additional parameters necessary to make the definition complete and meaningful?

- Does the formation of high saturation zones with associated dry-out zones above and below the repository reduce or increase postemplacement GWTT from the repository to the accessible environment? Can the concept of a disturbed zone be deleted from the GWTT regulation without compromising the usefulness of GWTT as a measure of the performance of the geologic setting?

- Can an equivalent composite medium (ECM) adequately represent a fractured porous medium under partially-saturated conditions for purposes of calculating the extent of the disturbed zone or GWTT?

- What level of structural detail is necessary to assure that a model is representative of the physical site?

- Can stochastic continuum methods provide analytical tools to predict GWTT distributions in unsaturated regimes based on the statistical structure of the unsaturated hydraulic conductivity and moisture retention functions?

- Is the earliest particle arrival a meaningful regulatory measure of performance, or can a percentile-based GWTT provide a realistic alternative to current regulation?

- What would be the effects of anisotropy on GWTT calculations for the Yucca Mountain site?

- Would stochastic GWTT results be different if a larger number of realizations were used?

- In probabilistic calculations, does the number of independent particle "flights" within a realization reduce the necessary number of realizations required?

Future computational analyses for GWTT will be aimed at clarifying these technical aspects and evaluating the merits of other quantitative approaches.

6 REFERENCES

Ababou, R., D. McLaughlin, L.W. Gelhar, and A.F.B. Thompson. 1989. Numerical simulation of three-dimensional saturated flow in randomly heterogeneous porous media. *Transport in Porous Media* 4: 549-565.

Ababou, R. 1991. *Approaches to Large Scale Unsaturated Flow in Heterogeneous, Stratified, and Fractured Geologic Media.* NUREG/CR 5743. Washington, D.C.: Nuclear Regulatory Commission (NRC).

Ahola, M., and B. Sagar. 1992. *Regional Groundwater Modeling of the Saturated Zone in the Vicinity of Yucca Mountain, Nevada. Iterative Performance Assessment - Phase II.* CNWRA 92-001. San Antonio, Texas: Center for Nuclear Waste Regulatory Analyses (CNWRA).

Andrews, R.W., A.M. LaVenue, and J.A. McNeish. 1989. Evaluating the effect of sampling and spatial correlation in ground-water travel time uncertainty coupling geostatistical, stochastic, and first order, second moment methods. *Proceedings of Conference on Geostatistical, Sensitivity, and Uncertainty Methods for Ground-Water Flow and Radionuclide Transport Modeling.* B.E. Buxton, ed. Columbus, Ohio: Battelle Press: 539-558.

Bagtzoglou, A.C., A.F.B. Thompson, and D.E. Dougherty. 1991. Probabilistic simulation for reliable solute source identification in heterogeneous porous media. *Water Resources Engineering Risk Assessment.* J. Ganoulis, ed. Berlin, Unified West Germany: Springer-Verlag: (G29): 189-201.

Bagtzoglou, A.C., G.W. Wittmeyer, and B. Sagar. 1992a. Parallel computing of subsurface flow problems with the Connection Machine (CM) system. in *Chapter 9: Performance Assessment Research, Report on Research Activities for Calendar Year 1991.* CNWRA 91-01A. San Antonio, Texas: CNWRA.

Bagtzoglou, A.C., G.W. Wittmeyer, R. Ababou, and B. Sagar. 1992b. Application of a massively parallel computer to flow in variably saturated heterogeneous porous media. Volume 1. *Numerical Methods in Water Resources.* T.F. Russell, R.E. Ewing, C.A. Brebbia, W.G. Gray, and G.F. Pinder, eds. Computational Mechanics Publications & Elsevier Applied Science: 695-703.

Bagtzoglou, A.C., A.F.B. Thompson, and D.E. Dougherty. 1992c. Projection functions for particle-grid methods. *Numerical Methods for Partial Differential Equations* 8: 325-340.

Brandshaug, T. 1989. *Variation of Heat Loading for a Repository at Yucca Mountain.* NUREG/CR-5428. Minneapolis, Minnesota: Itasca Consulting Group, Inc.

Brandshaug, T. 1991. *A Thermomechanical Far-Field Model of Yucca Mountain.* SAND85-7101. Albuquerque, New Mexico: Sandia National Laboratory (SNL).

Buscheck, T.A. 1991. Impact of repository-heat-driven hydrothermal flow on repository performance: Benefits form high repository thermal loading. *Presentation to Yucca Mountain Project - Project Manager's/Technical Program Office Meeting.*

Buscheck, T.A., and J.J. Nitao. 1992. The impact of thermal loading on repository performance at Yucca Mountain. *Proceedings of the Third International Conference on High-Level Waste Management.* La Grange Park, Illinois: American Nuclear Society: 1003-1017.

Code of Federal Regulations 10 CFR Part 60. 1992. Disposal of high-level radioactive wastes in geologic repositories. Washington, D.C.

Dagan, G. 1982. Stochastic modeling of groundwater flow by unconditional and conditional probabilities 2. The solute transport. *Water Resources Research* 18(4): 835-848.

Dagan, G. 1989. *Flow and Transport in Porous Formations.* Berlin, Unified West Germany: Springer-Verlag: 465.

Eriksson, L.G. 1991. The MD design — A cool concept for geologic disposal of radioactive waste. *Proceedings of the Second International Conference on High-Level Waste Management.* La Grange Park, Illinois: American Nuclear Society (ANS).

Green, R.T., and B. Sagar. 1992. *Options for Elimination of Technical Uncertainties from the Groundwater Travel Time Rule.* June, 1992. CNWRA Letter Report. San Antonio, Texas: CNWRA.

Harr, M.E. 1987. *Reliability Based Design in Civil Engineering.* New York, New York: McGraw-Hill: 290.

Iman, R.L., J.M. Davenport, and D.K. Zeigler. 1980. *Latin Hypercube Sampling.* SAND78-1473. Albuquerque, NM: SNL.

Johnson, G.L., and D.N. Montan. 1990. *Thermal Calculations Pertaining to a Proposed Yucca Mountain Nuclear Waste Repository.* UCRL-ID-103534. Livermore, California: Lawrence Livermore National Laboratory (LLNL).

Klavetter, E.A., and R.R. Peters. 1986. *Estimation of Hydrologic Properties of an Unsaturated, Fractured Rock Mass.* SAND84-2642. Albuquerque, New Mexico: SNL.

Nitao, J.J. 1988. *Numerical Modeling of the Thermal and Hydrological Environment Around a Nuclear Waste Package using the Equivalent Continuum Approach: Horizontal Emplacement.* UCID-21444. Livermore, California: LLNL.

Nitao, J.J. 1989. *V-TOUGH - An Enhanced Version of the TOUGH Code for the Thermal and Hydrologic Simulation of Large-Scale Problems in Nuclear Waste Isolation.* UCID-21954. Livermore, California: LLNL.

Papp, T. 1992. The importance of the site for the safety of a repository for Spent Nuclear Fuel in Sweden. *Proceedings of the Third International Conference on High-Level Radioactive Waste Management*. La Grange Park, Illinois: ANS: 2136-2144.

Peters, R.R., E.A. Klavetter, I.J. Hall, S.C. Blair, P.R. Heller, and G.W. Gee. 1984. *Fracture and Matrix Hydrologic Characteristics of Tuffaceous Materials from Yucca Mountain, Nye County, Nevada*. SAND84-1471. Albuquerque, New Mexico: SNL.

Pruess, K. 1987. *TOUGH User's Guide*. LBL-20700, NUREG/CR-4645. Berkeley, California: Lawrence Berkeley Laboratory (LBL).

Reference Information Base. 1992. YMP/CC-0002. Nevada Operations Office/Yucca Mountain Project Office. Las Vegas, Nevada: Department of Energy (DOE).

Rice, W.A. 1984. *Preliminary Two-Dimensional Regional Hydrologic Model of Nevada Test Site and Vicinity*. SAND837466. Albuquerque, New Mexico: SNL.

Rubin, Y., and G. Dagan. 1992. Conditional estimation of solute travel time in heterogeneous formation: Impact of transmissivity measurements. *Water Resources Research* 28(4): 1033-1040.

Runchal, A., and B. Sagar. 1992. *PORFLOW: A Multifluid Multiphase Model for Formulating Flow, Heat Transfer, and Mass Transport in Fractured Porous Media*. User's Manual, Version 2.40. CNWRA 92-008. San Antonio, Texas: CNWRA.

Sandia National Laboratory. 1987. *Site Characterization Plan Conceptual Design Report. Volume 4*. SAND84-2641. Albuquerque, New Mexico: SNL.

Site Characterization Plan. 1988. *Nuclear Waste Policy Act, Section 113*. Volume III, Part A, Chapter 7.4.1.2: Anticipated Thermal History. DOE/RW-0199. Washington, D.C.: U.S. DOE.

Smith, L., and R.A. Freeze. 1979a. Stochastic analysis of steady state groundwater flow in a bounded domain 1. One-dimensional simulations. *Water Resources Research* 15(3): 521-528.

Smith, L., and R.A. Freeze. 1979b. Stochastic analysis of steady state groundwater flow in a bounded domain 2. Two-dimensional simulations. *Water Resources Research* 15(6): 1543-1559.

Tompson, A.F.B., R. Ababou, and L.W. Gelhar. 1989. Implementation of the three-dimensional turning bands random field generator. *Water Resources Research* 25(10): 2227-2243.

Thompson, A.F.B., E.G. Vomvoris, and L.W. Gelhar. 1987. *Numerical Simulation of Solute Transport in Randomly Heterogeneous Porous Media: Motivation, Model Development, and Application*. UCID-21281. Livermore, California: LLNL.

U.S. Nuclear Regulatory Commission. 1990. *Preliminary Performance Assessment for a HLW Repository at Yucca Mountain, Nevada. Nevada.* Washington, D.C.: NRC.

van Genuchten, M.Th. 1980. A closed-form equation for predicting the hydraulic conductivity of unsaturated soils. *Soil Science Society of American Journal.* 44: 892-898.

Wang, Y.S.Y. 1992. Variations of hydrological parameters of tuff and soil. *Proceedings of Third International Conference on High-Level Radioactive Waste Management.* Las Vegas, Nevada: ANS and American Society of Civil Engineers (ASCE): 727-731.

Weiner, R.F., W.C. Patrick, and D.T. Romine. 1990. *Identification and Evaluation of Regulatory and Institutional Uncertainties in 10 CFR 60.* Vol. 1 and 2, CNWRA 90-003. San Antonio, Texas: CNWRA.

Wittmeyer, G.W., and B. Sagar. 1992. Performance assessment research. *Report on Research Activities for Calendar Year 1991.* W.C. Patrick, ed. CNWRA 91-01A. San Antonio, Texas: CNWRA.